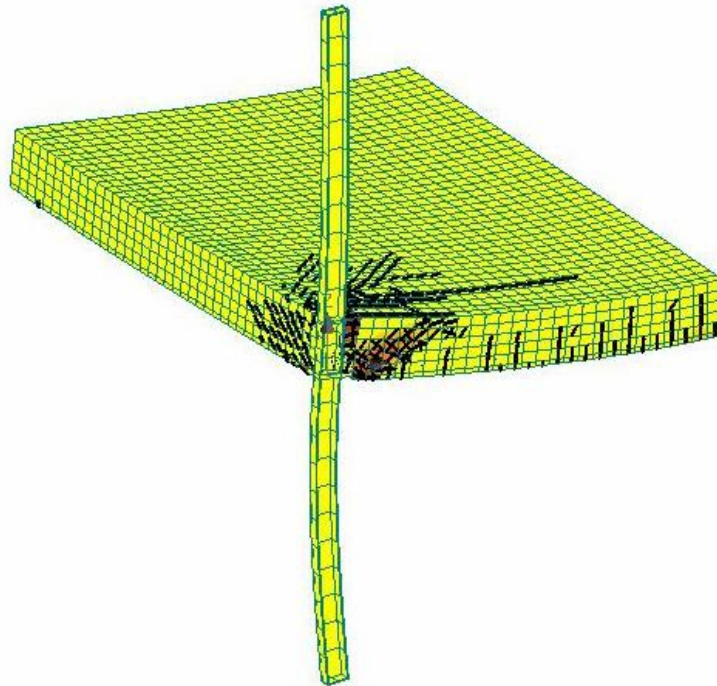


CHALMERS



Punching Shear in Reinforced Concrete Slabs Supported on Edge Steel Columns

Assessment of response by means of nonlinear finite element analyses

Master of Science Thesis in the Master's Programme Structural Engineering and Building Performance Design

SOFIA ERICSSON
KIMYA FARAHAHANINIA

Department of Civil and Environmental Engineering
Division of Structural Engineering
Concrete Structures
CHALMERS UNIVERSITY OF TECHNOLOGY
Göteborg, Sweden 2010
Master's Thesis 2010:101

MASTER'S THESIS 2010:101

Punching Shear in Reinforced Concrete Slabs Supported on Edge Steel Columns

Assessment of response by means of nonlinear finite element analyses

*Master of Science Thesis in the Master's Programme Structural Engineering and
Building Performance Design*

SOFIA ERICSSON
KIMYA FARAHANINIA

Department of Civil and Environmental Engineering
*Division of Structural Engineering
Concrete Structures*

CHALMERS UNIVERSITY OF TECHNOLOGY

Göteborg, Sweden 2010

Punching Shear in Reinforced Concrete Slabs Supported on Edge Steel Columns
Assessment of response by means of nonlinear finite element analyses

*Master of Science Thesis in the Master's Programme Structural Engineering and
Building Performance Design*

SOFIA ERICSSON

KIMYA FARAHANINIA

© SOFIA ERICSSON & KIMYA FARAHANINIA, 2010

Examensarbete / Institutionen för bygg- och miljöteknik,
Chalmers tekniska högskola 2010:101

Department of Civil and Environmental Engineering
Division of Structural Engineering
Concrete Structures
Chalmers University of Technology
SE-412 96 Göteborg
Sweden
Telephone: + 46 (0)31-772 1000

Cover:

Deformed shape and crack pattern of the investigated model that failed in punching shear.

Department of Civil and Environmental Engineering Göteborg, Sweden 2010

Punching Shear in Reinforced Concrete Slabs Supported on Edge Steel Columns
Assessment of response by means of nonlinear finite element analyses

Master of Science Thesis in the Master's Programme Structural Engineering and Building Performance Design

SOFIA ERICSSON

KIMYA FARAHANINIA

Department of Civil and Environmental Engineering

Division of Structural Engineering

Concrete Structures

Chalmers University of Technology

ABSTRACT

Punching shear is a phenomenon in flat slabs caused by concentrated support reactions inducing a cone shaped perforation starting from the top surface of the slab. Although generally preceded by flexural failure, punching shear is a brittle failure mode and the risk of progressive collapse requires a higher safety class in structural design. The design approach with respect to punching shear assumes that the slab is subjected to hogging moments in both main directions above the column which postulates that the slab is either continuous or that the slab-column connection is moment resisting. Little research has been conducted on flat slabs supported on edge columns of steel. The need for further investigation derives from the low stiffness of steel edge columns in comparison to concrete slabs, which is believed to result in very little moment transfer through the connection. This causes reason to believe that the slab strip perpendicular to the edge shows resemblance to a simply supported beam.

In order to investigate the behaviour of such flat slabs simulations by nonlinear finite element analyses have been performed using the software ATENA developed by Červenka Consulting. Initially, conducted experiments were simulated in order to validate the modelling technique and the FE-analyses showed good agreement for peak loads and structural responses during loading.

A geometrically simple prototype of a reinforced concrete element supported on its edge by a steel column was used in the present work. As the simulation of punching shear failure was successful the comparison to the case when concrete columns are used showed certain similarities. The critical events that preceded punching failure were similar to what had been observed in previous investigations where concrete columns were employed. The behaviour of the strip perpendicular to the edge did however resemble the action of simply supported beams as shear cracks propagated from the bottom surface. Nevertheless, the presence of tangential cracks on the top surface and the triaxial state of compression in the concrete close to the supporting column depicted that some restraint could be expected.

Key words: flat slab, punching shear failure, edge steel column, reinforced concrete, FE-analysis, ATENA

Contents

ABSTRACT	I
CONTENTS	III
PREFACE	VII
NOTATIONS	VIII
INTRODUCTION	1
1.1 Background and problem description	1
1.2 Purpose	1
1.3 Scope	1
1.4 Method	2
2 ENGINEERING PRACTICE	3
2.1 Reinforced concrete slabs	3
2.2 Column-slab connection	5
3 DESIGN APPROACH FOR FLAT SLABS	7
3.1 Load distribution	7
3.2 Moment distribution	8
3.3 Reinforcement design	9
4 PUNCHING SHEAR	10
4.1 Observations on punching shear	10
4.1.1 Slabs supported on interior columns	10
4.1.2 Slabs supported on corner columns	13
4.1.3 Slabs supported on edge columns	16
4.1.4 Summary of observations	21
4.2 Design resistance with regard to punching shear	21
4.2.1 Punching shear resistance at interior columns	23
4.2.2 Punching shear resistance at edge and corner columns	24
5 OBJECT OF INVESTIGATION	26
5.1 Previous investigation on steel column supported slabs	27
5.2 Case study	27
6 NONLINEAR FE-ANALYSIS AND NUMERICAL METHODS	29
6.1 Nonlinearity	29
6.2 Numerical solution methods	30
6.2.1 The Newton-Raphson iteration	30

6.2.2	The Arc Length iteration	32
6.2.3	The Line Search method	34
7	MODELLING OF REINFORCED CONCRETE IN ATENA	35
7.1	Material models	35
7.1.1	Concrete model	36
7.1.2	Reinforcement model	41
7.2	Structural definition	42
7.3	Solution control setting	44
8	VALIDATION OF MODELLING TECHNIQUE	45
8.1	Laboratory tests for comparison	45
8.1.1	Material data	45
8.1.2	Geometrical data and loading	46
8.1.3	Results and observations from experiments	47
8.2	Simulation of laboratory tests	48
8.2.1	Material properties	51
8.2.2	Finite elements	51
8.3	Results from analyses of test specimens	52
8.3.1	Corner column supported slab <i>R1</i>	52
8.3.2	Edge column supported slab <i>No. 2</i>	59
8.4	Comments on verification	65
8.4.1	Predicted punching load for specimen <i>No. 2</i>	66
8.4.2	Previous comparisons with ATENA	66
9	NUMERICAL INVESTIGATION OF CASE STUDY	67
9.1	General modelling considerations	67
9.1.1	Geometrical specifications	68
9.1.2	Boundary conditions and loading	69
9.1.3	Material models	70
9.2	Modelling scheme	71
9.2.1	Simulation of punching shear failure	71
9.2.2	Mesh convergence study	72
9.2.3	Influence of the reduced compressive strength as lateral tensile strains develop	74
9.3	Results from FE-Analyses	74
9.3.1	Analysis of <i>A1</i>	75
9.3.2	Analysis of <i>A2</i>	80
9.3.3	Analysis of <i>A3</i>	82
9.3.4	Influence of the parameter $r_{c,lim}$ on model <i>A3</i>	88
9.4	Comments on results	91
9.4.1	Models failed in bending, <i>A1</i> and <i>A2</i>	91
9.4.2	Model failed in punching, <i>A3</i>	92
9.4.3	Summary of investigation	95

10	CONCLUSIONS	96
11	REFERENCES	99
11.1	Literature references	99
11.2	Electronic references	100
11.3	Complementary literature	100
APPENDIX I	Design of prototype slab	
APPENDIX II	Material properties	
APPENDIX III	Reinforcement arrangement in the validation models	
APPENDIX IV	Reinforcement arrangement in the prototype models	
APPENDIX V	Predicted punching load according to EC2	
APPENDIX VI	Convergence criteria	

Preface

The work presented in this report has been carried out at Tyréns Structural Design Department in Gothenburg and constitutes the final curriculum of our studies at the Master of Science Programme ‘Structural Engineering and Building Performance Design’, Chalmers University of Technology.

The initiator and main supervisor of this project has been MSc Bengt Johansson at Tyréns in Gothenburg, whose long experience in the field of structural engineering we have benefited from. We would like to thank Bengt Johansson for having appealed to and enabled this project. Throughout the project, we have been supported by our assistant supervisor PhD Mikael Hallgren at Tyréns in Stockholm and also PhD Dobromil Pryl at the Cervenka software support in Prague. We are very grateful for their appreciative inputs and support, especially Mikael Hallgren who has dedicated much time and effort into our work. Furthermore, we would like to thank the employees at Tyréns who have been supportive during the realisation of this project. We would especially like to thank BSc Sara Kader who has been very helpful and has dedicated much time into introducing us to practical engineering.

We would like to cordially thank and express our great appreciation to our examiner Professor Björn Engström for being of much help and guidance throughout the project and for sharing his many perspectives on the subject of punching. We would also like to thank Associate Professor Mario Plos who has shared his knowledge about finite element modelling and provided us with helpful information.

Göteborg June 2010

Sofia Ericsson & Kimya Farahaninia

Notations

Roman upper case letters

A_s	Reinforcement area
A_{sw}	Area of shear reinforcement within control perimeter
$A_{s,x}$	Reinforced area in the y-z plane
E	Modulus of elasticity (Young's modulus) for concrete
E_0	Initial modulus of elasticity for concrete
E_s	Steel modulus of elasticity
EI	Concrete slab stiffness
EI_{pe}	Column stiffness
G_F	Fracture energy of concrete
L	Column length
M_a	Transferred moment in slab-column connection
P	Column reaction
P_b	Column reaction at bending failure
P_p	Column reaction at punching failure
S_F	Crack shear stiffening factor
$V_{R,c}$	Punching shear resistance without shear reinforcement
$V_{Rd,c}$	Design punching shear resistance without shear reinforcement
$V_{Rd,cs}$	Design punching shear resistance with shear reinforcement

Roman lower case letters

a	Length of concrete slab along edge
b	Length of concrete slab perpendicular to edge
c_a	Side of supporting plate along slab edge
c_b	Side of supporting plate perpendicular to slab edge
c_{ts}	Factor governing tension stiffening of concrete
d	Effective depth of concrete section
d	Column side
d	Aggregate size
d_a	Column side in FE-model
d_b	Column side in FE-model
$d_{c,x}$	Column side in tests specimens, x-direction
$d_{c,y}$	Column side in tests specimens, y-direction
f_c	Concrete compressive strength
$f_{c,cube}$	Concrete compressive strength based on cube tests
$f_{c,cylinder}$	Concrete compressive strength based on cylinder tests

f_{ck}	Characteristic concrete compressive strength
f_t	Concrete tensile strength
$f_{t,s}$	Limiting steel stress in case of strain hardening
f_y	Yield strength of reinforcing steel
f_{yd}	Design yield strength of reinforcing steel
f_{yw}	Yield strength of shear reinforcement
f_{ywd}	Design yield strength of shear reinforcement
$f_{ywd,ef}$	Effective value of design yield strength of shear reinforcement
h	Thickness of slab
k	Size effect of the effective depth
l	Span length
l_x	Distance between columns along the edge
l_y	Distance between columns perpendicular to the edge
m_{Ed}	Design moment per unit width
m_{Rd}	Resisting moment per unit width
m_x	Bending moment per unit width in x-direction
m_{xy}	Twisting moment per unit width
m_y	Bending moment per unit width in y-direction
p_x	Side of neoprene bearings in x-direction
p_y	Side of neoprene bearings in y-direction
$r_{c,lim}$	Reduction limit of f_c as lateral tensile strains develop
s_{max}	Maximum crack spacing
s_r	Radial distance between rows of shear reinforcement
t	Thickness of hollow steel section
t_p	Thickness of supporting steel plate
t_p	Thickness of neoprene bearing
q	Surface load
u_0	Control perimeter of the column
u_1	Control perimeter
u_1^*	Reduced control perimeter
u_{out}	Outer control perimeter outside shear reinforcement when provided
$v_{Rd,c}$	Design shear strength per unit width without shear reinforcement
$v_{Rd,cs}$	Design shear strength per unit width with shear reinforcement
$v_{Rd,max}$	Recommended maximum value of shear strength per unit width
w_d	Critical compressive displacement
z	Internal level arm of reinforced concrete section

Greek lower case letters

α	Coefficient for thermal expansion
α_s	Angle between shear reinforcement and plane of slab
β	Coefficient for plastic flow direction
γ_c	Partial safety factor for concrete
ε_{cp}	Plastic strain at compressive edge
ε_{lim}	Limiting strain in case of strain hardening
η	Variable for support moment transfer
μ	Poisson's ratio
ν	Reduction factor for concrete with shear cracks
ρ	Concrete density
ρ_l	Ratio of bonded flexural reinforcement
ρ_{lx}	Ratio of bonded flexural reinforcement in x-direction
ρ_{ly}	Ratio of bonded flexural reinforcement in y-direction
ϕ	Diameter of reinforcement bar
ψ	Coefficient accounting for connection type

1 Introduction

1.1 Background and problem description

Steel columns in flat slab systems, a common solution in multi-storey residential buildings and office complexes, are favourable due to their sparse demand for space and possibility to be hidden inside non load-carrying walls. They make it possible to use large areas of glass in the façades and allow a more flexible window positioning.

The critical failure mode for flat slabs is punching shear; a phenomenon in slabs caused by concentrated support reactions inducing a cone shaped perforation starting from the top surface of the slab. The design approach with respect to punching shear is in various codes based on experimental results and observations from reinforced concrete slabs supported on concrete columns. The design method for punching shear assumes that the slab is subjected to hogging moments in both main directions above the column. This either requires that the slab is continuous, or in the case of edge and corner supported flat slabs, that the connection is moment-resisting in the direction perpendicular to the simply supported edge. Due to the relatively low stiffness of edge columns the slab can be regarded as nearly simply supported on the column with very little moment transfer through the connection. In contrary to interior columns, edge columns follow the rotation of the slab strip in the direction perpendicular to the edge.

During the last decades several researchers have investigated punching failure at edge and corner columns of reinforced concrete. The common feature of these objects has been the presence of unbalanced moments in the direction perpendicular to the edge of the slab. Knowingly there has been little research where the features of steel columns have been employed. As steel columns are less stiff than concrete columns, they are expected to be more prone to responding to the deformation of the slab.

1.2 Purpose

The purpose of this project has been to simulate punching failure of reinforced concrete slabs supported at their edges on slender steel columns in order to study the structural behaviour during this phenomenon. Furthermore, the aim of the study has been to provide information that can be of use when appropriate designs of reinforced concrete slabs supported on steel columns are sought.

1.3 Scope

The project considered reinforced concrete flat slabs supported on their edges by steel columns of square hollow sections. A geometrically simple prototype of a reinforced concrete slab has been analysed. The study also considers the influence of flexural reinforcement amount as it governs the failure mode. Moreover, the effect of concrete compressive strength reduction as cracking propagates has been assessed.

The considered slab was neither provided shear reinforcement nor drop panels for the enhancement of the punching shear capacity. Material models included nonlinear responses, such as concrete cracking and plastic behaviour and yielding of the reinforcing steel. Neither concrete shrinkage nor creep has been considered. Openings near columns are commonly present in practice, reducing the area of concrete that resists transverse shear, although this effect has not been dealt with in the present study.

1.4 Method

The project was initiated by the study of results and conclusions from former research, further employed as a point of reference. The steel column supported flat slabs have been investigated by means of nonlinear finite element analyses with Cervenka software ATENA 3D, version 4.3.4. In order to ensure the accuracy of the modelling technique, comparisons against available experimental data have been carried out. The purpose of these comparisons was to confirm that the FE-models were able to resemble the actual responses that were observed during experiments.

2 Engineering practice

The term flat slab is used for reinforced concrete slabs supported by one or several columns as illustrated in Figure 2.1 (a). This type of structural system can be performed in various ways, profiting from the sparse demand of space the columns, particularly steel columns, require. Flat slabs are not provided with any intervening beams or girders; the loads are directly transferred to the supporting columns resulting in low structural heights. Furthermore, the absence of beams and girders and particularly load-bearing walls allows for more freedom in planning.

A common structural system in case of flat slabs is to have a stabilising core of reinforced concrete that holds elevator shafts and main staircase in the centre, placing columns along the building's edges as illustrated in Figure 2.1 (b). When needed, additional stabilising can be obtained by the use of shear walls. In multi-residential buildings, reinforced concrete walls are often used to separate apartments from one another, providing good acoustic insulation and distinct fire cells. In the following, a brief description is given for the structural elements considered in the present work.

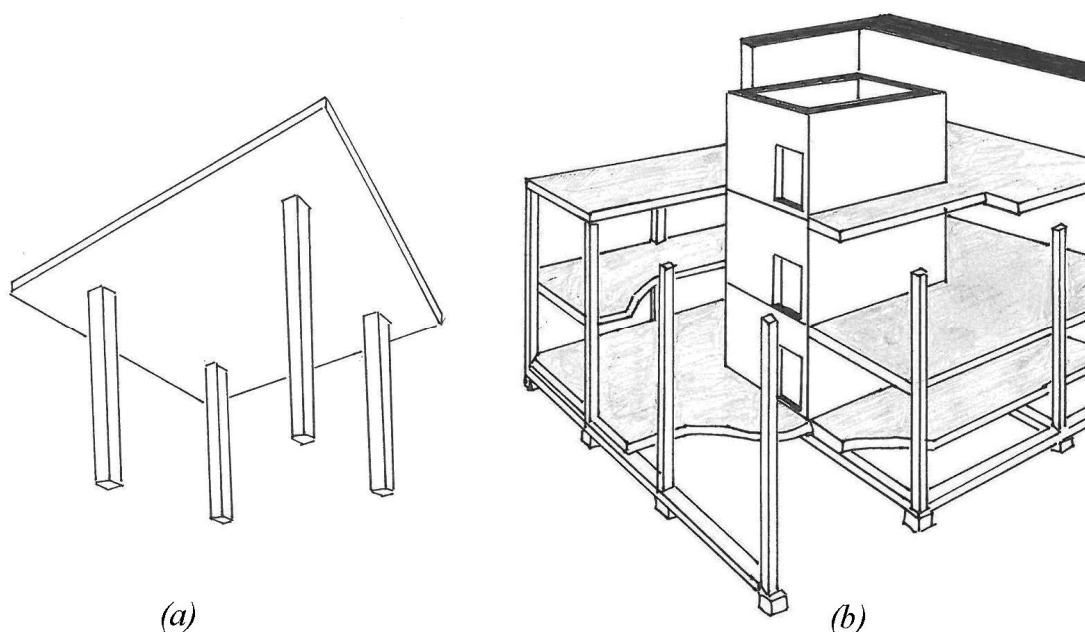


Figure 2.1 (a) Flat slab. (b) Flat slab system with a stabilising core and shear walls of reinforced concrete.

2.1 Reinforced concrete slabs

Reinforced concrete slabs can be of various types; where for residential buildings in Sweden a majority of the slabs used are composite floor plate floors. The choice of slab depends on various factors, such as structural heights, span lengths and the need for ducts.

Composite floor plate floors consist of prefabricated reinforced concrete plate elements and in-situ cast concrete, where the prefabricated units function as remaining

formwork. The precast member is usually rather thin (40–60 mm) and the reinforcement consists of a horizontal grid of steel bars in two perpendicular directions, corresponding to the required bottom reinforcement. Lattice girders are often present and serve two main purposes; increasing the rigidity of the prefabricated elements, which is beneficial during transport and construction, and providing transverse reinforcement and hence a mechanical bond in the joint between two units. A schematic illustration of a composite floor plate element is shown in Figure 2.2.

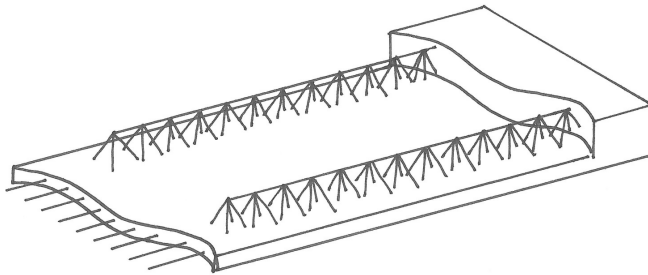


Figure 2.2 Prefabricated element and lattice girders of composite floor plate floor over which concrete is cast in-situ.

Before casting concrete above the prefabricated elements additional reinforcement is provided where needed. The slab carries the load mainly in the direction of the lattice girders. However, it can also transfer load in the weaker direction provided that the joints between the precast members are connected properly with additional reinforcement in the transverse direction. When needed, the composite floor plate floor can be prestressed, allowing longer spans and keeping deflections within limits. Span lengths of about 7 m can be expected for non-prestressed slabs, whilst for prestressed slabs a span length of about 10 m can be achieved. In residential buildings this type of slab commonly has distances of 3-5 m between the edge columns. The advantage and hence popularity of composite floor plate floors lies in their little demand of formwork and reinforcement labour. Nevertheless, one drawback is that the in-situ cast concrete requires desiccation to acceptable levels of relative humidity before proceeding with the next level of the construction. Throughout the time of concrete hardening the concrete develops its strength and propping is necessary. This type of slab is therefore not always preferable in tall buildings with many floors when rapid construction is desirable.

Lift slabs are flat slabs cast at ground level and thereafter elevated to the right position in the structural system. Steel collars are embedded in the concrete to function as a connection between the slab and the steel or concrete column, but also to facilitate the erection. The provided connection between the slab and the column is not sufficiently stiff to be considered as moment-resisting and therefore no or little moment will be transferred between the slab and the column in the direction perpendicular to the edge of the slab. Although not commonly used in Sweden today, lift slabs are of interest in this report since the lack of moment transfer make resemblance to the connections studied in this project. A flat slab system using lift slabs with steel columns is illustrated in Figure 2.3.

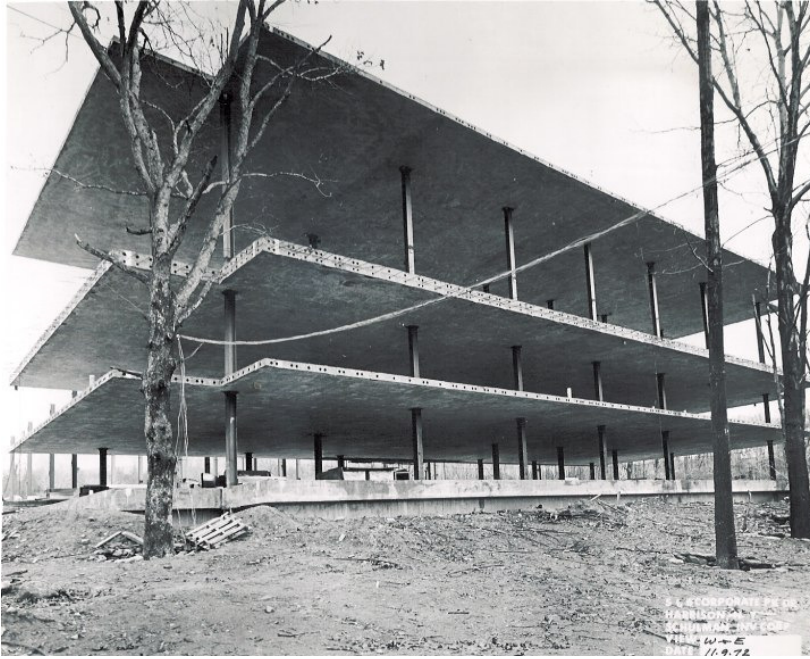


Figure 2.3 A structural system using lift slabs. (Baumann Research and Development Corporation, 2004)

2.2 Column-slab connection

When the building's exterior consists of non load-bearing walls or is a glass façade, columns can be used for the vertical load transfer at the building's edges. Regardless of the type of column that is chosen, given that it has sufficient capacity to withstand the forces it is subjected to, the column's cross-section is determined with respect to the possibility of connection to other structural members.

Concrete columns are solid sections of concrete provided with both longitudinal and transverse reinforcement. Although concrete has a high compressive strength the reinforcement needs to be provided in order to compensate for the brittleness of concrete and to guarantee correct functioning under bending action. The longitudinal bars are positioned in corners and when needed around the edges, whilst the transverse reinforcement is spread out over the length to keep the longitudinal reinforcement in place and to prevent buckling. Concrete columns can be made in various shapes and sizes. However, to certify a correct performance the minimum section must be relatively large, each side about 300 mm.

Steel columns can be of varying sections and detailing, giving different performances and aesthetic forms of expressions when being exposed. Hollow sections with almost equal stiffnesses in both directions are apposite when mainly subjected to normal forces. Aside with H-sections these column sections are predominant in residential and office buildings.

The varieties of the connection between slab and column are many and the possibilities are somewhat limited to the tolerances regarding production on site. Thus when designing slabs with respect to punching shear resistance it is important to

consider the limitations of practical execution. The connection is required to enable the load transfer from the slab to the column and in some cases the joint is sufficiently rigid to allow moment transfer. In the case of a concrete column, the connection can be considered as rigid since a part of the flexural reinforcement generally continues down the column from the slab (bent-down bars). Although the slab and the column are not cast together the two parts constitute a continuous structure.

The connection between a steel column and the slab can be executed in different ways. In this work, a common execution with square hollow steel columns has been treated. The detailing of the connection is such that two columns from adjacent storeys are connected through the slab by a hollow steel profile of the same cross sectional dimensions as the columns; see Figure 2.4. In the region around the column, the slab is recessed and entirely cast in-situ in order to get a homogenous concrete slab, which is normally done to reduce the risk of shear failure in the joint between the precast unit and the in-situ cast concrete. The purpose of the column continuity is to increase the performance of the vertical load transfer and to help avoid spalling and splitting of the concrete. The slab rests on the lower column on a rectangular steel plate, where the larger side is parallel to the slab's edge. Seeing as the plate is not bonded to the slab, the slab might lift from the support plate under the action of bending. The horizontal pins function as minimum tying with regard to progressive collapse.

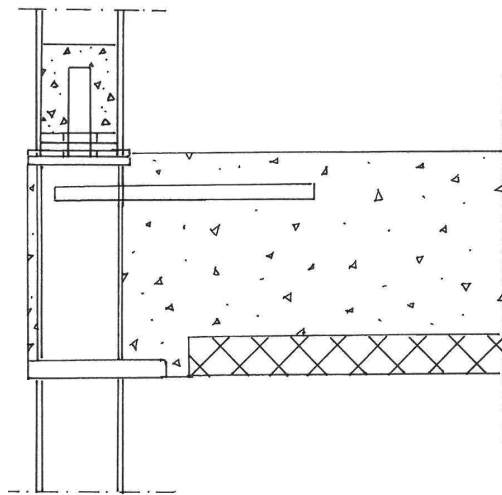


Figure 2.4 Detailing of the slab-column connection used in the present study.

3 Design approach for flat slabs

Reinforced concrete has the advantage of allowing the designer to somewhat influence the design moment distribution as the moment capacity of the slab is determined by the reinforcement amount. Slabs may be designed in accordance to the theory of plasticity due to their nonlinear behaviour including plasticity in the ultimate state. The plastic response of the material and the statically indeterminacy of flat slabs imply that equilibrium conditions can be fulfilled for several alternative moment distributions. In the following sections, the design and structural behaviour of flat slabs are further explained.

3.1 Load distribution

Slabs can be considered to carry the load in one or two directions, distinguishing them into one-way or two-way slabs. One-way slabs are supported on opposite supports, whilst bidirectional supports enable two-way action. Flat slabs are always two-way slabs as the load is transferred in both main directions and distributed between the supports. By dividing the slab into portions, the load carried to each column is distinguished. The portions are separated from one another by so called 'load-dividing lines', i.e. lines that indicate where the shear force is zero. The size of each portion depends on the moment distribution and the exact position can be derived once the statically indeterminate parameters have been chosen. For a flat slab, as shown in Figure 3.1, a reasonable estimation of the position of the load dividing lines in relation to the span length l is:

- Span between fixed edges and column: $0.5l - 0.5l$,
- Span between partially fixed edge and column: $0.45l - 0.55l$,
- Span between simply supported edge and column: $0.4l - 0.6l$,
- Span between columns: $0.5l - 0.5l$.

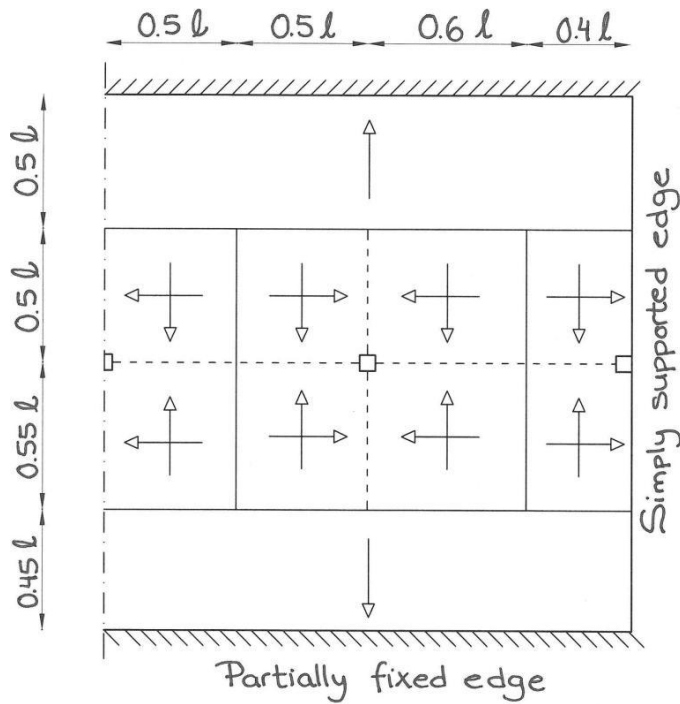


Figure 3.1 Reasonable load distribution of flat slab.

3.2 Moment distribution

The Strip Method is a method commonly used, aside from the yield line theory¹, for the design of reinforced concrete slabs. In contrary to the yield line theory, the Strip Method postulates that for any moment distribution that fulfils equilibrium, the solution is on the safe side in relation to the true plastic solution. The method originates from Arne Hillerborg (1959) and is based on the lower bound theorem of the theory of plasticity. The equilibrium equation for a slab element is generally expressed as:

$$\frac{\partial^2 m_x}{\partial x^2} + \frac{\partial^2 m_y}{\partial y^2} - 2 \frac{\partial^2 m_{xy}}{\partial x \partial y} = -q \quad (3.1)$$

where: m_x and m_y are bending moments in x and y-directions [kNm/m]

m_{xy} is the torsional moment [kNm/m]

q is the surface load [kN/m²]

Due to the difficulties of proportioning reinforcement for torsional moments, an alternative formulation for the equilibrium condition was suggested where these are chosen to zero and the load is fully resisted by flexural moment capacities. The reinforcement is then arranged in two perpendicular directions and the equilibrium condition yields:

¹ Yield line theory is an upper bound plastic approach to determine the limit state of a slab by assuring that the yield lines establish a kinematically possible collapse mechanism.

$$\frac{\partial^2 m_x}{\partial x^2} + \frac{\partial^2 m_y}{\partial y^2} = -q \quad (3.2)$$

Regardless of the satisfactory equilibrium and safety conditions, it is important to bear in mind that there are more or less effective solutions of reinforcement design, why good engineering practice should be adopted in order to avoid improper serviceability, lack of ductility and poor economy.

3.3 Reinforcement design

In a design situation, given the load distributions, each strip is designed for one-way action where design moments are determined by means of equilibrium conditions. When statically indeterminate strips are present, support moments are first chosen in accordance to provided guidelines. Once the support moments are determined, the field moments can be obtained by equilibrium conditions within a strip. When columns are placed across a line, the row of columns corresponds to one main strip. According to the theory of plasticity any moment distribution can be chosen provided that it fulfils equilibrium, nevertheless guidelines are set up to assure good serviceability behaviour and to respect the limited plastic rotation capacity of the reinforced slab section. Given the moment distributions, it is possible to determine the required reinforcement amount by considering the moment resistance achieved by force couples in the slab section. The design moment per unit width (m_{Ed}) is to be resisted by the sectional resistance of the reinforced section (m_{Rd}), according to the following expression:

$$m_{Ed} \leq m_{Rd} \quad (3.3)$$

where: $m_{Rd} = f_{yd} \cdot A_s \cdot z$

f_{yd} is the design yield strength of reinforcement

A_s is the area of contributing reinforcement in section

z is the internal level arm

In order to account for serviceability requirements, the transverse distribution of the resisting moments in the main strip needs to be considered. This may result in a concentration of reinforcement in areas where crack widths need to be restricted.

4 Punching shear

In addition to the design of flexural capacity of a flat slab the shear capacity above the columns need to be addressed. The intersection between the column and the slab is critical as the concentrated forces can induce a cone shaped perforation through the slab thickness. The perforation is formed as the cracks on the top surface caused by hogging moments extend downwards to the perimeter of the column. While a ductile flexural failure is characterised by an almost constant load-carrying ability with increasing displacements, the rapid loss of resistance in punching failure indicates a brittle failure and is therefore far more dangerous. The punching phenomenon has been under investigation mainly during the 1960's and 1970's when laboratory tests and extensive research were conducted. These experiments treated slabs supported on concrete columns. As more rational production methods have been desired, concrete columns have in some extent been replaced by steel columns. This chapter gives a brief overview of the research and how punching shear of reinforced concrete is accounted for in Eurocode 2 (EC2).

4.1 Observations on punching shear

Several researchers have conducted laboratory tests to study the structural behaviour of reinforced concrete slabs supported on columns. Some of the performed tests and their results are presented in this section. In the available literature two major groups of tests can be distinguished. The first group deals with punching failure where the shear stress in the vicinity of the column is assumed to be uniform, which is the case for most interior columns. The other group deals with non-symmetric shear stresses around the column due to unbalanced moments over the column. Unbalanced moments are caused by span discontinuity across the slab's edge and lateral loads from for instance wind. For edge and corner columns, unbalanced moments are always present due to span discontinuity. The available experiments can be divided into yet another two groups; those with and those without shear reinforcement. In the present study shear reinforced flat slabs have not been treated.

Knowingly, no laboratory tests on slabs supported on edge columns of steel have been performed. The importance of distinguishing between columns of steel and concrete depends on the difference in stiffness; where normally steel columns have a much lower stiffness than reinforced concrete columns. It should therefore be kept in mind that the observations presented in this section apply to the case where transference of moments can be expected in the connection. Furthermore, most experiments have been conducted on isolated slab-column specimens, which may not always correspond to the response of the same region in a complete structure.

4.1.1 Slabs supported on interior columns

The structural response of reinforced concrete slabs supported on interior columns was experimentally investigated by Kinnunen and Nylander (1960). The test specimens consisted of circular slab portions supported on circular columns placed in

the centre and loaded along the circumference. Kinnunen and Nylander observed two main failure modes; namely, yielding of the flexural reinforcement at small reinforcement ratios (failure in bending) and failure of the slab along a conical crack within which a concrete plug was punched. In Figure 4.1 typical fracture surfaces of the specimens that experienced punching failure are illustrated.

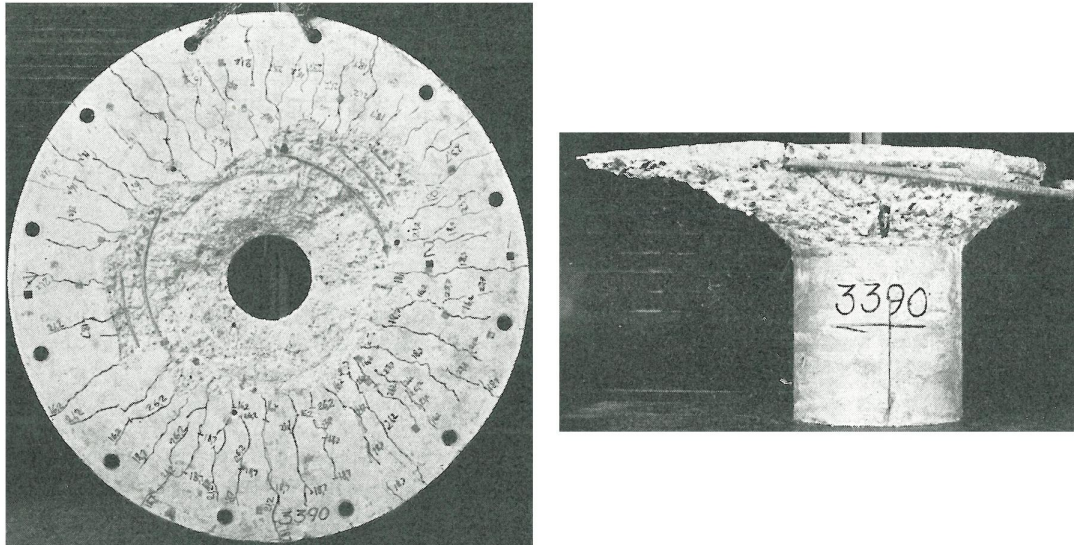


Figure 4.1 Left: typical view of the slab portion outside the shear crack (note that all cracks are radial); right: typical view of the slab portion within the shear crack. (Kinnunen and Nylander, 1960)

The initiation of cracking was similar in all the test specimens that suffered punching failure, starting with the formation of flexural cracks in the bottom surface of the slab caused by sagging moments. The crack propagation on the top surface of the concrete slab is illustrated in Figure 4.2.

- (a) Initially tangential cracks were encountered on the top surface of the slab above the column. These were flexural cracks due to the hogging moments.
- (b) Crack propagation continued with the formation of radial cracks starting from the tangential cracks.
- (c) Thereafter additional tangential cracks were formed outside the circumference of the column.
- (d) After further loading the latter tangential cracks deviated from their original vertical direction into an inclined course towards the column face on the bottom surface of the slab.
- (e) With the increase of vertical displacements the cracking extended to the edge of the column. The final shear crack either coincided with or was located outside the outermost tangential crack that was observed before failure.

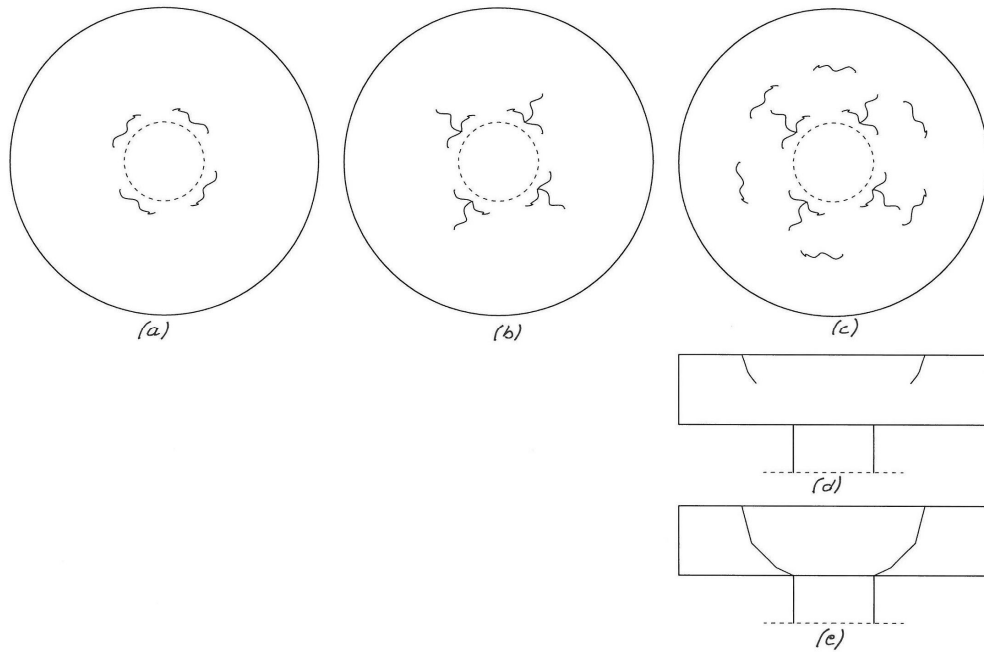


Figure 4.2 Crack propagation for Kinnunen's and Nylander's tests on centrally supported slabs.

Based on their experiments Kinnunen and Nylander developed a model describing the punching mechanism. Not only did the model agree well with the test results, it was also the first model that thoroughly described the flow of forces. Their observations during the tests led to the mechanical model, illustrated in Figure 4.3, where the slab is divided in several parts bounded by the propagated shear cracks and the radial cracks. From the column to the bottom of the shear crack, an imaginary compressed conical shell is developed that carries the outer portion of the slab. During the tests it was discovered that the outer portion could be regarded as a rigid body since it behaved accordingly. When a load is applied the slab portion is believed to rotate around a centre of rotation placed at the root of the shear crack.

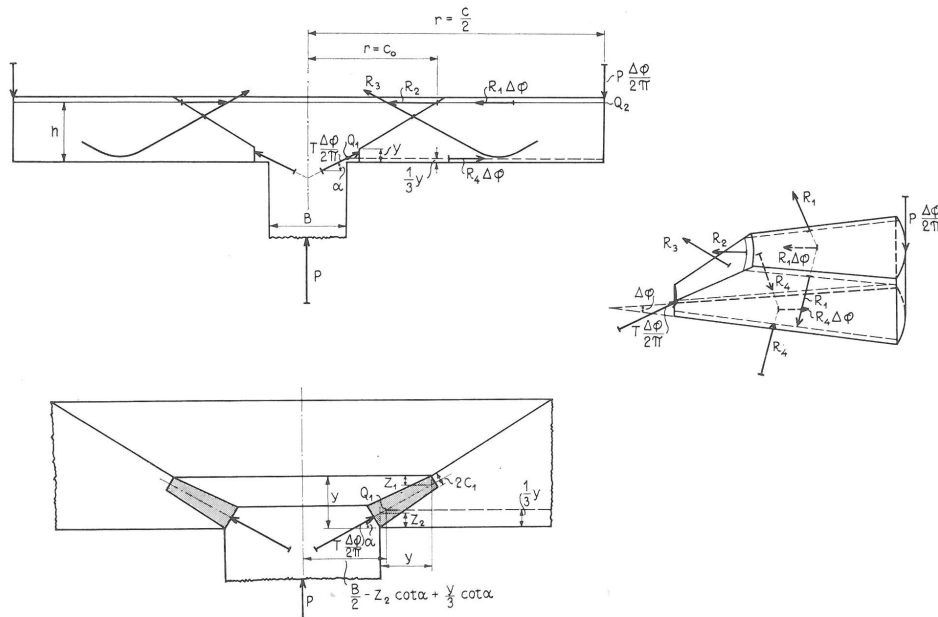


Figure 4.3 Mechanical model of Kinnunen and Nylander (1960).

The punching shear failure criterion is related to the tangential strain at the bottom of the slab. The conical shell is subjected to compression in all three directions, resulting in an increased concrete compressive strength. During loading the tangential compressive strain at the bottom of the slab increases until the internal concrete bond in the transverse direction is impaired. When the maximum value is reached the enhanced effect decreases and there is a loss of strength in the conical shell. These observations led to the formulation of the failure mode of the conical shell in compression, formulated by Kinnunen and Nylander (1960) as:

“...failure occurs when the tangential compressive concrete deformation on the bottom of the slab under the root of the shear crack reaches a characteristic value at which the favourable embedment of the conical shell is impaired.”

The model proposed by Kinnunen and Nylander has constituted the foundation for many researchers who have proposed modified models. Among these Hallgren (1996) developed a fracture mechanical failure criterion that depends on the ultimate tangential strain and is based on the concept that punching shear failure is initiated when the concrete is close to horizontal cracking in a zone at a certain distance from the column face. The formation of this crack causes loss of confinement at the slab-column intersection and the shear crack is enabled to penetrate through the compressed zone and cause a complete loss of load-bearing capacity.

4.1.2 Slabs supported on corner columns

During the 1970's, two sets of experiments on corner supported concrete slabs were carried out at the Royal Institute of Technology in Stockholm, both conducted by Ingvarsson (1974), (1977). The test specimens from the first set of experiments consisted of square concrete slabs supported on square columns. The observed crack

propagation was similar for all the specimens tested. Cracking was initiated by flexural cracks at the bottom face of the slabs in the span. With increased loading flexural cracks were also observed at the top faces above the columns. In addition to these, inclined cracks along the edges near the columns were formed, believed to be caused by torsional moments. For the specimens that failed in shear, shear cracks propagated just prior to the load increment that caused the rupture. For the three specimens that experienced shear failure (specimen Nos. 1, 4 and 5) a schematic plot of the crack path is shown in Figure 4.4.

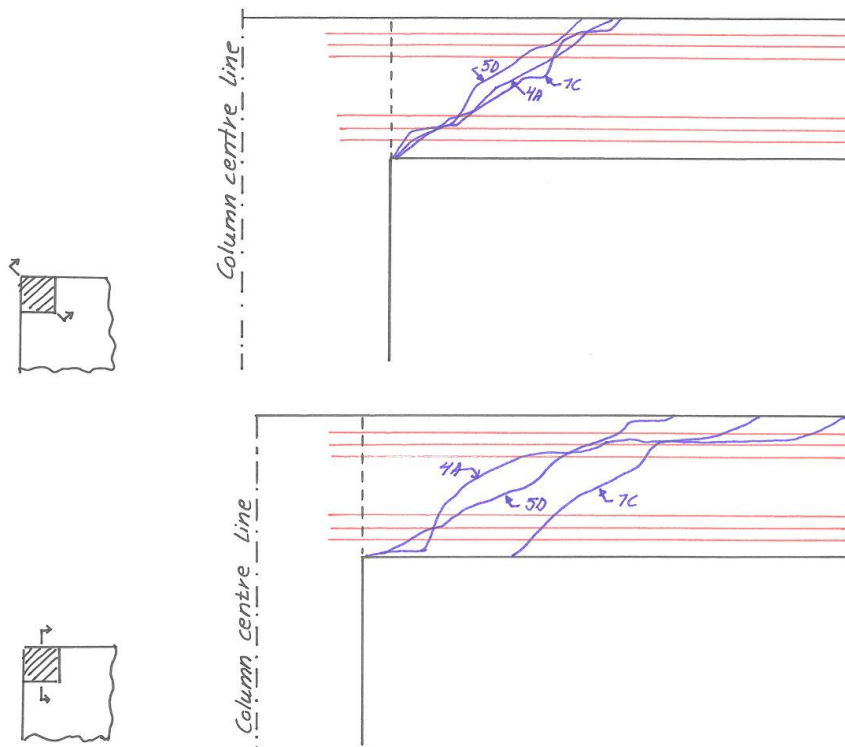


Figure 4.4 For specimen Nos. 1, 4 and 5, a schematic plot of the shear crack extensions at punching failure, where A, C and D denote the corner column at which punching failure was experienced. (Modified from Ingvarsson, 1974)

It was observed that the behaviour at failure for several of the specimens differed from the observations from the, by Kinnunen and Nylander (1960), performed experiments on interiorly supported slabs. While corner supported slabs experienced tensile strains in the tangential direction, the centrally supported slab had compressive strains in the same direction. In the radial direction reverse strains were observed. These differences are illustrated in Figure 4.5. According to Ingvarsson, the difference in behaviour indicated that corner supported slabs are prone to shear failure rather than punching shear, similar to the behaviour of beams.

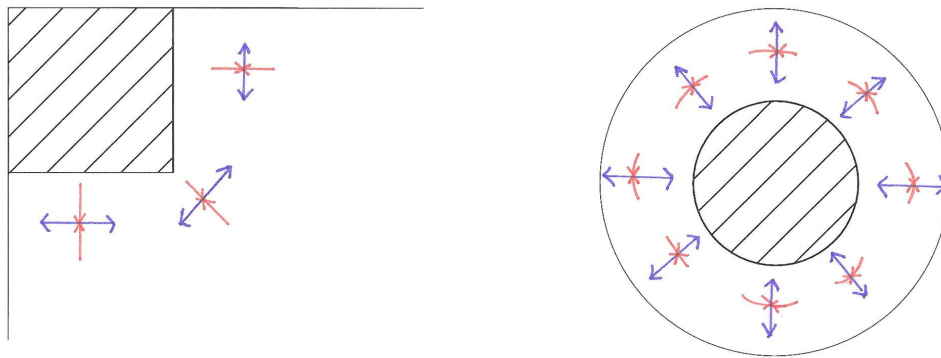


Figure 4.5 Reverse directions of strains were observed on the bottom surfaces near the columns between slabs supported on corners and interiorly.

The second set of experiments was performed in the same manner, now on square plates with rectangular columns of varying sizes and reinforcement arrangements (specimens denoted *R1 - R3*). These tests showed that, for slabs without shear reinforcement, the inclination of the shear crack decreased from the edge towards the internal corner of the column and then increased towards the other edge. This was also observed in the first set of experiments as was illustrated by Figure 4.4. Thus the perforation did not resemble the same cone shaped perforation as the punching cone for slabs centrally supported on columns. A schematic plot with contour lines of the failure surfaces from the two sets of experiments is illustrated in Figure 4.6.

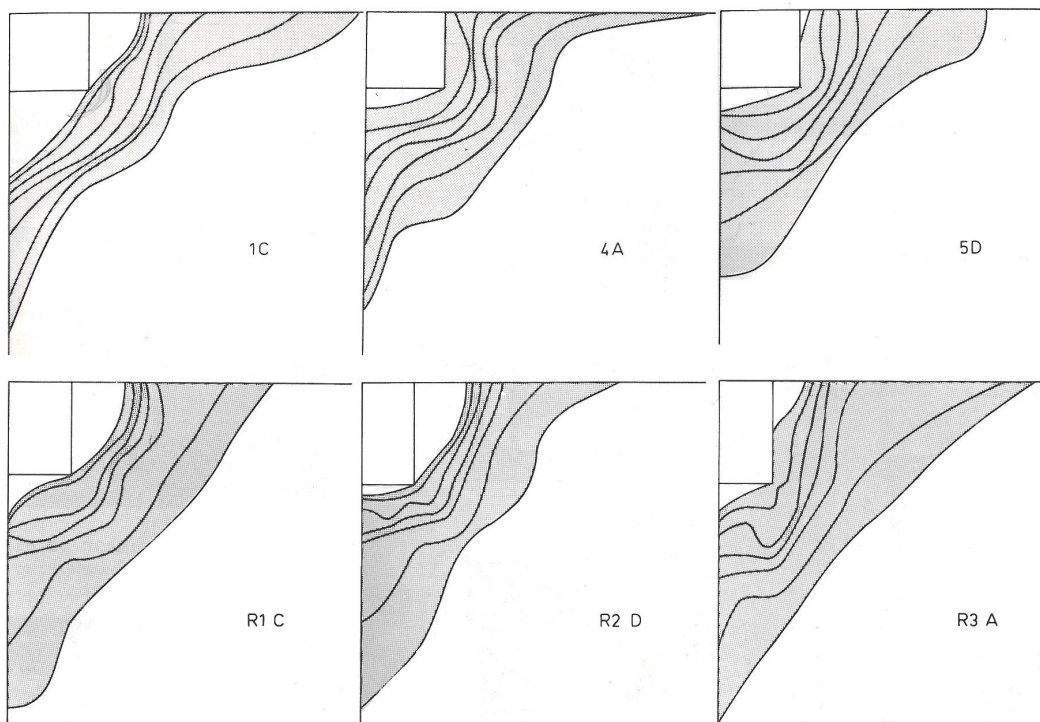


Figure 4.6 Failure surfaces from the experiments conducted by Ingvarsson (1977) represented by contour plots where each line decreases 20 mm ($H/6$) from the innermost line. (Specimens Nos. 1, 4 and 5 and *R1 - R3*; A - D denote the failed corner.)

4.1.3 Slabs supported on edge columns

An experimental study on punching shear of slabs supported on edge columns was conducted by Andersson (1966). Three cases were studied in order to compare different structural solutions; slab *I-a*, *I-b* and *I-c*. Specimen *I-a* simulated a slab between two floor levels supported on square columns; the columns were then relatively stiff compared to the slab. Specimen *I-b* was a slab supported by underlying square columns on pinned supports and specimen *I-c* resembled specimen *I-a* apart from the employment of a rectangular column. By the use of a rectangular column Andersson could study the influence of the eccentricity on the punching capacity.

Specimens *I-a* and *I-c* experienced shear failure. Both specimens had a similar crack pattern, illustrated in Figure 4.7. During loading tangential and radial cracks developed at the top part of the slab. Inclined cracks occurred along the column supported edge, believed to be caused by torsional moments. Rupture arose when a shear crack reached the bottom of the slab in vicinity of the column face parallel to the edge. At failure the inclined cracks along the edge were wide in specimen *I-a*, which indicated that the failure might have started as a torsional-shear failure. The approximate positions of the cracks that caused failure are illustrated in Figure 4.8.

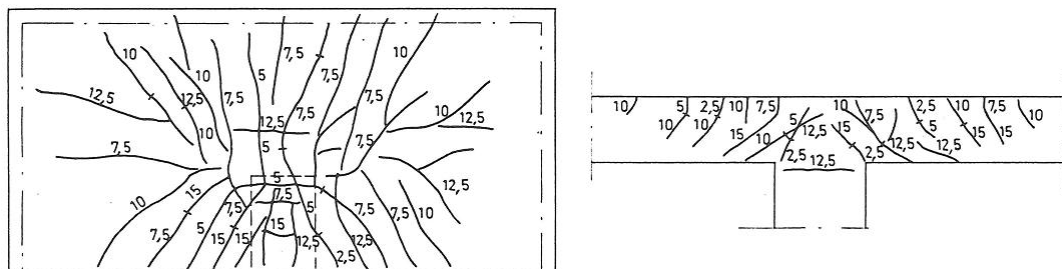


Figure 4.7 Crack patterns of specimen *I-c*. (Andersson, 1966)

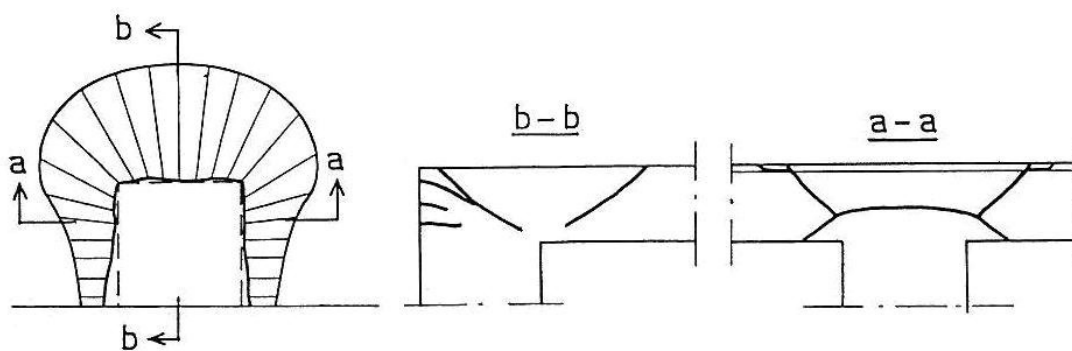


Figure 4.8 Approximate positions of the cracks that caused failure of test slab No. *I-a*. (Andersson, 1966)

Specimen *I-c* experienced punching shear failure. The inclined cracks appearing along the column supported edge were smaller than in specimen *I-a*. This was explained by the larger cross sectional area of the column resisting the torsional moments. In specimen *I-b* no shear crack was visible at failure, therefore deducted pure bending. Andersson proposed that this behaviour might be due to the development of a smaller

torsional moment and the employment of a higher concrete quality. From the tests Andersson concluded that the behaviour of the concrete in proximity to the interior face of the column is similar to a centrally loaded interior column. Therefore also at edge columns the failure could be explained by the tangential strain reaching a critical value. However, the problem is complicated by torsional moments occurring along the two sides of the column perpendicular to the slab's edge. Andersson also noted that the eccentricity of the column highly influenced the ultimate load.

Kinnunen (1971) continued his research on punching shear with an investigation on flat slabs supported at their edges. The characteristic crack pattern of the slabs is presented in Figure 4.9. The cracks occurring in the vicinity of the column were both radial and tangential, where the tangential cracks formed an angle of 45-90° with the slab's edge. The flexural cracks that were observed in the bottom surfaces of the slabs were in the mid-span parallel to the slab's edges, whilst curved in the area closer to the column.

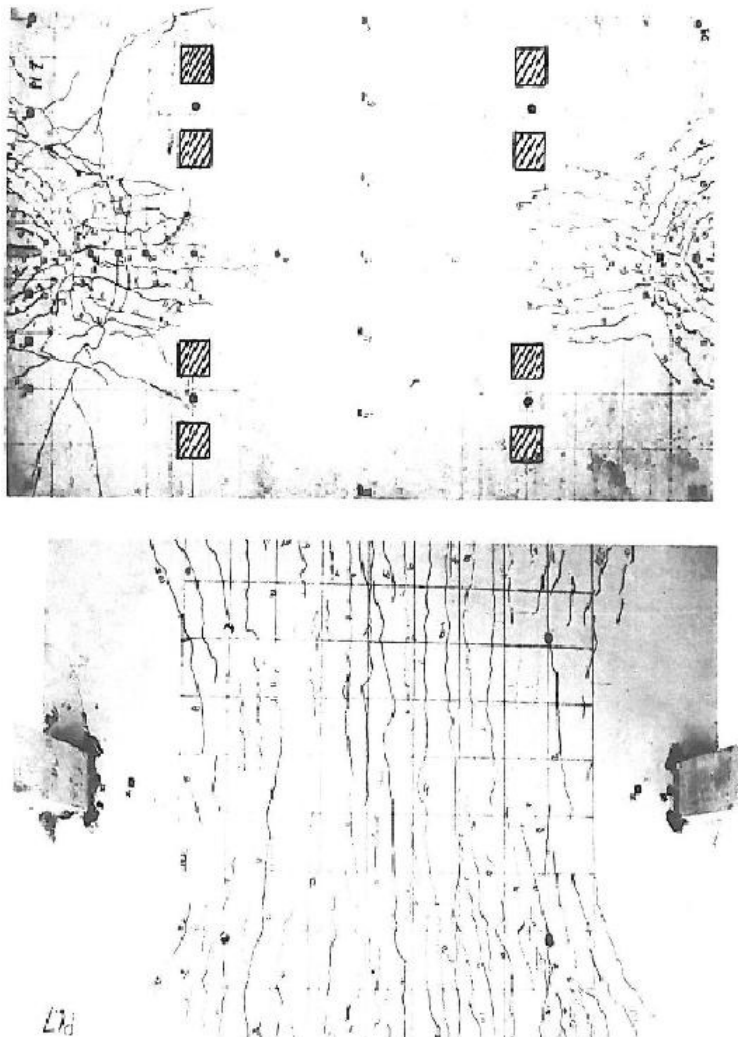


Figure 4.9 Characteristic crack patterns on the top and the bottom surface respectively of the edge supported slab. (Kinnunen, 1971)

In the investigation, the specimens Nos. 1-3 were not provided with shear reinforcement and specimen No. 3 had the largest amount of flexural reinforcement. In these slabs rupture started with a shear crack in the slab portion surrounding the compressed face of the column. The failure mode was classified as local punching for specimens Nos. 1 and 2, since no failure cracks occurred in the slab along the edge, as shown in Figure 4.10.



Figure 4.10 Crack development along the edge of the slab, specimen No. 2. (Kinnunen, 1971)

In specimen No. 3 large cracks were noticed along the edges, although these were secondary cracks occurring after the punching failure. The crack development along the edge of the specimen is illustrated in Figure 4.11.



Figure 4.11 Crack development along the edge of the slab for specimen No. 3. (Kinnunen, 1971)

Shear cracks were formed parallel and perpendicular to the edge in all three specimens. As shown in Figure 4.12, these cracks had roughly the same inclination.

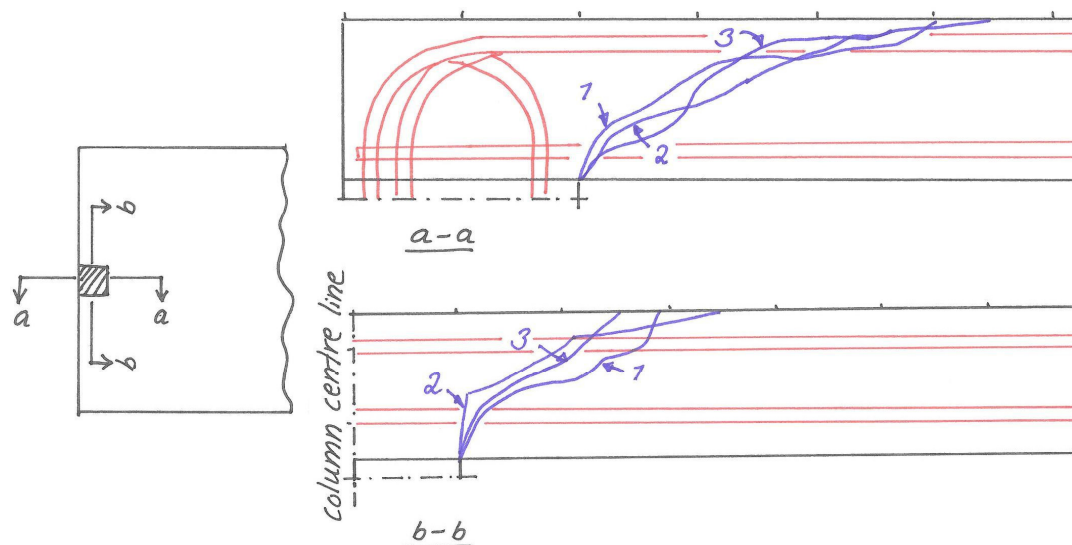


Figure 4.12 Propagation of shear cracks that caused failure, in specimen Nos. 1, 2 and 3. (Modified from Kinnunen, 1971)

The crack notations helped to establish an idea of the crack propagation at failure. The distance from the internal edge of the column to the shear crack at the slab's top face was determined as seen in Figure 4.13. Since this distance was determined to $1.8h$ for

interior columns, Kinnunen deduced that the expected response of the slab in proximity of the internal face of the column should be similar to the behaviour in the region close to a centrally loaded interior column.

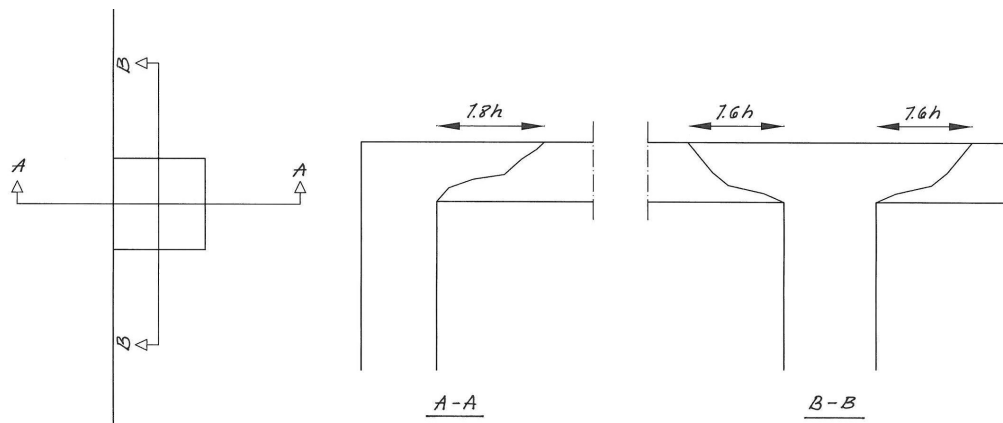


Figure 4.13 Crack propagation at failure for Kinnunen's tests on edge columns.

At the faculty of Civil Engineering in Belgrade an experimental investigation on post-tensioned lift slabs supported on edge columns was carried out by Marinković and Alendar (2008). Apart from the experimental study, the research included a finite element analysis of one of the test specimens in order to deeper analyse the punching mechanism and the state of stresses and strains. Three specimens were tested; *S1*, *S2* and *S3*. They were all of the same size, with the same amount and distribution of tendons and equally prestressed. What distinguished the specimens was the size of the steel collar and the amount of flexural reinforcement in the area subjected to hogging moments. Specimen *S1* and *S2* had a steel collar with angles on all sides whilst specimen *S3* was provided with the smallest steel collar with angles merely on two opposite sides of the column. Specimen *S1* was provided with reinforcement designed according to minimum requirements, while the other two contained a larger reinforcement ratio to assure punching shear failure to be decisive. Pure punching occurs when the flexural reinforcement ratio is sufficient enough to prevent yielding of reinforcement prior to failure. All three specimens behaved elastically up to the level of service load, when the first cracks appeared. Specimen *S2* and *S3* suffered brittle punching shear failures, preceded by concrete splitting at the bottom of the slab and followed by crushing of the concrete as demonstrated in Figure 4.14. The punching of specimen *S2* was followed by large deformations and yielding of the reinforcement, and was therefore classified as a secondary punching failure. Specimen *S3* failed without prior indications of larger cracks, deformations or yielding of reinforcement and was therefore considered a primary punching failure.

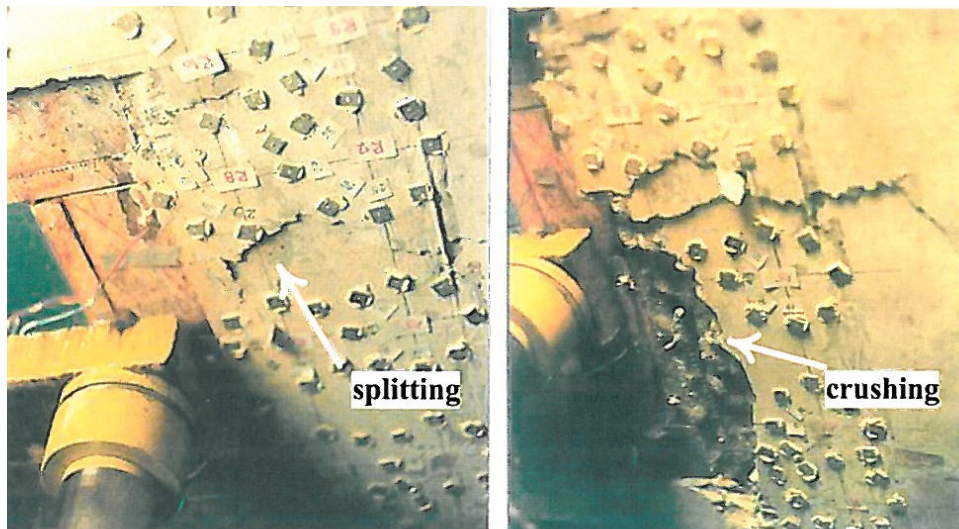


Figure 4.14 Splitting of concrete prior to failure, followed by crushing at failure. (Marinković and Alendar, 2008)

Marinković and Alendar noticed that the size of the steel collars influenced the punching shear capacity. Specimen *S2* had a larger punching strength than *S3*. The failure surface formed outside the collar's edges; the beneficial influence from the collar on the critical perimeter can be seen in Figure 4.15.



Figure 4.15 Failure surfaces of specimen *S2* and *S3*, where *S2* had a larger steel collar than *S3*. (Marinković and Alendar, 2008)

The nonlinear FE-analysis of specimen *S3* showed that the critical part was found at the bottom of the slab in proximity to the interior corners of the steel collar. This zone was under the effect of high triaxial compressive principal stresses, while a biaxial stress state could be found outside this area. However, the FE-analysis showed that failure did not start in the zone with the highest principal stresses, but in an adjacent area where a compressive strain converted into a tensile strain high enough to cause cracking. The stress conversion was caused by the dilation of the zone with the high compressive principal stresses. The dilation was restrained by the surrounding zones, resulting in increased strength of the highly stressed zone while the strength of the surrounding zone decreased due to the imposed tensile stresses. The induced tensile stresses lead to splitting of the concrete in this area, causing sudden concrete crushing in the highly compressed zone.

4.1.4 Summary of observations

Regardless of the position of the column the failure seems to be caused by the shear crack from the top surface reaching the compressed region and causing the capacity provided by the compressive zone to cease. In all experiments the failure mode has been related to measured strains. However, comparing the reported strains from the different experiments is complex and most likely not reliable due to the strains dependency on crack propagation, other events in adjacent regions and the inaccuracy of the monitoring equipment.

For the case of corner supported slabs the failure surface was diagonal across the corner rather than having a smooth shape with a radius around the support. Along the edges the punching cone was more vertical through the thickness of the slab and more inclined within the centre. The strain configuration in the slab near the corner columns differed from what had previously been observed for interior columns. Here it seemed as if the two simply supported edges enabled the slab to expand in the tangential direction.

For their internal regions (direction perpendicular to the simply supported edge), the tests on edge supported flat slabs showed resemblance to the punching failure observed for interior columns. The punching cone reminds of that of the corner column; more vertical through the depth at the slab's edges and more inclined at the inner face of the column. As the strip perpendicular to the edge is nearly simply supported it experiences compression in the bottom regions due to inclined compressive struts carrying the shear forces. It appears as if the cracks on the two opposite sides of the column reach the compressed zone which loses its capacity, giving the shear crack on the interior face of the column the possibility to propagate and cause rupture.

Similarities between the interior face of edge supported slabs and interiorly supported slabs have been observed. Due to the presence of hogging moment along the edges, these similarities would be expected for the two faces perpendicular to the edge rather than for the interior face. This could perhaps be explained by the free movement that is enabled for the concrete along the simply supported edge, as seemed to be the case for corner supported slabs.

The experiments and the FE-analysis performed by Marinković and Alendar (2008) also indicated that punching failure of edge columns resemble the failure mode of interior columns as failure occurs when tensile strains in the bottom part of the slab reach a critical value, enabling the adjacent shear crack to penetrate to the column face.

4.2 Design resistance with regard to punching shear

The design resistance to punching shear is, generally in building codes, an empirically derived formulation based on various tests. The resistance is determined along a control perimeter where the nominal shear force per unit width is compared to the shear resistance per unit width of the control section. In sections subjected to hogging moments the presence of tensile reinforcement increases the punching shear capacity.

This gain is believed to be an effect of the flexural reinforcement intersecting the crack and preventing the crack from dilation.

If the capacity provided by the reinforced section is insufficient, the performance needs to be enhanced by taking different measures. To directly increase the resisting section the slab thickness and supporting cross section can be increased. The slab thickness can be increased locally by using a drop panel (more or less limited to concrete columns). The parameters that govern the section increase are however seldom possible to influence and shear reinforcement needs to be provided. There are several types of shear reinforcement available, such as studs, stirrups, bent bars and bolts. When utilised, they provide a localised increase of the shear capacity in the area around the column.

The recommendations given in Eurocode 2 (2005) regarding punching shear resistance are largely based on section 6.4.3 in the CEB-FIP Model-Code on Concrete Structures (1993). Both provisions consider the following parameters:

- Concrete cylinder strength, $f_{c,cylinder}$
- Flexural reinforcement ratio in the tensile zone, ρ_l
- Size effect of the effective depth, k
- Shear capacity of the shear reinforcement, $f_{yw} \cdot A_{sw}$

The recommendations use a conventional formulation identical to the mono-directional case of a beam although a control perimeter is considered instead of a beam width (see Figure 4.16). The control perimeter is defined as the assumed crack periphery on the top surface of the slab and is in EC2 taken as $2.0d$ from the face of the support, where d denotes the effective slab depth. However, it is important to bear in mind that the control perimeter does not predict the actual punching cone as it is dependent on detailing.

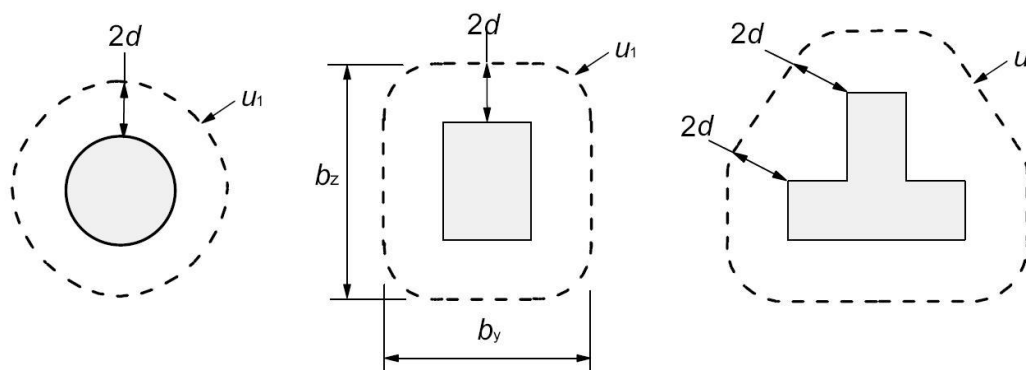


Figure 4.16 Control perimeter for interior columns. (Eurocode 2, 2005)

Prior to the current formulation of the control perimeter, u_l was taken at a distance $1.5d$ from the column. It was concluded that this definition resulted in non-conservative results for higher concrete strengths, why the formulation in the CEB-FIP Model Code was adopted. According to Walraven (2002), the formulation given by the Model Code is advantageous for two reasons. First, it makes the limiting shear

stress more uniform for varying column sizes. Secondly, the same formulation as for normal shear of members without shear reinforcement can be used for punching.

4.2.1 Punching shear resistance at interior columns

For interior columns where the loading is symmetric and where no shear reinforcement is present, the design punching shear capacity $V_{Rd.c}$ is evaluated according to (4.1), using the control perimeter u_1 involved as shown in Figure 4.16 and the effective depth of the slab from the compressed edge d (taken as a mean for the effective depths in the two main directions):

$$V_{Rd.c} = v_{Rd.c} \cdot u_1 \cdot d \quad (4.1)$$

The design punching shear strength $v_{Rd.c}$ is determined as:

$$v_{Rd.c} = \frac{0.18}{\gamma_c} k \cdot (100 \cdot \rho_1 \cdot f_{ck})^{1/3} \quad (4.2)$$

where: γ_c is the partial safety factor for concrete (recommended value $\gamma_c = 1.5$)

$$k = 1 + \sqrt{\frac{200\text{mm}}{d}} \leq 2.0$$

$$\rho_1 = \sqrt{\rho_{1x} \cdot \rho_{1y}} \leq 0.02$$

ρ_{1x} and ρ_{1y} are reinforcement ratios in the main directions [-]

f_{ck} is the concrete characteristic compressive strength [MPa]

Shear reinforcement may be required if the capacity is insufficient. The design punching shear capacity $V_{Rd.cs}$ is then determined as follows:

$$V_{Rd.cs} = v_{Rd.cs} \cdot u_1 \cdot d \quad (4.3)$$

Where the design punching shear strength for shear reinforced slabs $v_{Rd.cs}$ is evaluated using (4.2) as:

$$v_{Rd.cs} = 0.75v_{Rd.c} + 1.5 \frac{d}{s_r} \cdot A_{sw} \cdot f_{ywd,eff} \cdot \frac{1}{u_1 \cdot d} \cdot \sin(\alpha_s) \quad (4.4)$$

where: s_r is radial distance between circular rows of shear reinforcement

A_{sw} is area of shear reinforcement within the control perimeter

α_s is inclination between shear reinforcement and the plane of the slab

The design value of the effective yield strength $f_{ywd,ef}$ [MPa] is related to the effective depth d [mm] as:

$$f_{ywd,ef} = \min(250 + 0.25d, f_{ywd}) \quad (4.5)$$

The recommended maximum value of the punching capacity is limited to $v_{Rd,max}=0.5v \cdot f_{cd}$, where v is a reduction factor for concrete with shear cracks. $v_{Rd,max}$ acts on the control perimeter u_0 which is the perimeter of the column. The value for v is determined as:

$$v = 0.60 \left(1 - \frac{f_{ck}}{250 \text{MPa}} \right) \quad (4.6)$$

According to the Swedish national annex, $v_{Rd,max}$ is also limited by:

$$v_{Rd,max} \leq 1.60 v_{Rd,c} \cdot \frac{u_1}{u_0} \quad (4.7)$$

Furthermore, the punching shear strength $v_{Rd,c}$ has to be checked at a control perimeter u_{out} at the distance $1.5d$ from the outermost shear reinforcement.

4.2.2 Punching shear resistance at edge and corner columns

For edge and corner column supported slabs the eccentricity caused by unbalanced moments must be accounted for in the design of punching shear capacity. There are two ways to consider the eccentricity, either by introducing an eccentricity factor or by using a simplified approach. If accounting for the eccentricity by the eccentricity factor, the control perimeter is determined as illustrated in Figure 4.17. In the latter approach uniform shear on a reduced perimeter u_1^* is assumed, as seen in Figure 4.18; thereby the evaluation is similar to the one of interior columns. However, if only eccentricity in one direction is present the two approaches will result in the same punching shear resistance.

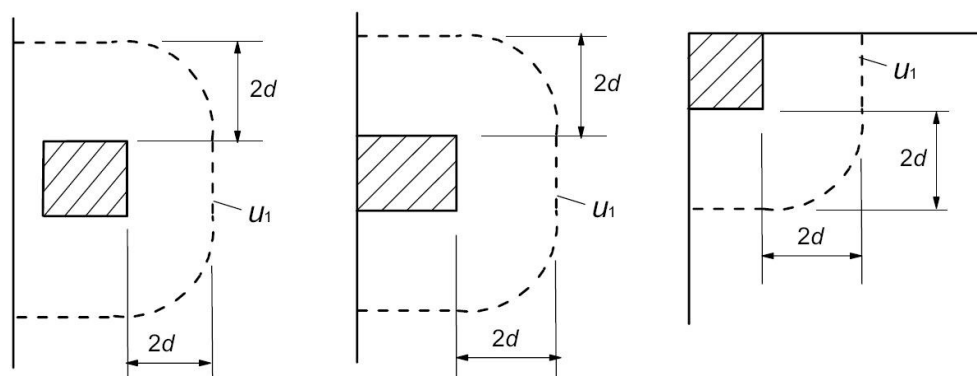


Figure 4.17 Control perimeter for edge and corner supported slabs. (Eurocode, 2005)

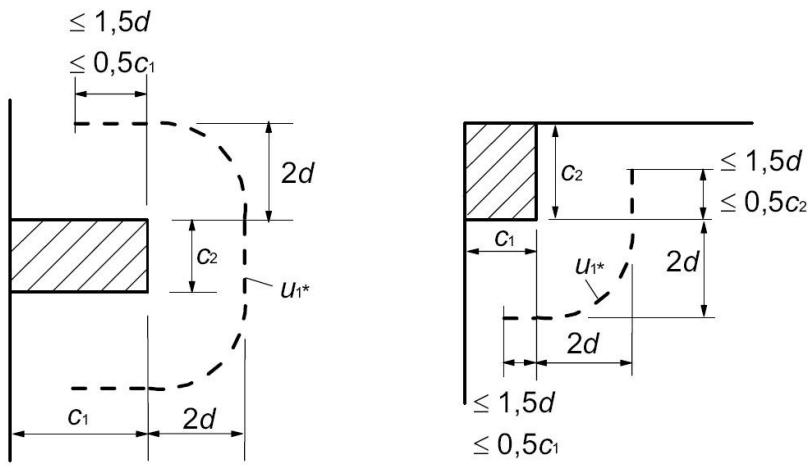


Figure 4.18 Reduced control perimeter for edge and corner supported slabs. (Eurocode, 2005)

5 Object of investigation

As previously mentioned, the small moment transfer between the slab and edge columns of steel is what have caused reason for additional investigation of the punching phenomenon of edge supported flat slabs. Slender steel columns connected to stiff concrete slabs are not likely to behave as frame structures, as is the case for approximately equally stiff concrete columns and concrete beams.

The relation between the stiffness ratio and the transferred moment was formulated by Andersson (1965) during his studies of flat slabs supported on edge columns. Andersson developed an approximate method for determining the moment transfer at edge columns in flat slabs which is based on the elasticity theory of Timoschenko². Through the derivative of the moment equation with respect to the support rotation, the transferred moment can be determined as a function of the span ratio a/b and the rigidity ratio between the column and the slab. From the graph in Figure 5.1 it is deductable that the moment transferred through the connection decreases as the slab stiffness increases compared to that of the column.

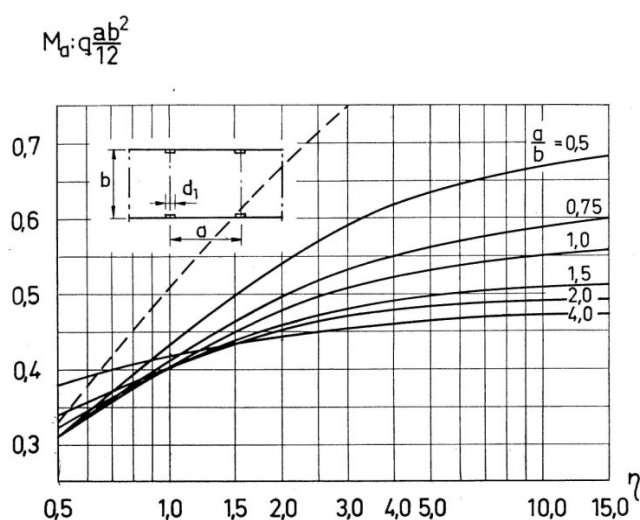


Figure 5.1 Transferred moment, M_a , as a function of the variable η and the span ratio a/b . (Andersson, 1965)

The variable η , related to the stiffnesses and span lengths, is expressed as:

$$\eta = \frac{3}{2} \cdot \frac{EI_{pe} \cdot \psi}{L \cdot EI} \cdot \frac{b}{a} \quad (5.1)$$

where: EI_{pe} is the column stiffness

EI is the concrete slab stiffness

L is the column length

² Timoschenko developed solutions for the behaviour of plates and shells according to elastic theory.

ψ is a coefficient for connection type (1.0 for hinged, 1.33 for fixed)

a and b are the span lengths

For a concrete slab on steel columns with equally distant spans a very small value of η is obtained, which postulates that no significant moment transfer through the connection will occur.

5.1 Previous investigation on steel column supported slabs

The behaviour of reinforced concrete slabs supported on their edges by steel columns was investigated by Jensen (2009), using linear finite element analyses. Jensen concluded that the connection between the edge column and the slab ought to be regarded as a pinned support. The small hogging moment over the column in the direction perpendicular to the edge and the large difference in stiffness between the steel column and the slab would make the edge resemble a simple support without any significant ability to transfer moment. The additional shear capacity, provided when the connection is subjected to compression in both directions, is according to Jensen not gained in this case since there is only a significant hogging moment parallel to the simply supported edge. Designing with respect to punching failure is based on the increased shear capacity and the current method for design was not believed to be appropriate in this case. The slab portion parallel to the edge should, according to Jensen, be regarded as a continuous beam over the steel column (acting as a pinned support) and the slab in the direction perpendicular to the edge should be regarded as a simply supported beam. Jensen suggested that these fictitious beams should be designed with respect to shear with the conventional approach for beam design.

According to the formulation in EC2 the punching shear capacity can be enhanced by additional flexural reinforcement in the tensile zone, increase of the slab thickness, increasing the cross-sectional area of the support or by employing shear reinforcement. The flexural reinforcement that is to be considered is a question of interpretation. According to EC2 it is the tensed reinforcement that enhances the punching capacity. For interior columns the tensed reinforcement is positioned in the top part of the slab in both directions, but for edge columns it becomes a question of interpreting the connection with reference to moment transfer. If the strip perpendicular to the simply supported edge is considered to not transfer moments, as is the case for steel columns, the slab is subjected to sagging moments and the bottom reinforcement is tensed. It should therefore be the contribution from the bottom reinforcement that is considered in shear design, since the increase of capacity is caused by the reinforcement traversing the crack and limiting its propagation.

5.2 Case study

The aim when defining a case study has been to achieve a sample that can be related to realistic objects. Adjacent to the region of an edge column balconies are often present, however their presence might aggravate the interpretation of results from the

analyses and have therefore been excluded in the present study. In order to establish a general case, the case study considered derives from an infinite flat slab supported at equal distances along its continuing edges (l_y) and also interiorly (l_x) by rectangular steel columns, as illustrated in Figure 5.2. Span lengths were chosen such that the reaction forces in the steel columns corresponded to what could be expected in similar structures and are here considered being 5 m in both directions. An arbitrary corner supported element along the edge has been considered and is bound by one edge and three load dividing lines.

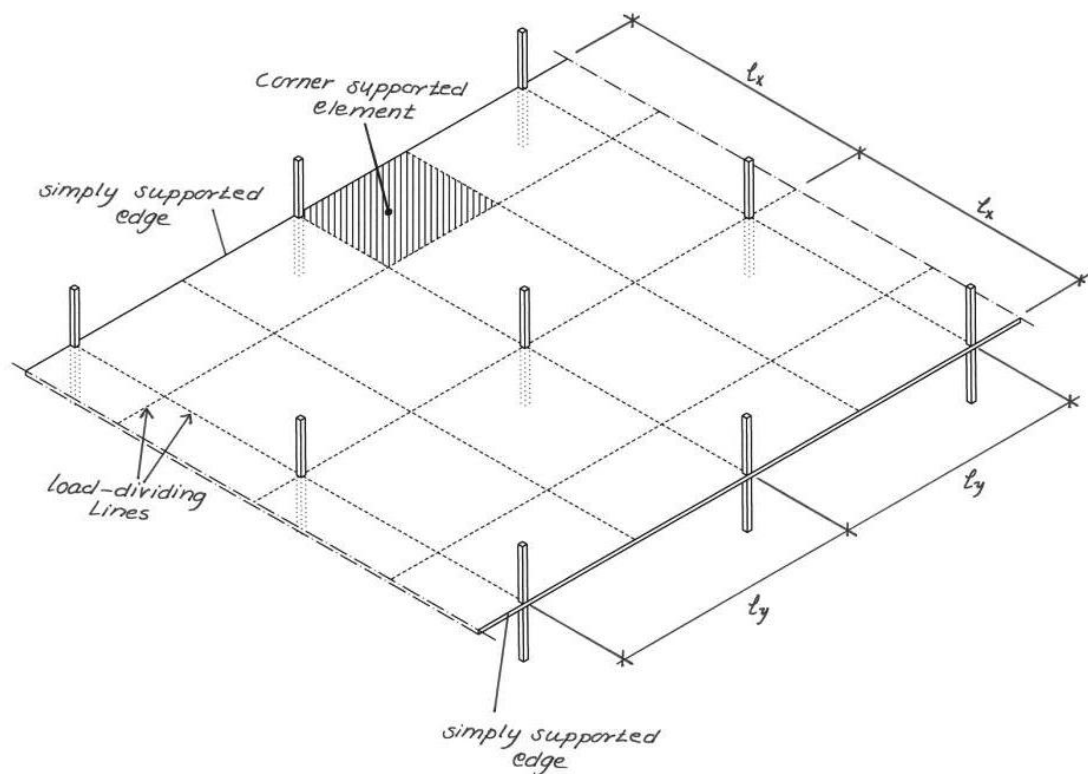


Figure 5.2 Infinite flat slab from which a corner supported element has been considered and further investigated.

The case study considers a concrete slab with the total slab thickness of 250 mm, which corresponds to realistic dimensions in residential buildings using composite floor plate floors and with the concrete strength class C30/37. The type of the reinforcing steel was chosen to B500B. These characteristic features constitute the case study and are constant throughout the parametric study.

The reinforcement in the concrete slab was originally designed according to the Strip Method, described in Chapter 3. Since the behaviour of the slab is influenced by the design, the amount and arrangement of flexural reinforcement has been varied in order to study its influence on the failure mode.

6 Nonlinear FE-analysis and numerical methods

The finite element method is used to numerically solve field problems³. In structural engineering this method is employed by dividing the structure into finite elements, each allowed to only one spatial variation. Since element variations are believed to be more complex than limited by a simple spatial variation, the solution becomes approximate. Each element is connected to its neighbouring element by nodes. At these nodes equilibrium conditions are solved by means of algebraic equations. The assembly of elements in a finite element analysis is referred to as the mesh. Due to the approximation of the spatial variation within each element the solved quantities over the entire structure are not exact. However, the overall solution can be improved by assigning a finer mesh to the structure.

6.1 Nonlinearity

In a nonlinear analysis it is possible to follow nonlinear structural responses throughout the loading history as the load is applied in several distinguished steps. These load steps, or increments, are considered as a form of nonlinearity, superordinate to the types of nonlinearity that will be described further on. A mathematical description of the overall structural response is presented by the following equation system:

$$\underline{A}x = \underline{b} \quad (6.1)$$

where: \underline{A} is the structural matrix

x is the vector of displacements

\underline{b} is the unknown vector containing internal forces

Within each load step a number of iterations are carried out until equilibrium is found for the equation system.

Nonlinearity can also be employed for constitutive, geometrical and contact relations all of which have been used in the simulations in this work. Nonlinear constitutive relations consider the range of material responses from elastic to plastic behaviour; it is possible to account for nonlinear material behaviours, such as cracking of concrete and yielding of reinforcement. These in turn cause redistribution of forces within the structure. Geometrical nonlinearity accounts for the ongoing deformations of the structure including the change of force direction. The analysis accounts for the changing structural matrix due to deformations and uses an updated matrix for the consequent load increment. When fluctuating contact between two adjacent parts of a structure is experienced, contact nonlinearity accounts for the changes of contact forces and presence of frictional forces.

³ Field problems are problems that are mathematically described by integral expressions or differential equations.

6.2 Numerical solution methods

In order to solve nonlinear equation systems iterative solution methods are used. Their scope is to find approximate numerical solutions to the equation systems that correlate the external forces to the structural response. In ATENA iterations are carried out using either one of the two default solution methods, namely *Newton-Raphson* or *Arc Length*. Both methods can be enhanced by means of the *Line Search* iteration. Within an analysis it may be appropriate or even necessary to switch between solution methods due to regional responses in the load-displacement function.

6.2.1 The Newton-Raphson iteration

The Newton-Raphson (N-R) iteration is an iterative solution method using the concept of incremental step-by-step analysis to obtain the displacement u_i for a given load P_i . N-R method keeps the load increment unchanged and iterates displacements and is therefore suitable to use in cases when load values must be met. The N-R iteration can also be used for incremental increase of the deformation u . The search for the unknown deformation is described by the tangent of the load-displacement function. This is known as the tangent stiffness $k_{t,i}$ and describes the equilibrium path for each increment. The N-R iteration scheme is illustrated in Figure 6.1 which describes the search for the unknown deformation when a load is applied.

For the case where the initial deformation is u_0 the method according to which equilibrium is found can be described as follows. For the load increment ΔP_1 the corresponding displacement u_1 is sought. By means of the initial tangential stiffness $k_{t,0}$ the displacement increment Δu can be determined as:

$$\Delta u = k_{t,0}^{-1} \cdot \Delta P_1 \quad (6.2)$$

Adding this increment to the previous displacement u_0 gives the current estimate u_A of the sought displacement u_1 according to:

$$u_A = u_0 + \Delta u \quad (6.3)$$

The current error, or load imbalance, e_{PA} is defined as the difference between the desired force P_1 and the spring force $k \cdot u_A$ deduced by the estimated displacement u_A . The stiffness k is evaluated from the tangent of the function at the point where u_A is found.

$$e_{PA} = P_1 - k \cdot u_A \quad (6.4)$$

However, since the deformation has not been deduced by the current force P_1 this solution is not exact. If the error is larger than the limiting tolerance another attempt is made to find equilibrium. The new displacement increment Δu starting from the point a is calculated by means of the previous imbalance e_{PA} . Hence a displacement u_B closer to the desired u_1 is determined:

$$\Delta u = k_{tA}^{-1} \cdot e_{PA} \quad (6.5)$$

$$u_B = u_A + \Delta u \quad (6.6)$$

Analogously, if the displacement u_B does not meet the tolerances for the load imbalance according to (6.4) yet another iteration within this load increment is carried out, now starting from point b . The iterations continue until the load imbalance approaches zero, the analysis then enters the next load increment ΔP_2 where these iterations are carried out until the load equilibrates to P_2 and the analysis has converged to a numerically acceptable solution u_2 for the load step.

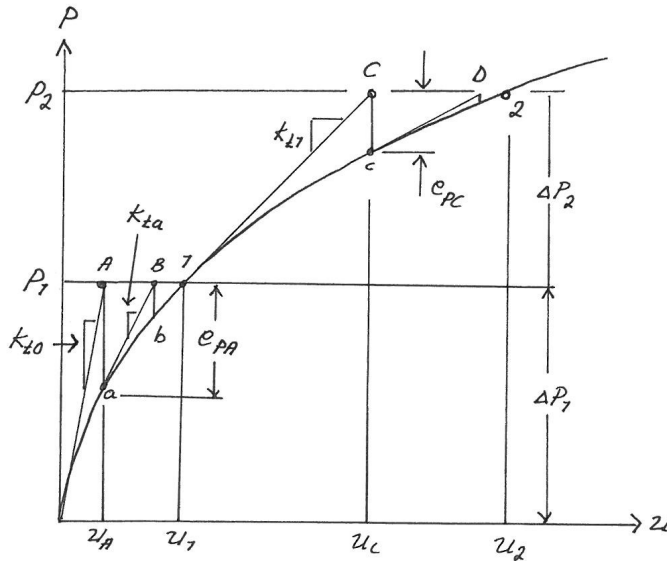


Figure 6.1 Newton-Raphson iteration scheme.

Continued iterations normally cause force errors to decrease, succeeding displacement errors to approach zero and the updated solution to approach the correct value of the displacement. Moreover, smaller load increments can enhance the probability of finding equilibrium within each step.

The nonlinearity of the equations lies in the internal forces and the stiffness matrix having nonlinear properties. The stiffness matrix is deformation dependent and is therefore updated for each repetition. However, the recalculation of the stiffness matrix is very time consuming why this dependency can be neglected within a load increment in order to preserve linearity of the stiffness tangent. When neglected, the stiffness matrix is calculated based on the value of the deformations prior to the load increment. This simplification is referred to as the modified Newton-Raphson iteration where the stiffness matrix is only updated for the first iteration in each step (see Figure 6.2). Apart from increasing computing pace, the drawback of this simplification is reduced accuracy.

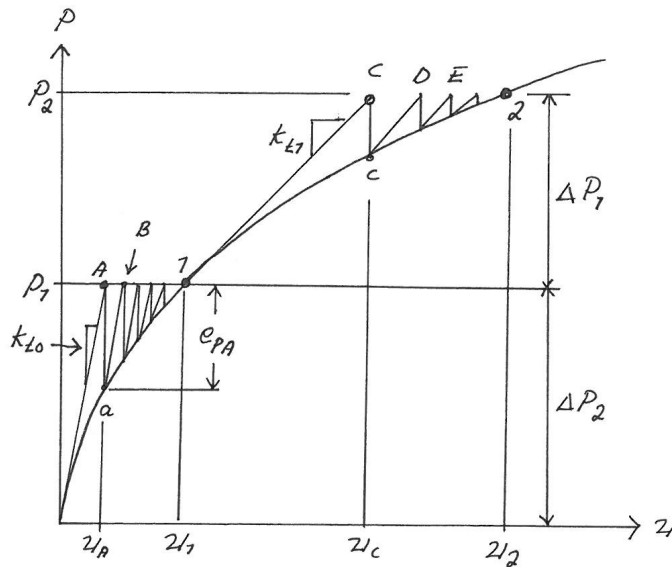


Figure 6.2 Modified Newton-Raphson iteration scheme.

In the beginning of an analysis quite large load increments can be used. However, when the structure experiences significant loss of stiffness, normally during excessive crack propagation or when approaching failure load, increments need to decrease in order to achieve equilibrium. The use of smaller load increments can sometimes be insufficient since the stiffness reduction implies increasing deflections while loading decreases. Graphically this is visualised as the change of tangent direction. When the stiffness tangent becomes negative iterations by means of the N-R method fail to find the sought solution. The Arc Length iteration is such a method.

6.2.2 The Arc Length iteration

In the Arc Length (A L) iteration a load multiplier is introduced that increases or decreases the intensity of the applied load in order to obtain convergence within a step faster. With this method the solution path is kept constant and increments of both forces and displacements are iterated as shown in Figure 6.3. At the end of each step both loading and displacement conditions become fixed. The fixation is performed by establishing the length of the loading vector.

In the N-R formulation the degrees of freedom were associated with the displacements, but for this method an ulterior degree of freedom for the loading must be introduced; the load multiplier λ .

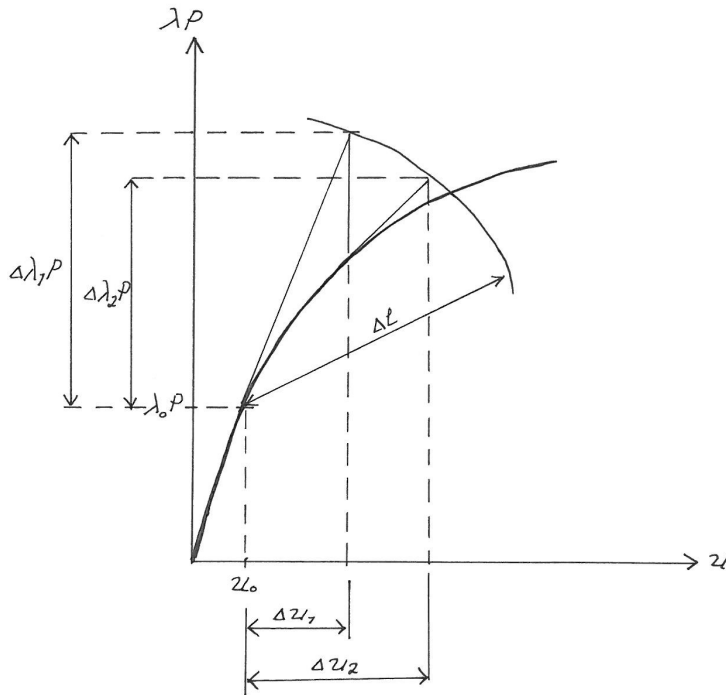


Figure 6.3 Arc Length iteration scheme.

Depending on the structural response the value of λ varies throughout the analysis leading to an increase or decrease of the increment within the step. The value is based on the previous iteration. If convergence difficulties are encountered λ is reduced, whilst for easily converged responses the value is increased resulting in larger load increments.

The Arc Length method presents some advantages compared to the Newton-Raphson as it is very robust and computational efficient. For this reason it can provide good results even when the N-R method cannot be used. For instance it is well applicable when large cracks occur and is also able to capture behaviours when the stiffness is decreased, such as snap-through and snap-back phenomena (see Figure 6.4).

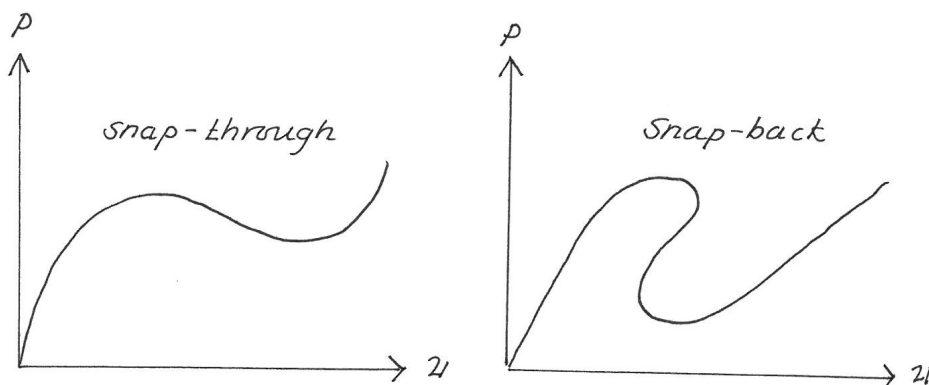


Figure 6.4 Snap-through and Snap-back phenomena.

6.2.3 The Line Search method

The Line Search method is a feature for optimisation of iteration techniques. The scope of the Line Search method is to speed up the analysis in case of well-behaving load-deformation relationships or to damp possible oscillations in the case of convergence problems. The method introduces a new parameter η which becomes the iterative step length. The parameter η is set to a value and solved by iteration until the work done by the out-of-balance forces on the displacement increment is minimised. The definition of minimum is chosen in the program and the limits for η are either chosen to standard values in ATENA or prescribed by the user.

7 Modelling of reinforced concrete in ATENA

The modelling and simulations presented in this report have been performed using the ATENA 3D version 4.3.4 software for nonlinear finite element analysis of civil engineering structures (further on referred to as ATENA). In this chapter, implemented theories and modelling considerations are presented.

7.1 Material models

In ATENA, features can be prescribed according to the three methods for material input, namely; direct definition, load from file or select from catalogue. The *direct definition* contains a list of materials with predefined material parameters. These parameters can be set to default values generated by ATENA or manually defined by the user. The generated parameters are based on codes and other empirically derived expressions. When selecting concrete material from the ATENA *catalogue* it can be specified whether mean, design or characteristic values are to be used.

Realistic nonlinear finite element analyses of reinforced concrete structures require proper and adequate definitions of material models. When simulating a structural response by means of nonlinear finite element analyses, there are a few aspects regarding the input parameters that need to be addressed. First and foremost it is important to distinguish between the different aims of analyses before determining the material parameters. If attempting to simulate an actual response, i.e. behaviour of a conducted experiment, material values as close as possible to the properties of the actual specimen are desirable. If the aim is to simulate the real response of a non-conducted experiment it is appropriate to assign *mean values* to the material models. If the purpose of the simulation is to obtain an appropriate design, a safety format must be adopted. In case of an analysis for design, the material parameters should be chosen as the lower characteristic values with applied partial safety factors. Then, according to the ATENA Manual (2009), the obtained ultimate load from the analysis corresponds to the design resistance. If other safety margins than those proposed by EC2, *characteristic values* can be combined with the safety factors that are of interest. However, Broo, Lundgren and Plos (2008) have recently confirmed that the use of design values in an analysis does not only scale the response but can in some cases simulate non-realistic responses. Then it is more appropriate to use mean values for the analysis and scale the results for design purposes by means of a global safety factor. How this safety factor should be determined is currently under investigation at the Division of Structural Engineering, Chalmers University of Technology.

In ATENA, material properties are automatically generated by the input of concrete compressive strength or the yield strength of steel. However, all values of the generated material properties, especially regarding concrete, are not always in correspondence to the expressions given in EC2 or MC90 and have therefore been manually assigned to the materials within this study. The derivations of these values together with the other material inputs are presented in **Appendix II**. For those parts of a structure where the response is not of interest linearly elastic constitutive relations are assigned the material models, taking the Young's modulus of elasticity E into

account. In the present study, stress analysis of neither concrete nor steel columns has been of interest, why they were modelled as linear-elastic.

7.1.1 Concrete model

Concrete with nonlinear material behaviour experiences two stages of structural response. As concrete is assumed to be homogenous and isotropic prior to crack initiation, the material is generally modelled with a linear-elastic relation. After cracking several constitutive relations that are capable of describing the nonlinear behaviour in three dimensions need to be employed in the material model.

For nonlinear analyses of concrete in ATENA the fracture-plastic model *CC3DNonLinCementitious2* is recommended and is capable of describing concrete cracking, crushing and plastic behaviour. This model combines the constitutive relations for tensile and compressive responses as shown in Figure 7.1.

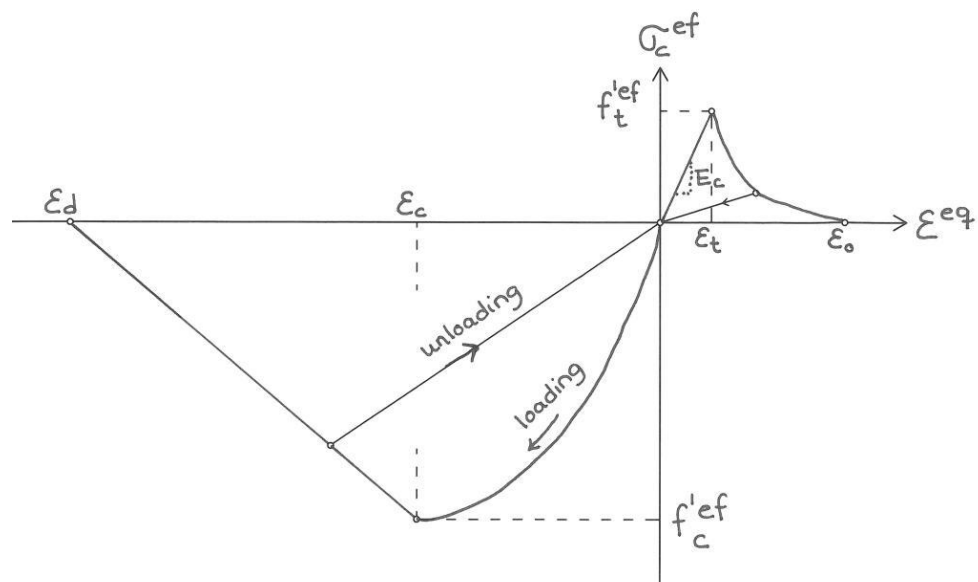


Figure 7.1 Constitutive stress-strain relation of *CC3DNonLinCementitious2*.

The *CC3DNonLinCementitious2* material model employs the Rankine failure criterion for the tensile fracture model. Two fundamentally different approaches to model failure and cracking in concrete have been introduced throughout the last decades, namely the *discrete* and the *smearred approach*. The smeared crack approach is more advantageous than the discrete one, giving satisfying accuracies of global results at low computational costs. In the material model the smeared crack approach is implemented and the features of the cracks are smeared over an entire element. It is important to bear in mind that the smeared crack model disables the cracks to fully open and thus the transfer of tensile stresses through the crack is somewhat higher than in reality. The Rankine failure criterion enables both *fixed* and *rotated crack models* which are both available in ATENA. In both models a crack is formed as the principal stresses reach the concrete tensile strength. In the fixed crack model the crack direction is given by the direction of the principal stress at the moment of crack initiation and is thereafter fixed. Whilst in the rotated crack model the direction of the

crack coincides with the direction of the principal stress. If the latter changes, the direction of the crack rotates. In a real reinforced concrete structure the cracks might change their courses; however they are cannot rotate as the rotated crack model proposes. The fixed crack model was assumed to give more realistic description of the cracking progress in this study.

Cracking in a three-dimensional material normally implies a non-uniform state of stresses, with both tensile and compressive principal stresses in any given node. The presence of tensile stresses perpendicular to the compressive stresses in the cracked concrete softens and weakens the compressive strength. Since the tabulated values of compressive strength of concrete is based on uniaxial cylinder tests, the strength needs to be reduced by means of a constitutive relationship accounting for the presence of both tensile and compressive stresses. In the *CC3DNonLinCementitious2* material model this is done according to the Men etrey-William failure surface. The biaxial failure law is presented in Figure 7.2.

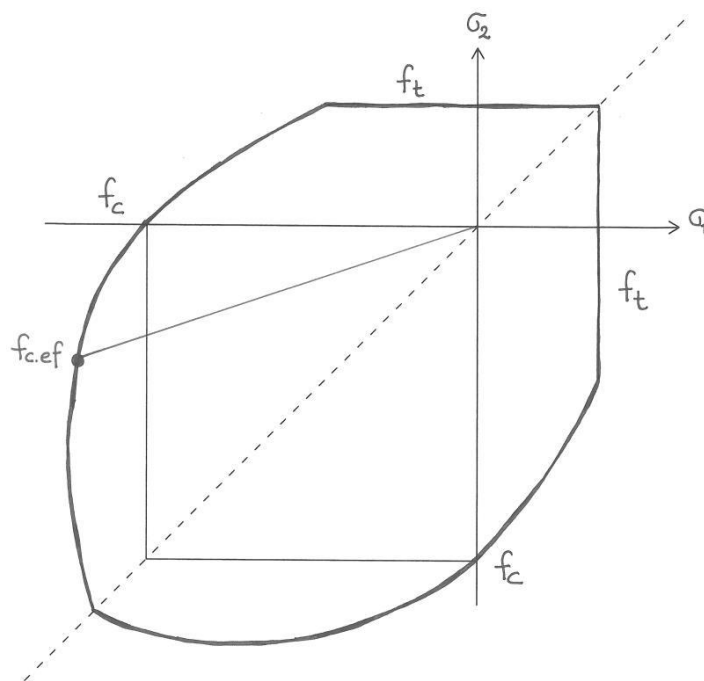


Figure 7.2 Biaxial failure law when both tensile and compressive stresses are present.

The concrete material model has been developed such that the two separate models for tensile and compression can be used simultaneously which enables the simulation of crack closure, which might lead to the presence of negative crack widths. Furthermore, the interaction between the two models also considers the decrease of tensile strength after crushing.

The parameters involved in the *CC3DNonLinCementitious2* material model and their default formulations in ATENA are presented in the following. The effect of some of these parameters have been investigated by  oman and Blomkvist (2006) where simulations in ATENA have been compared to results from experiments conducted by Broms. Their conclusions regarding parametrical influence have been benefited from in the present work.

The *basic features* of *CC3DNonLinCementitious2* (Table 7-1) consider the concrete elasticity and shear; tensile and compressive strengths. The values of E_0 , f_t and f_c have been calculated according to EC2 since the values deviate slightly from the defaults generated by ATENA.

Table 7-1 *Material parameters concerning basic features in the CC3DNonLinCementitious2 material model.*

E_0 [GPa]	Young's modulus (initial value): $E_0 = (6000 - 15.5 f_{cube}) \sqrt{f_{cube}}$
μ [-]	Poisson's ratio: $\mu = 0.2$
f_t [MPa]	Tensile strength: $f_t = 0.24 f_{cube}^{2/3}$
f_c [MPa]	Compressive strength: $f_c = -0.85 f_{cube}$

The *tensile features* (presented in Table 7-2) consider cracking and tension stiffening of concrete. The default expression for the fracture energy G_F deviates from the expression in MC90 and has been manually set in the present work. It is not normally required to specify the crack spacing s_{max} if the value is believed to be smaller than the element widths of the concrete material, as was the case for the concrete brick elements in the present work. For cases when concrete is heavily reinforced the crack development is somewhat hindered by the concrete's contribution to the stiffness of the member. Concrete between neighbouring cracks resists some of the present tensile forces. This effect is referred to as tension stiffening and is implemented in ATENA by considering a limiting value c_{ts} below which the tensile stress cannot drop in the descending branch of the fracture model. The effect of tension stiffening has not been included in the present study.

Table 7-2 *Material parameters concerning tensile features in the CC3DNonLinCementitious2 material model.*

G_F [Nm/m ²]	Fracture energy: $G_F = 0.000025 f_t$
s_{max} [m]	Crack spacing: <i>Inactivated</i>
c_{ts} [-]	Tension stiffening: <i>Inactivated</i>

The *compressive features* in the *CC3DNonLinCementitious2* material model contain the parameters presented in Table 7-3. The critical compressive displacement w_d defines the concrete softening when the compressive strength f_c has been reached and is described as a linear decrease of the compressive strength involved as shown in Figure 7.3, where L_d denotes the band size. Rather than to define the compressive constitutive relation using strain, a compressive displacement is used in order to reduce its dependency to the mesh. Öman and Blomkvist (2006) showed that

deviations of w_d from the default value in ATENA had little effect on the response. Thus this parameter was not further considered and the default value has been used for the simulations in the present study.

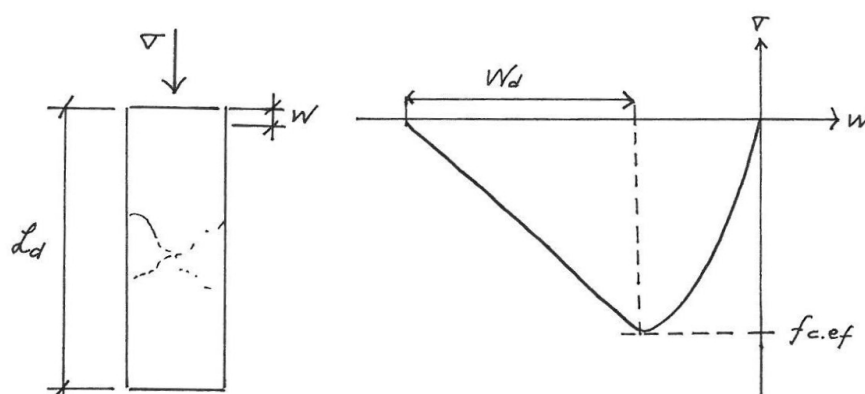


Figure 7.3 Softening displacement in compression.

The plastic part of the compressive strain is defined by the parameter ε_{cp} involved as shown in Figure 7.4. The investigation of Öman and Blomkvist (2006) showed that ε_{cp} does not affect the response markedly when simulating punching shear. In the present study ε_{cp} is however manually set to the value obtained by the MC90 expression, derived as presented in **Appendix II**.

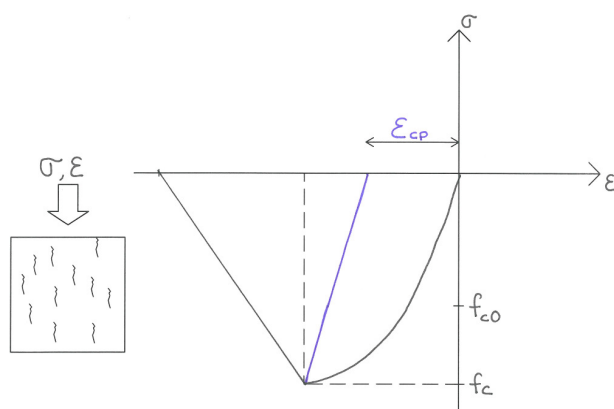


Figure 7.4 Plastic strain, ε_{cp} , at the compressive peak.

The parameter $r_{c,lim}$ governs the decrease of concrete compressive strength as the concrete enters its cracked state and is based on the compression field theory of Vecchio and Collins (Collins and Mitchell, 1991). It states that the compressive strength, derived from cylinder tests, should decrease when the transverse tensile strain increases in the concrete. Cracked concrete is weaker and softer than the concrete specimens used for testing. In the cylinders the concrete is subjected to very small transverse tensile stresses, whereas cracked reinforced concrete may be subjected to large transverse tensile strain. The parameter is related to the transverse tensile strain and the decrease of the compressive strength depends on how severely the concrete is cracked. The reduction is illustrated in Figure 7.5. The default value in ATENA allows a maximum decrease of 80%.

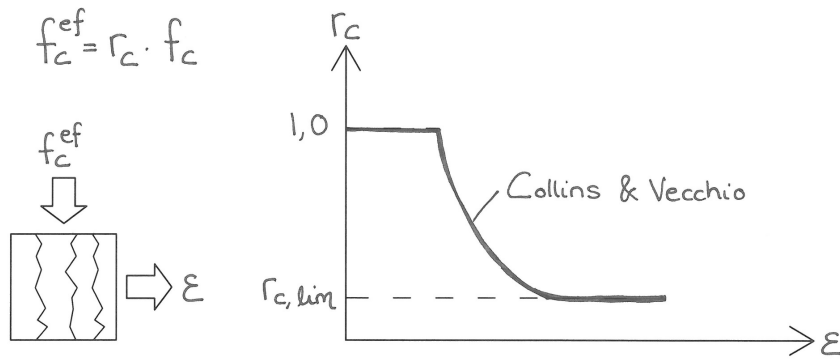


Figure 7.5 Compressive strength reduction due to development of lateral tensile strains.

Table 7-3 Material parameters concerning compressive features in the CC3DNonLinCementitious2 material model.

w_d [m]	Critical compressive displacement: $w_d = -0.0005\text{m}$
ϵ_{cp} [-]	Plastic strain at compressive edge: $\epsilon_{cp} = \frac{f_c}{E_0}$
$r_{c,lim}$ [-]	f_c -reduction due to lateral tensile strains: <i>Inactivated</i> ($\leq r_{c,lim} = 0.2$)

The parameters considering the *shear behaviour* of concrete are presented in Table 7-4. The shear stiffness factor relates the tensile and shear stiffnesses of a crack and depends on the crack widths. In the conducted simulations in this work the default value of S_F has been used and aggregate interlock has not been activated.

Table 7-4 Material parameters concerning shear features in the CC3DNonLinCementitious2 material model.

S_F [-]	Crack shear stiffness factor: $S_F = 20$
MCF [-]	Aggregate interlock: <i>Inactivated</i>
d [m]	Aggregate size: <i>Inactivated</i>

Other parameters employed in the concrete material model are presented in Table 7-5. The coefficient for plastic flow direction β enables simulation of volume change when the concrete is subjected to compression. The default value of β is in ATENA 0, i.e. no change of volume. Negative values of β postulate that the concrete will be compacted, whilst positive values of β results in concrete expansion. Only during high triaxial state of stresses a negative value of β (volume decrease) is reasonable,

however this is still not likely to occur since the stress in one direction will decrease and result in concrete expansion when crushing occurs. This expansion was observed in the experiments carried out on lift slabs by Marinkovic and Alendar (2008). According to Öman and Blomkvist (2006), the range of this coefficient that most likely would give satisfying results lies in the interval 0-1. In the simulations conducted in this study the coefficient has been set to the default value in ATENA.

Table 7-5 Other parameters used in the *CC3DNonLinCementitious2* material model.

EXC [-]	Failure surface eccentricity: $EXC = 0.520$
β [-]	Plastic flow: $\beta = 0$
ρ [kN/m ³]	Concrete density: $\rho = 23\text{kN/m}^3$ (C30/37)
α [1/K]	Coefficient for thermal expansion: $\alpha = 1.2 \cdot 10^{-5}/\text{K}$
FCM [-]	Fixed crack model coefficient: $FCM = 1$

7.1.2 Reinforcement model

Reinforcement is a predefined material model in ATENA where the tensile and compressive responses are identical. The parameters to prescribe are modulus of elasticity E_s , yield strength f_y and stress-strain law. The stress-strain law can either be linear (elastic), bilinear (elastic-perfectly plastic) or multilinear. In the multilinear definition all four stages of steel response are represented, namely; elastic state, yield plateau, hardening and fracture. There is also an alternative formulation of the bilinear stress-strain law that considers strain hardening which allows the stresses to increase after yielding to $f_{t.s}$. The parameter $f_{t.s}$ is bound by rupture of the steel bar at ε_{lim} . Using the multilinear constitutive relation requires more detailed input. The concepts for the other constitutive relations of reinforcing steel are shown in Figure 7.6.

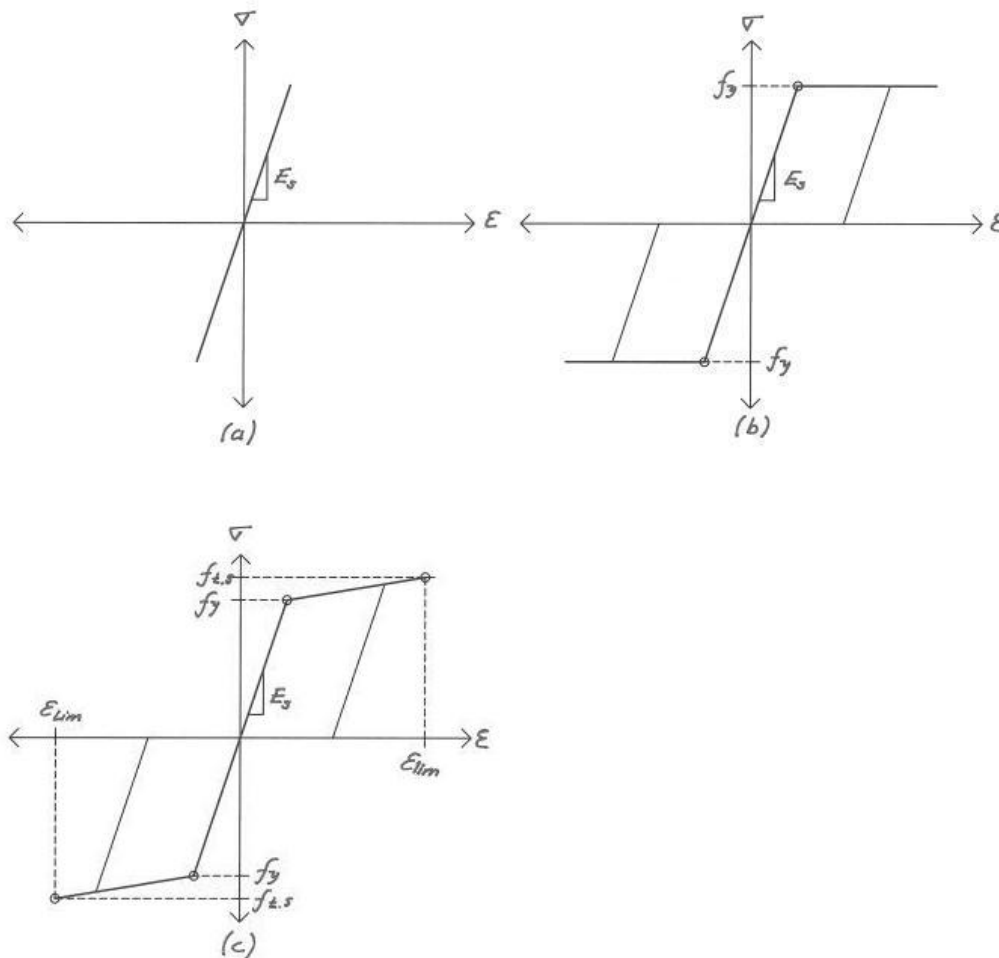


Figure 7.6 Constitutive relations for reinforcing steel; (a) Linear, (b) Bilinear, (c) Bilinear with strain hardening.

For reinforcing steel, unlike for concrete, there is little deviation in material strength parameters. Hence, when the mean values for steel have been considered the characteristic values have been assumed to be fairly representative.

7.2 Structural definition

The gross geometrical properties are defined as *macroelements* which can be formed as prisms, spheres or other geometrical shapes. For irregular structures an assembly of macroelements can be used. However, the shared *surfaces* of adjacent macroelements require special attention. These surfaces, or *contacts*, are automatically prescribed a rigid connection. In order to provide full compatibility between meshes that share the same surface the contact needs to be assigned a mesh compatibility feature. For the case when no connection or less restrained connection is desirable the contact features can be edited and assigned either no connection or *contact element – GAP*. The latter requires an interface material in which the restraint parameters are assigned. In the present study the contact between the concrete slab and the steel column or its caps has been assigned this feature, preventing the transference of tensile stresses.

Element types are assigned to each macroelement. Macroelements representing concrete material normally consist of 3D solid elements. In some cases where mainly bending is of interest concrete can be modelled with shell elements. Shell elements are thinner forms of 3D solid elements. The difference is that the strain distribution perpendicular to the shell surface is linear as shell elements postulate that cross sections remain plain after deformation. Moreover, the stress in this direction is neglected. Compared to 3D solid elements, shell elements are much more computationally effective.

Steel elements other than reinforcement bars, such as the steel column in the present study, are better represented by shell elements. An alternative to model the steel column is to assign *spring elements* along the line of the hollow steel section. Caution must however be taken as springs are uniaxial elements, allowing translation only in their longitudinal direction.

The reinforcement is modelled as 1D elements between joints and assigned a bar diameter. These 1D elements are embedded in the 3D concrete elements. Curved parts of bent and hairpin bars can be modelled as circular segments or for simplicity as straight lines. Apart from this discrete definition of reinforcement that uses truss elements, a smeared approach is also available where the reinforcement is spread along the macroelement by assigning a reinforcement ratio. The interaction between the steel bars and the surrounding concrete can be assigned either a *perfect bond* or a *bond-slip* relation. If a bond-slip relation is used it is possible to assign perfect connection at certain points. This feature is normally used when the structure is cut at a symmetry axis or when the bar is adequately fixed to an anchor. The parametric study of Öman and Blomkvist (2006) showed that the bond features between the reinforcement and the concrete was of less significance in their study of punching behaviour. Hence, in the present study perfect bond is assigned.

Boundary conditions can be assigned to nodes, lines or entire surfaces, depending on which most resembles the actual support. Allowing or preventing translations in any of the three coordinates assigns boundary conditions. In some cases attaching a steel plate on a boundary surface is favourable in order to obtain a rigid surface.

Three different *mesh element types* can be assigned in ATENA, namely; tetrahedron, brick and pyramid elements, where brick elements require that the macroelements is prismatic. Meshing of reinforcement cannot be affected in ATENA; discretely defined bars become embedded in the analysis, surrounded by meshed solid elements. Thus, the mesh of surrounding solid element governs the mesh of the bars. In the present study brick elements are used for concrete materials and steel columns, whilst tetrahedron elements are used for the other steel members.

With the purpose of obtaining a reasonable stress distribution in the modelled slabs, a proper mesh size is to be used. A coarse mesh might lead to a stiffer response, thus it is advised to have at least four to six elements over the thickness of the slab to capture the real stress distribution. The choice of a mesh size is highly influenced by the computation times and a small loss in accuracy might be balanced by precipitation of the analyses.

7.3 Solution control setting

During analysis, when attempting to reach equilibrium within a step the iterations continue until the *convergence criteria* are satisfied, which means that the iterations can stop when the result reaches a value close enough to the real solution for a load level. As iterations are performed, the obtained solution is controlled to see whether it has converged within preset tolerances. In ATENA the default values for tolerances of the different convergence criteria are presented in Table 7-6. The default values were used in the analyses within this study.

Table 7-6 Default values of error tolerances used in ATENA.

Criterion number	Convergence criteria	Tolerance
1	Displacement error tolerance:	1.00 %
2	Residual error tolerance:	1.00 %
3	Absolute residual error tolerance:	1.00 %
4	Energy error tolerance:	0.01 %

Taking small load steps increase the likelihood of reaching convergence at a load level. Difficulties with iterations can be caused by insufficient numbers of iterations, too conservative convergence tolerances or troubles with the specific solution method. To solve these difficulties one might decrease the load step, increase the tolerance limits or chose another solution parameter.

The analysis can be killed prior to having reached equilibrium due to extremely high convergence deviations. This is a measure taken in order to interrupt an analysis that is most likely corrupt or has reached failure. In the present work the analysis is abruptly executed within a step if the above errors are equal to or above a factor 10000 of the prescribed tolerances. After a completed step the analysis is interrupted if the errors exceed a factor 1000 of the prescribed tolerances. The analysis must however be reviewed after its completion in order to ensure that errors do not cause corrupt results. It is inappropriate to rely on results from load steps that have encountered high errors.

8 Validation of modelling technique

In order to validate that the modelling technique applied in the simulations of punching shear in reinforced concrete was reliable simulations have been conducted and compared to experimental data. Two test specimens have been modelled and the results from the experiments have been compared to data from the finite element analyses. It is however important to bear in mind that reported quantities from experiments are not always correct due to shortcomings of equipment and human error. There is also a natural scatter in results, which is not represented by single tests.

8.1 Laboratory tests for comparison

Two of the test specimens from the experiments described in Chapter 4 have been simulated in ATENA. The first simulated specimen was the corner supported slab denoted *R1* from the experiments conducted by Ingvarsson (1977). It consisted of a square slab supported on its corners by rectangular concrete columns. The other simulated specimen was the edge supported slab denoted *No. 2* in the report of Kinnunen (1971). Specimen *No. 2* was a rectangular slab supported on its opposite short edges by square concrete columns. Along its longer edges the slab was unsupported and believed to be limited by lines of shear force peaks. Both specimens experienced failure in punching shear.

During testing of the specimens, several types of data were measured throughout the loading; reinforcement strains, concrete compressive strains on the bottom surface near the columns, slab deflections and rotations. In addition, observations were made on crack propagation at each load step in order to distinguish the crack patterns. The comparisons have been limited to load-displacement responses, crack patterns and failure modes. Comparing for instance values of reinforcement strains is not advisable since the measured strains are much dependent on crack propagation in the adjacent parts of the structure.

8.1.1 Material data

As the reported concrete strengths for the compared specimens were determined according to a former Swedish standard, where the concrete samples had not been stored in water prior to testing, the reported strengths were about 10% higher than they would have been if tested according to the European standard and were therefore adjusted to correspond to valid standards. Material data for the two specimens are presented in Table 8-1.

Table 8-1 Material specifications of specimens R1 and No. 2.

Specimen	Concrete Slab – Compressive Strength			
	Reported		European Standard	
	$f_{c.cube}$ [MPa]	$f_{c.cylinder}$ [MPa]	$f_{c.cube}$ [MPa]	$f_{c.cylinder}$ [MPa]
R1	35.00	28.00	31.50*	25.20*
No. 2	32.65	-	29.39*	-
Specimen	Reinforcing Steel – Yield Strength			
	$\phi 6$	$\phi 8$	$\phi 10$	$\phi 12$
R1	-Not specified-	467 MPa	476 MPa	-
No. 2	-	-	420.72 MPa	422.68 MPa

*) estimated values corresponding to European Standard.

8.1.2 Geometrical data and loading

The considered specimens, with span lengths l_x and l_y and slab thicknesses h , were supported on rectangular columns with cross sections $d_{c,x}$ and $d_{c,y}$ and lengths L . For both specimens the reinforcement design was based on structural analysis according to the theory of elasticity as for frame structures. None of the specimens were provided with shear reinforcement. The columns were heavily reinforced in order to eliminate their failure. In specimen No. 2 torsional reinforcement (using hairpin bars) was provided to ensure the transmittance of support moments to the columns.

The slabs were loaded with several point loads in order to resemble uniformly distributed loads. The point loads were applied through neoprene bearings with the dimensions $p_x \times p_y \times t_p$. Loading was increased using equal increments until failure was observed. For further description of the loading arrangement, see Ingvarsson (1974) and Kinnunen (1971). The columns were connected to one another by tensile ties at the column foots. The ties were tensioned in order to create hogging moments corresponding to the self-weight of the slab and the loading equipment. Thus the results recorded from the experiments only consider the applied loads. The gross geometrical specifications for the two specimens are listed in Table 8-2. The reinforcement detailing is presented in **Appendix III**.

Table 8-2 Geometrical specifications of specimens R1 and No. 2.

Concrete Slab			
Specimen	l_x [mm]	l_y [mm]	h [mm]
R1	2000	2000	120
No. 2	3000	1800	130
Concrete Column			
Specimen	$d_{c,x}$ [mm]	$d_{c,y}$ [mm]	L [mm]
R1	215	145	1000
No. 2	200	200	1045
Neoprene Bearings			
Specimen	p_x [mm]	p_y [mm]	t_p [mm]
R1	100	100	10
No. 2	124	220	10

8.1.3 Results and observations from experiments

The column load at failure of specimen R1 had the average value of 104 kN. The average being based on the measured reactions in each of the four corner columns (see Table 8-3 below), within the load step that caused failure. The observed mode of failure was punching shear by the column denoted as C, although the results presented in Ingvarsson's report are for column B that was supported by roller bearings. Since only a quarter of the specimen was modelled in the FE-analysis (as further described in Section 8.2), the column had to be provided a fix bearing in order to prevent translation in all directions. This implies that the column denoted D has been modelled although compared to results from column B.

Table 8-3 Column loads at failure for specimen R1.

Columns Load at Failure					Failure	
A	B	C	D	Average	Corner	Mode
104 kN	100 kN	107 kN	106 kN	104 kN	C	Punching shear

The edge supported specimen *No. 2* experienced flexural cracks in the field and above the support at the same load level, corresponding to a column reaction of 60 kN. Punching failure occurred when the column reaction reached 128 kN. These observations are summarised in Table 8-4.

Table 8-4 Test data obtained during experiments for specimen No. 2.

Failure Mode	Punching shear
Column load at failure	128 kN
Column load at first flexural crack at top of the slab	60 kN
Column load at first flexural crack at bottom of the slab	60 kN

8.2 Simulation of laboratory tests

In order to reduce required computer capacity it was convenient and, due to symmetry, sufficient to only model a quarter of the test specimens. In the symmetries boundary conditions were introduced such that free movement was prevented in the direction with geometrical continuity. Apart from the symmetry lines, boundary conditions were added for the column supports. In both models, movement was hindered in all three directions (i.e. pinned support). In order to represent stiff support surfaces steel plates were attached to the column foots, onto which boundary conditions were prescribed.

The modelling principles are described by Figure 8.1 and Figure 8.2 and the geometrical specifications of the models are presented in Table 8-5 and Table 8-6. Note that for modelled specimen *No. 2* (as seen in Figure 8.2) the simply supported edge is along the x-axis, corresponding to the length a .

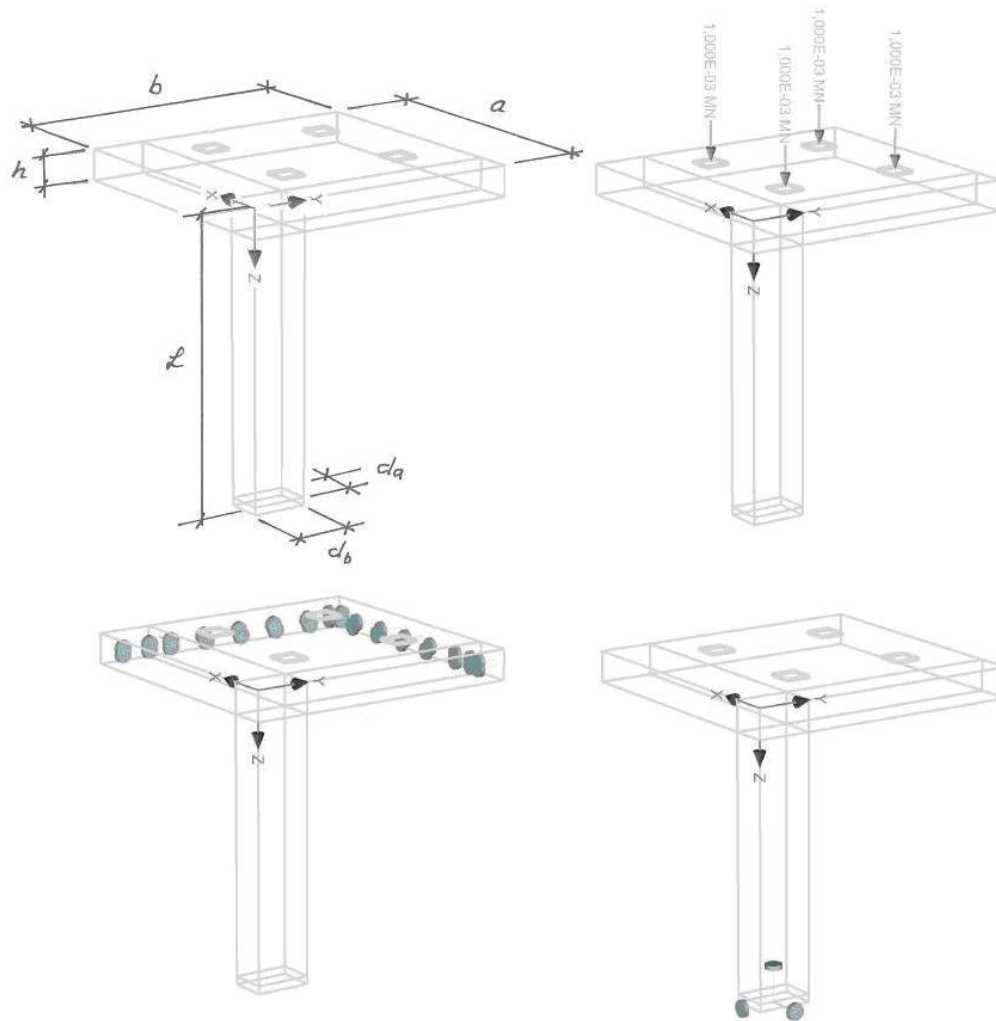


Figure 8.1 Model of specimen R1. (a): Geometrical specification (dimensions according to Table 8-5), (b): Application of loads on neoprene bearings, (c): Boundary conditions on symmetry sections, (d): Boundary conditions at column foot.

Table 8-5: Geometrical specifications for the simulations of models R1.

Concrete Slab		
a [mm]	b [mm]	h [mm]
1072.5	1107.5	120
Concrete Column		
d_a [mm]	d_b [mm]	L [mm]
215	145	1000

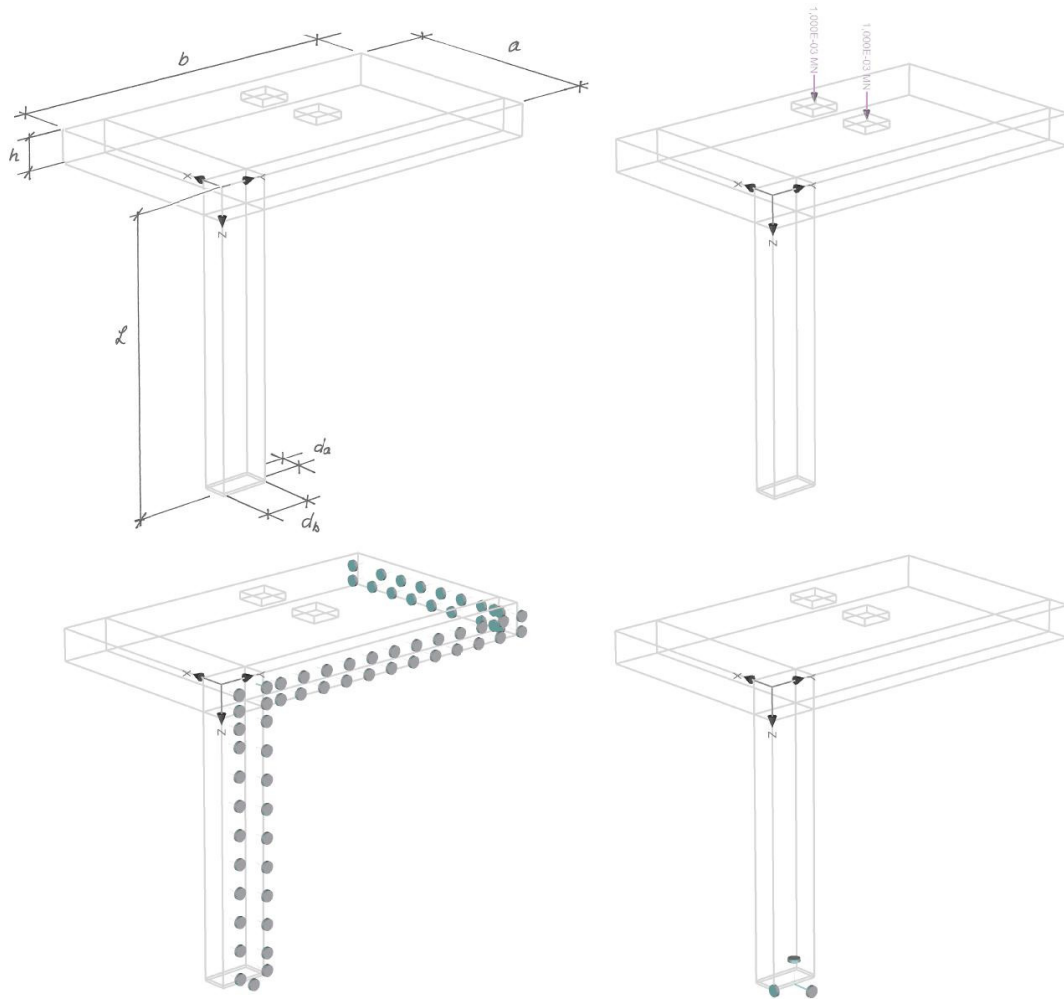


Figure 8.2 Model of specimen No. 2 (note that the simply supported edge is parallel to the x -axis). (a): Geometrical specification (dimensions according to Table 8-6), (b): Application of loads on neoprene bearings, (c): Boundary conditions on symmetry sections, (d): Boundary conditions at column foot.

Table 8-6: Geometrical specifications for the simulations of model No.2.

Concrete Slab		
a [mm]	b [mm]	h [mm]
900	1500	130
Concrete Column		
d_a [mm]	d_b [mm]	L [mm]
100	200	1045

8.2.1 Material properties

The two concrete slabs were modelled using the *CC3DNonLinCementitious2* material model in ATENA. The material parameters in this model have been derived from EC2 and MC90 as presented in Chapter 7 and are based on the strengths according to European standard. The derivations are presented in **Appendix II**. Since the behaviour and crack patterns of the columns were of less importance, the columns were modelled with linear-elastic concrete material, using a Young's modulus of elasticity representing that of cracked concrete, $0.4E_c$.

The neoprene bearing plates were modelled as linear-elastic with an increased modulus of elasticity in order to ensure that the surfaces remained plane and that unrealistic stress concentrations in the concrete were avoided. In both finite element analyses the modulus of elasticity was chosen to ten times the actual value for steel.

In the modelling of the corner supported slab (*RI*) a bilinear response with a horizontal top branch determined by f_y of the steel was prescribed, though during the modelling of the edge supported slab (*No. 2*) difficulties were encountered as the response was too ductile. This could be avoided by assuming a bilinear response with an inclined top branch representing strain hardening of steel. All flexural reinforcement was modelled, although stirrups in the columns were ignored since the columns were modelled as linearly elastic.

The prestressed ties have been ignored in the simplified FE-model. The scope of these ties was to eliminate the action of the self-weight, which is roughly equivalent to neglecting the body force.

8.2.2 Finite elements

In the validation models, solid elements were used. The concrete members of the test specimens were modelled with brick elements, whilst tetrahedral elements were used for the steel plates due to the lack of interest for their stress distribution. In order to ensure the generation of a qualitative mesh, the concrete slabs were divided into three and four macroelements for specimen *RI* and *No. 2* respectively. The surfaces between the adjacent macroelements were then prescribed mesh compatibility features. The meshed models can be seen in Figure 8.3, where specimen *RI* was divided into 10505 finite elements and specimen *No. 2* was divided into 11662 finite elements.

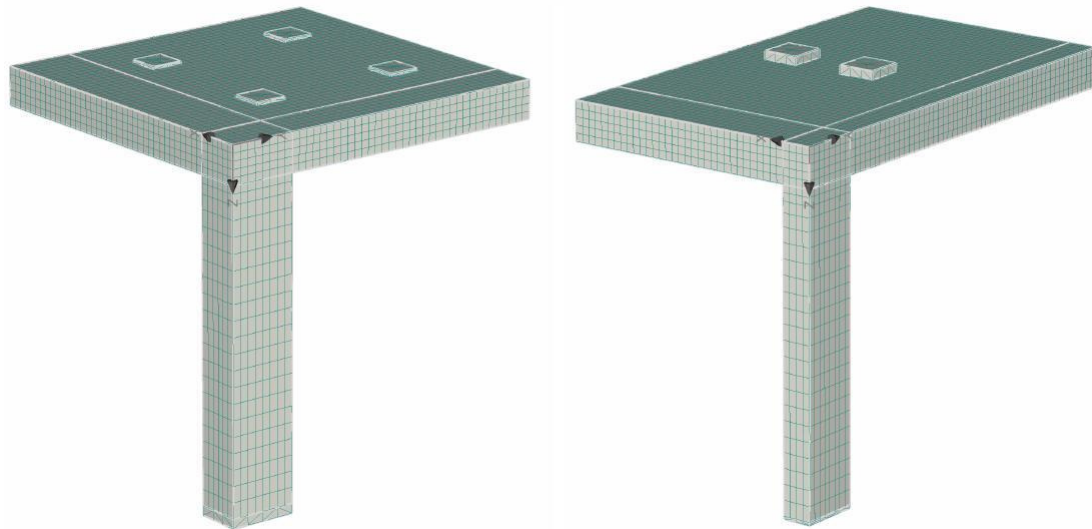


Figure 8.3 Mesh configuration of specimens R1 and No. 2.

Generally a mesh convergence is assessed to verify that the number of finite elements used in the analysis is sufficient, although the mesh is also verified by analysing the response of the models and compare them to test results. The measured value for comparison is chosen as the vertical displacement of the inner corner of the model, i.e. the centre deformation of the full scale structure. The lower limit for the mesh coarseness is set to five elements across the slab thickness since it is required in order to describe flexure. The chosen mesh was evaluated to be fairly accurate as the response from the FE-analyses showed good agreement with the reported observations.

8.3 Results from analyses of test specimens

For the conducted FE-analyses of specimens R1 and No. 2 crack patterns, state of stresses and ultimate loads have been studied to represent an idea of the structural responses and cause of failure.

8.3.1 Corner column supported slab R1

As illustrated in Figure 8.4 the column reaction P versus the vertical displacement u in the middle of the slab presents an idea of the structural response and the sequence of events are represented by A , B , C and D in the graph. The same response as reported in the test documentation by Ingvarsson (1977) is compared to the response from the analysis and shows good agreement for peak loads and the events as presented in the following. However, the analysis showed a somewhat stiffer behaviour than the response that was observed in the experiment. This is believed to be caused by the smeared crack formulation which means that the model responds with significantly decreased stiffness first after the crack is fully developed. In reality, cracking affects the response as cracks are initially formed.

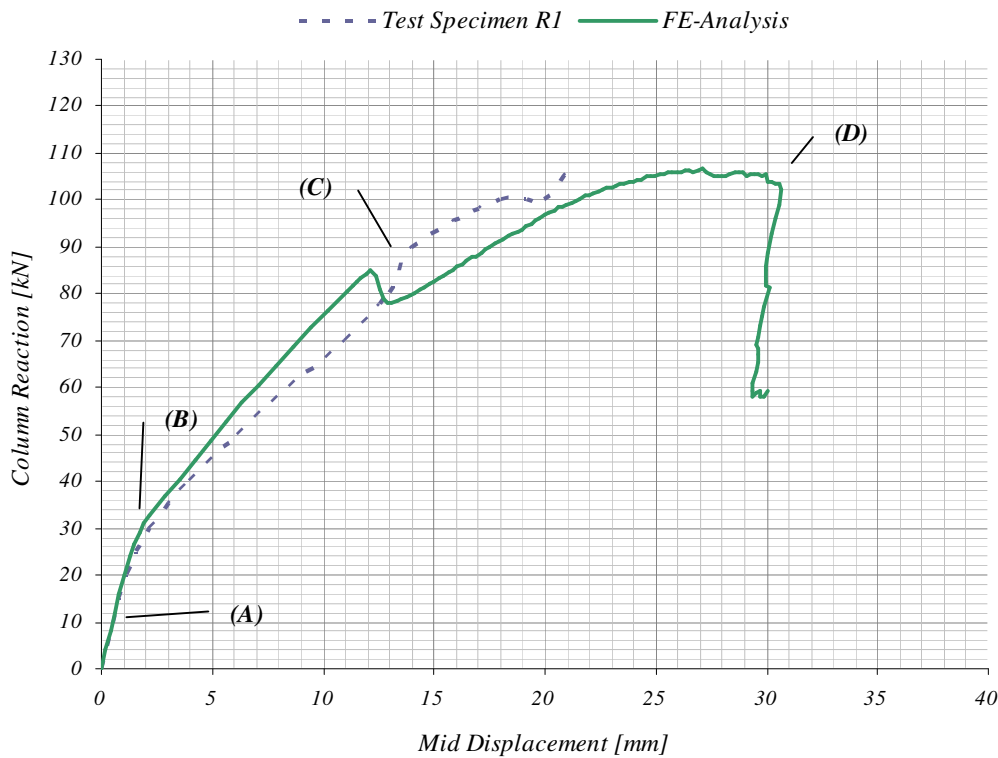


Figure 8.4 Comparison between response from experiment and FE-analysis for test specimen R1.

The response in the analysis was linear until the initiation of flexural microcracks on the bottom surface in mid-field. Although very small, the flexural microcracks caused a slight softening of the concrete (A). These microcracks appeared at load step 4, corresponding to a column reaction of 12 kN. In the following load step, flexural microcracks above the support were formed, also contributing to the softening response of concrete. Some of these cracks were inclined due to the presence of torsional moments. In Figure 8.5, all cracks that have been numerically derived are indicated, although in reality they would not have been visible as the maximum crack widths only reach values around 50 μm .

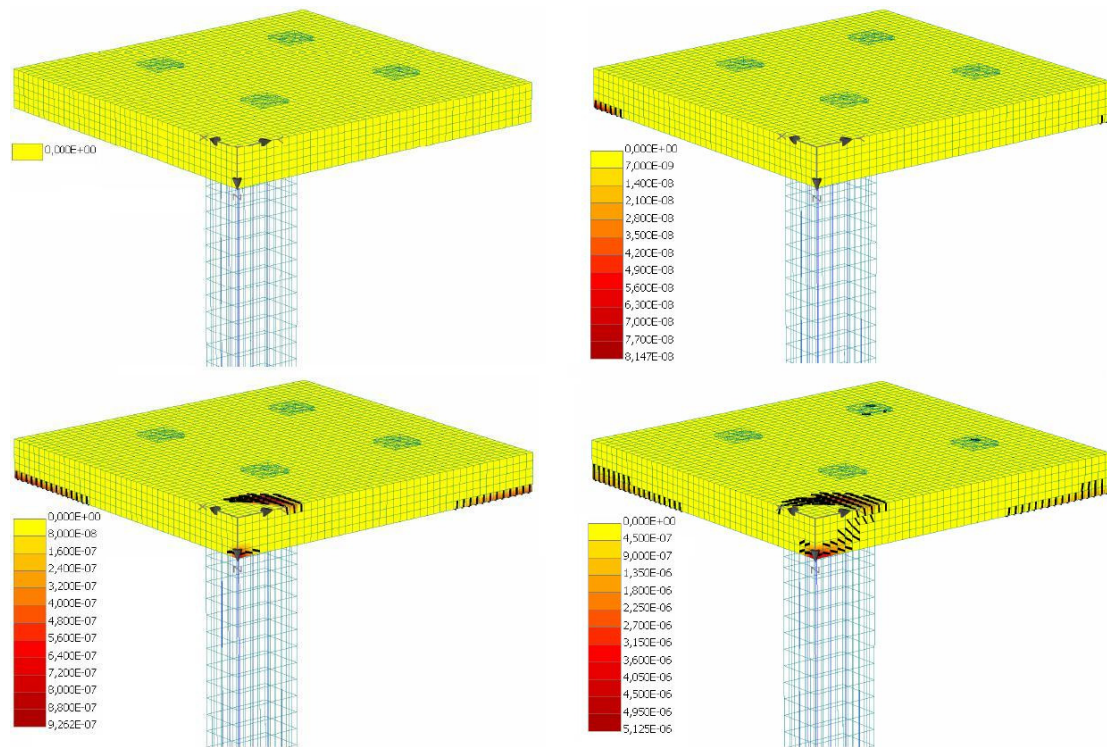


Figure 8.5 Initiation of flexural and torsional microcracks (no crack filter) causing concrete softening at event (A). Cracks are plotted against crack widths [m].

(a) $P=12$ kN (LS 3),

(b) $P=16$ kN (LS 4),

(c) $P=20$ kN (LS 5),

(d) $P=24$ kN (LS 6).

As the cracks above the column propagated, yet another stiffness decrease could be noticed on the load-displacement graph (B) as illustrated in Figure 8.4. This is believed to be caused by flexural microcracks above the column extended downwards across the section of the slab as seen in Figure 8.6 where all numerically derived cracks are visible. This event corresponds to the load where the column reaction is above 30 kN.

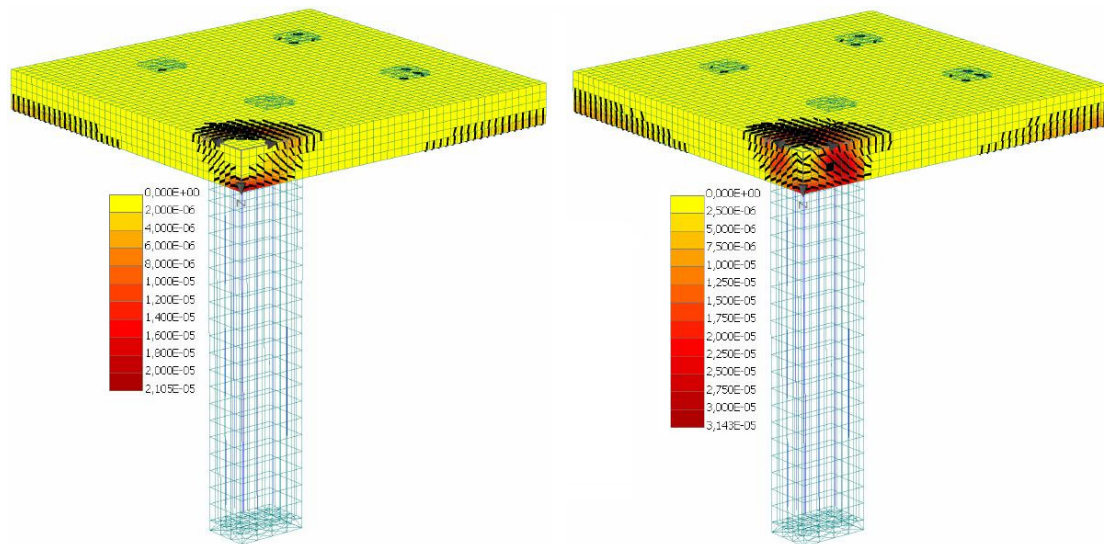


Figure 8.6 Propagation of microcracks above the column (no crack filter) plotted against crack widths [m] at event (B).

(a) $P=31$ kN (LS 9), (b) $P=37$ kN (LS 11).

With increased loading the cracks continued to propagate and crack widths increased. The snap-through response (C) between load steps 27 and 32 appeared to be caused by the combined effect of events occurring in the supported area. One cause is believed to be the propagation of shear cracks in the vicinity of the column as seen in Figure 8.7. These shear cracks cross the previously formed inclined cracks that were caused by torsional moments. In Figure 8.7, only cracks larger than 0.05 mm are illustrated. The corresponding column reaction at this event was about 84 kN. In addition to this, concrete crushing⁴ was initiated and the affected region spread along the faces of the column. The grey regions bounded by the dark blue lines in Figure 8.8 indicate where crushing was experienced. Furthermore, Figure 8.9 indicates that the reinforcing steel above the column experienced increased stresses and strains during the snap-through response. The reinforcement here (hairpin bars) was of poorer quality than the other bars in the slab. Tensile strains in the vertical direction appeared during the snap-through response as illustrated by the arrows outside the triaxial state of compression near the column corner in Figure 8.10.

⁴ Crushing is believed to occur when the compressed concrete has reached the limit for the principal plastic strain, ϵ_{cp} .

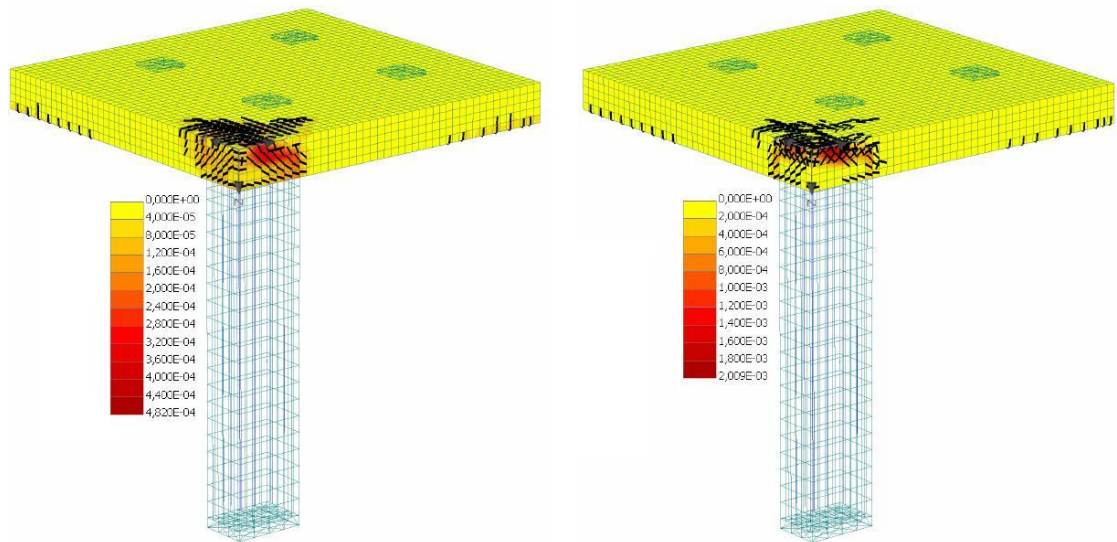


Figure 8.7 Propagation of shear cracks (cracks >0.05 mm) at event (C) plotted against crack widths [m].

(a) $P=84$ kN (LS 26),

(b) $P=79$ kN (LS 30).

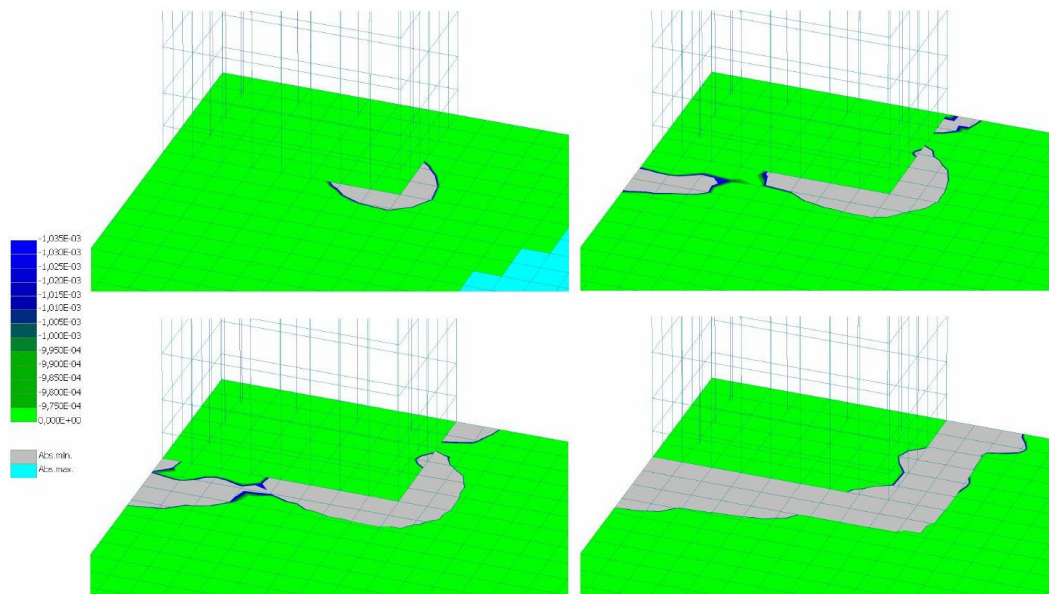


Figure 8.8 Principal plastic strains [-] indicate concrete crushing (grey regions).

(a) $P=83$ kN (LS 25),

(b) $P=79$ kN (LS 35),

(c) $P=85$ kN (LS 45),

(d) $P=105$ kN (LS 90).

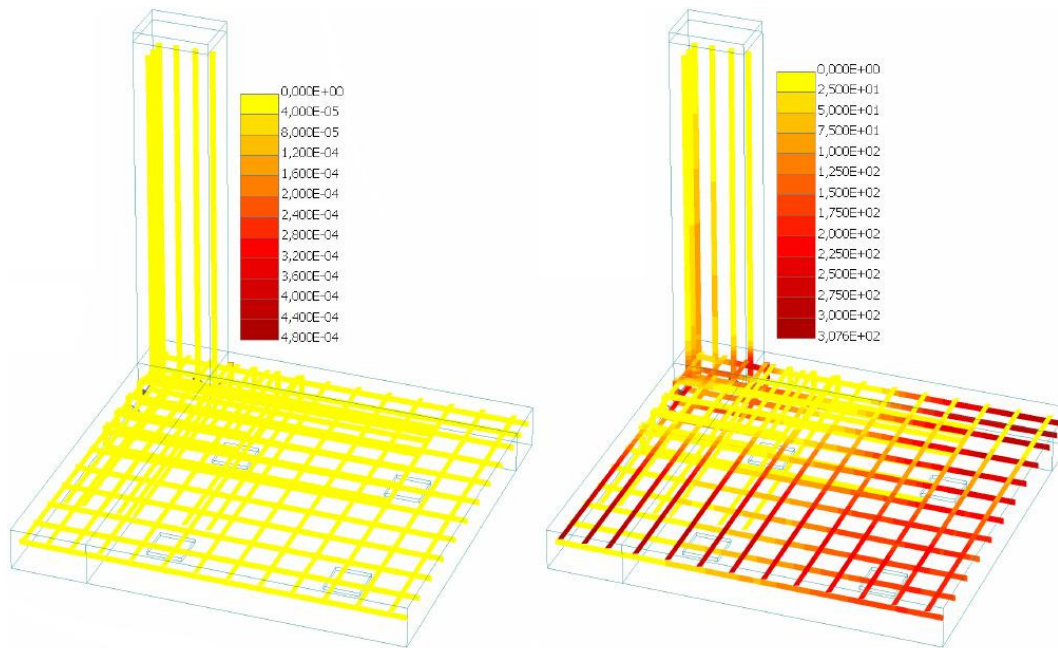


Figure 8.9 Increase of reinforcement strains [-] and stresses [MPa] above the column at $P=79$ kN (LS 30) corresponding to event (C).

(a) Principal strains, (b) Principal stresses.

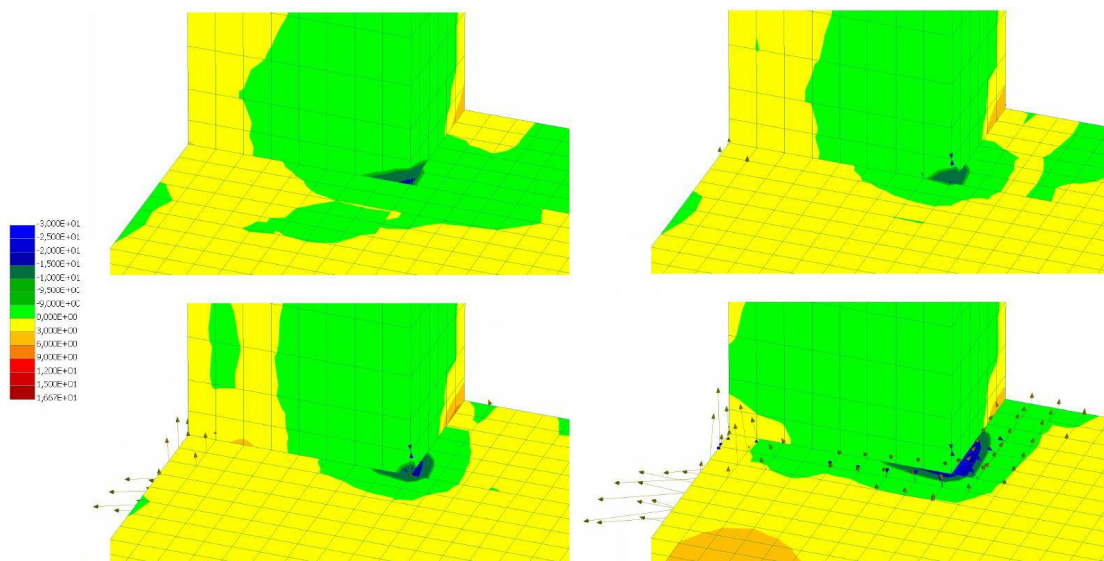


Figure 8.10 Initiation and propagation of tensile strains in the vertical direction on the bottom surface near the column plotted against principal tensile stresses [MPa] (negative stresses indicate triaxial compression).

(a) $P=83$ kN (LS 25), (b) $P=79$ kN (LS 30),
(c) $P=85$ kN (LS 45), (d) $P=105$ kN (LS 90).

Despite the critical events around (C) the structure still had resistance to withstand a further increase of shear forces. As loading increased the slab approached failure

which appeared to be caused by cracks that propagated towards the slab-column intersection in a nearly horizontal course. When reaching the compressed conical shell the horizontal crack provoked a sudden decrease of the column reaction from its peak around 105 kN (*D*), i.e. brittle failure. The state of stresses in the vicinity of the column prior to the failure, as was illustrated in Figure 8.10, indicated a state of triaxial compression as the maximum principal stresses (principal tensile stresses) were negative. This state was impaired as the crack reached the fully compressed zone in an almost horizontal course as indicated in Figure 8.11, resulting in increased tensile strains in the vertical direction.

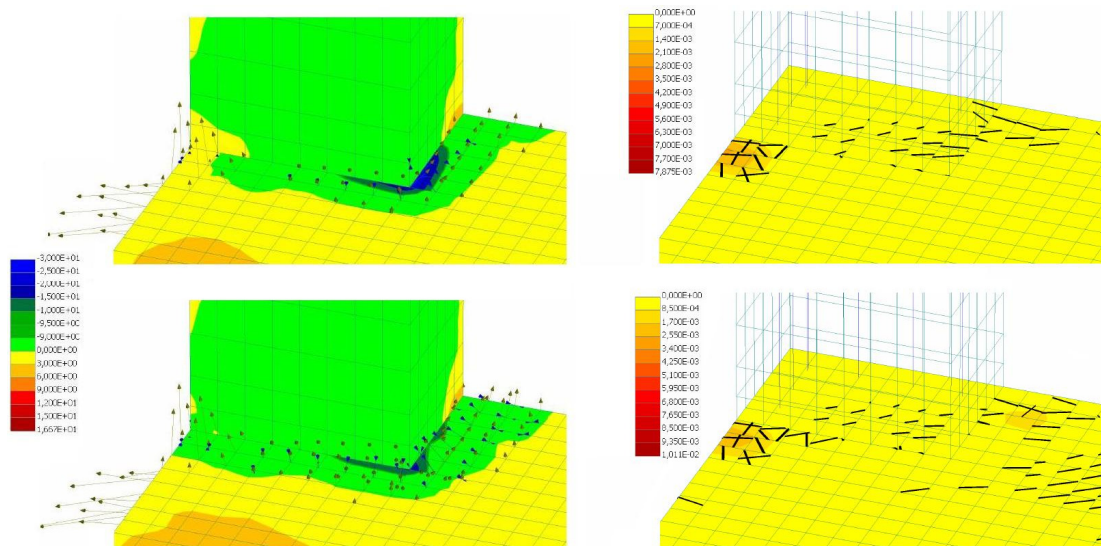


Figure 8.11 Cause of punching failure at $P=105$ kN corresponding to event (D). Left: tensors of principal strains plotted against principal tensile stresses [MPa]. Right: Cracks (> 0.05 mm) plotted against crack widths [m].

(a) LS 90,

(b) LS 115.

The deformed shapes of the slab prior to the sudden loss of capacity are illustrated in Figure 8.12 and clearly indicate failure in punching as the slab above the column experienced vertical displacements. Compared to the vertical displacements that were observed from the experiment, the analysis is quite well corresponding.

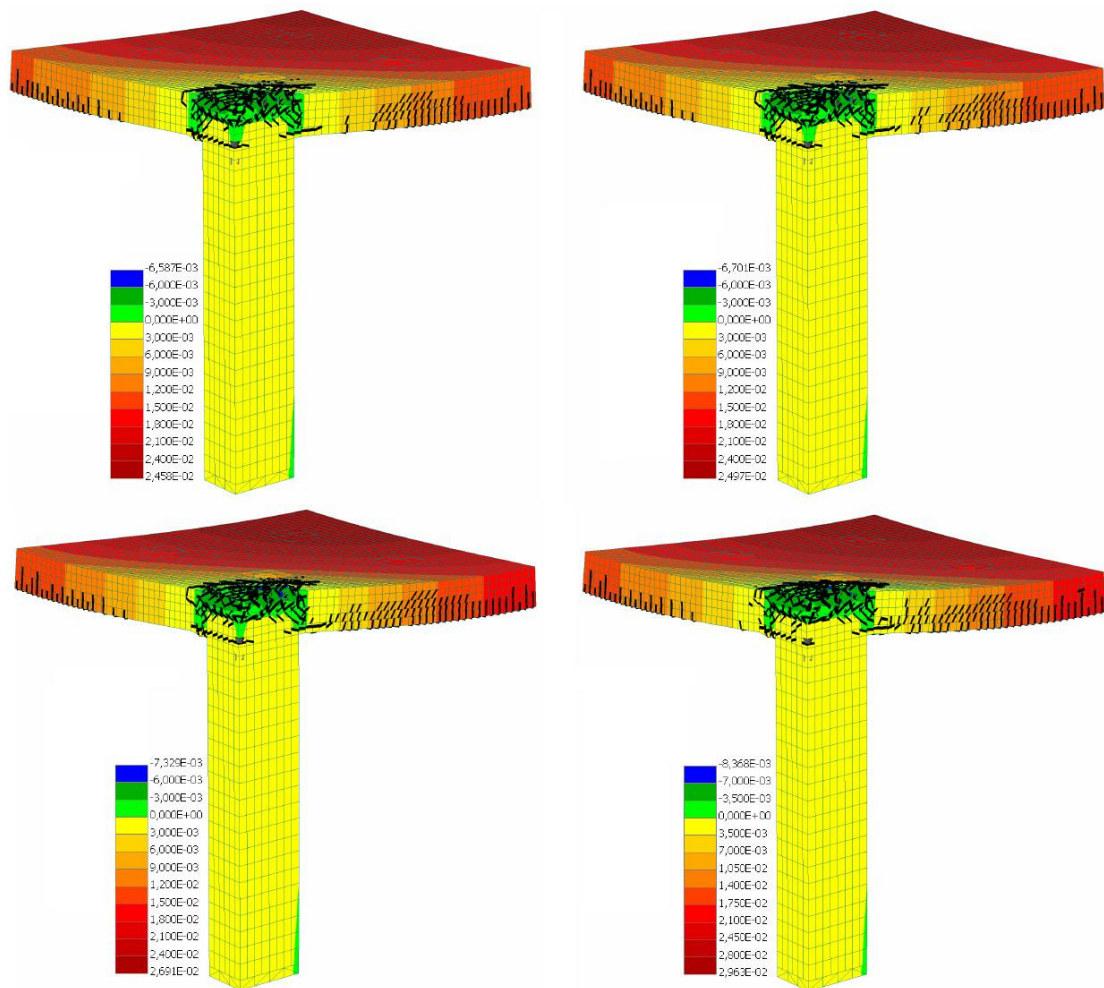


Figure 8.12 Deformed shapes (magnified by a factor 5) prior to failure and cracks (>0.05 mm) plotted against vertical displacement [m]. (Note the horizontal cracks in the vicinity of the column.)

(a) LS 88,

(b) LS 90,

(c) LS 100,

(d) LS 115.

8.3.2 Edge column supported slab No. 2

The structural response from the tests performed by Kinnunen (1971) and the FE-analysis are presented in Figure 8.13 by means of a load–displacement graph. The load-displacement relationships were well simulated although a slight deviation of the cracking loads was observed. The stiffer response was discovered also in the FE-analysis of the corner supported slab (RI), giving an indication of a stiffer response in ATENA. Both the test curve and the curve from the FE-analysis of the edge supported slab showed a typical punching failure; a brittle failure with a sudden loss of load-bearing capacity. However, the FE-analysis was able to capture the descending branch of the load-displacement curve after failure. In the load-displacement graph, the response from the FE-analysis is characterised by the events A, B, C and D.

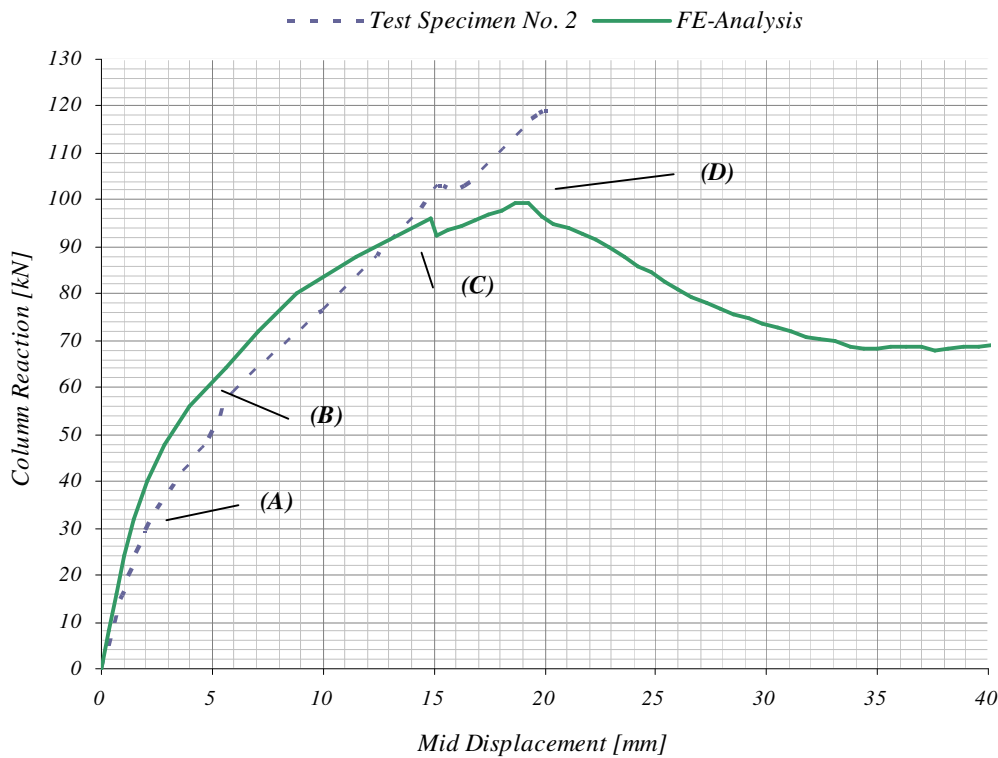


Figure 8.13 Comparison between response from experiment and FE-analysis for test specimen No. 2.

The displacements increased linearly with the load until (A), where the structural response was softened due to the propagation of microcracks. Figure 8.14 shows an illustration of the crack development, where all numerically derived cracks are visible. There was an increase of microcracks both in the bottom of the slab and around the column. The largest microcracks were found around the column, presented by darker areas in the illustration. On the top surface of the slab, microcracks in both main directions were present which gave an indication of hogging moments in both directions.

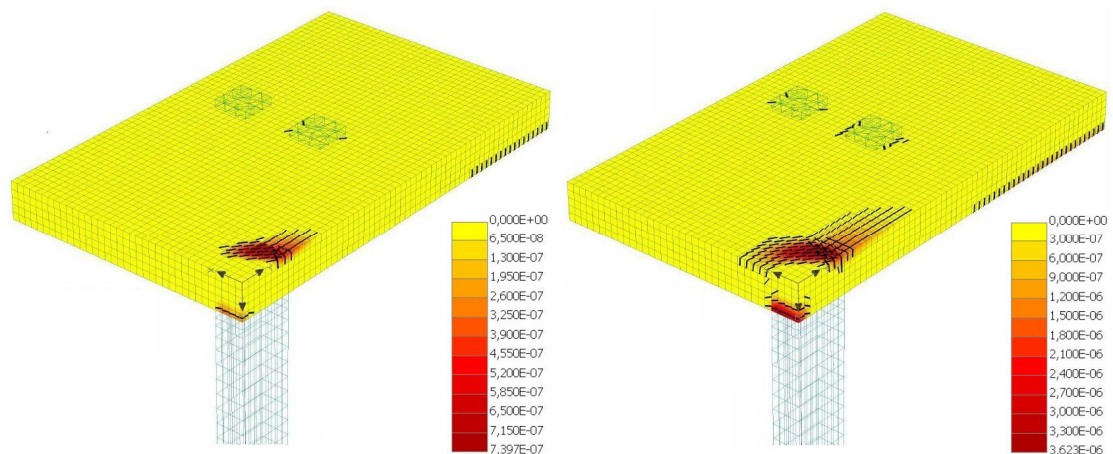


Figure 8.14 Crack initiation (no crack filter) at event (A) plotted against crack widths [m].

(a) $P=24$ kN (LS 3),

(b) $P=32$ kN (LS 4).

Thereon the curve continued to increase linearly until (B), where the structural stiffness was decreased due to more significant crack propagation. The crack pattern at load step 7 and 8, corresponding to a column load of about 60 kN, is illustrated in Figure 8.15. In the latter, larger inclined cracks were developed.

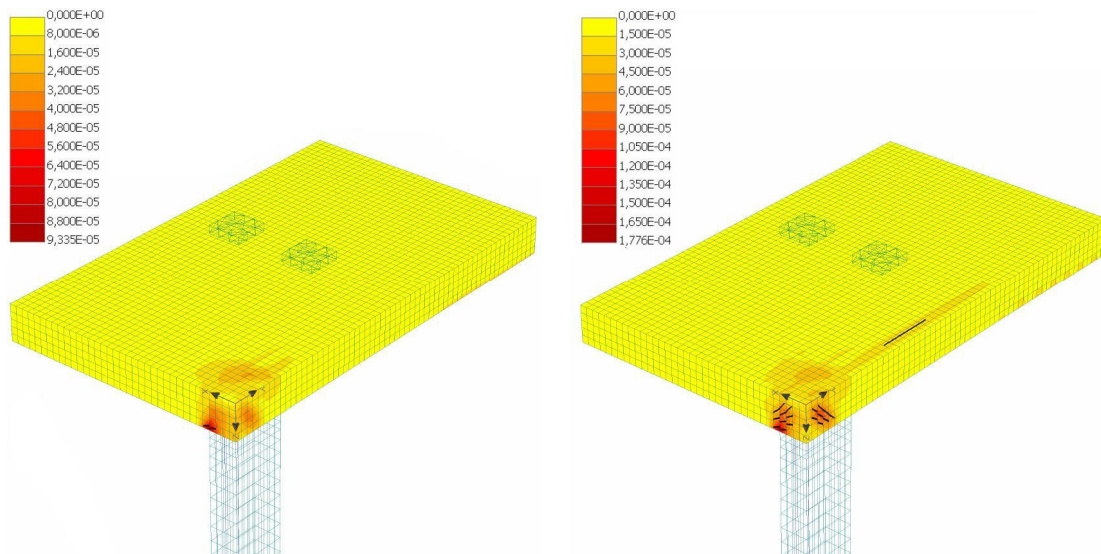


Figure 8.15 Crack development (cracks > 0.05 mm) at event (B) plotted against crack widths [m].

(a) $P=56$ kN (LS 7),

(b) $P=64$ kN (LS 8).

Figure 8.16 shows how microcracks extended towards the corner of the slab-column intersection in (B), resulting in a decrease of the triaxial compressive zone along the column face perpendicular to the simply supported edge.

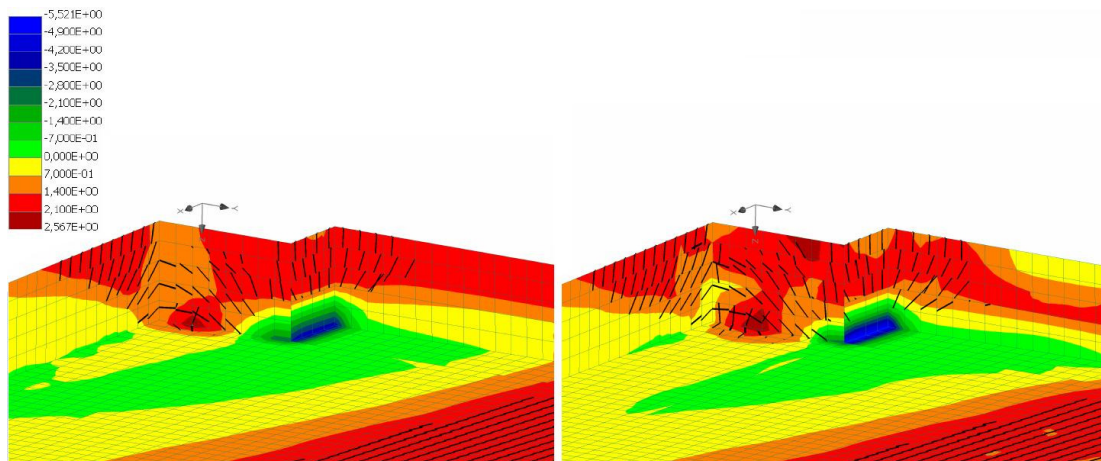


Figure 8.16 Crack propagation and principal tensile stresses [MPa] at event (B) (negative stresses indicate triaxial compression).

(a) $P=56$ kN (LS 7),

(b) $P=64$ kN (LS 8).

Even though the shear crack propagated towards the bottom face of the slab, the load-bearing capacity was not lost. The load-displacement relationship was still ascending until interrupted at event (C), which denominates a snap-through in the load-

displacement curve. The snap-through response was an effect of several occurrences causing a localised decrease of the load-bearing capacity. The analysis of the structural responses at (C) indicated that failure had been initiated.

Shortly before the snap-through, at a column load of 80 kN, the compression of the concrete exceeded the capacity and crushing of the concrete started. After increased loading the crushed area was spread along the column faces. The crushing progress is presented by the grey coloured areas in Figure 8.17, where it is the concrete in vicinity to the column face parallel to the edge that is majorly crushed.

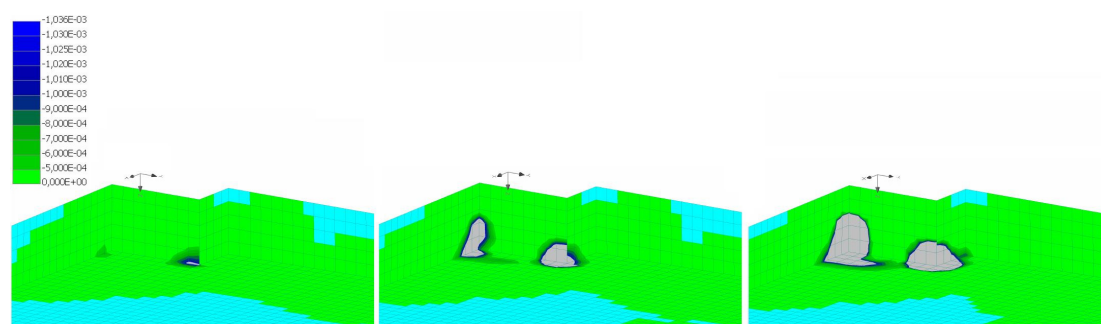


Figure 8.17 Principal plastic strains [-] indicate concrete crushing (grey regions) around the column at event (C).

(a) $P=80$ kN (LS 10), (b) $P=88$ kN (LS 11), (c) $P=94$ kN (LS 14).

Up to a column reaction of about 90 kN, the region around the column face parallel to the edge was triaxially compressed. This area was decreased at the peak of the snap-through and after further loading solely the corner was under a triaxial compressive state of stresses. The concrete in proximity of the column was instead found to be biaxially compressed due to the conversion of one compressive stress into tensile. The process is presented in Figure 8.18.

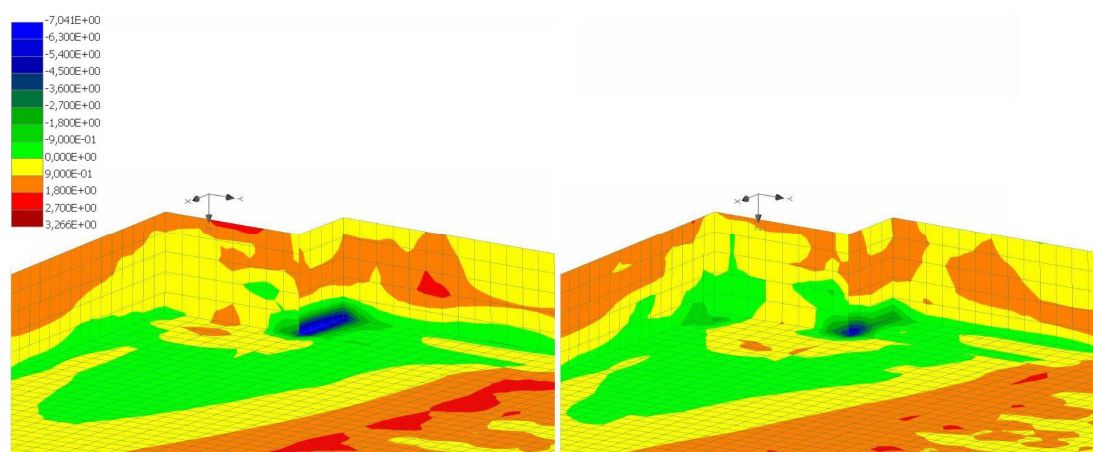


Figure 8.18 Principal tensile stresses [MPa], blue areas indicate triaxial compression at event (C).

(a) $P=88$ kN (LS 11), (b) $P=92$ kN (LS 13).

The decrease of the triaxial compression zone was caused by the formation of horizontal microcracks, visible in Figure 8.19 which illustrates the crack pattern after

the snap-through. The slab portion facing the column face perpendicular to the edge was subjected to the largest cracks, caused by torsion and shear. Some of the shear cracks had perforated and reached the bottom surface of the slab. The crack propagation together with the loss of the triaxial compressive zone and extensive crushing of the concrete seems to have impaired the structural capacity.

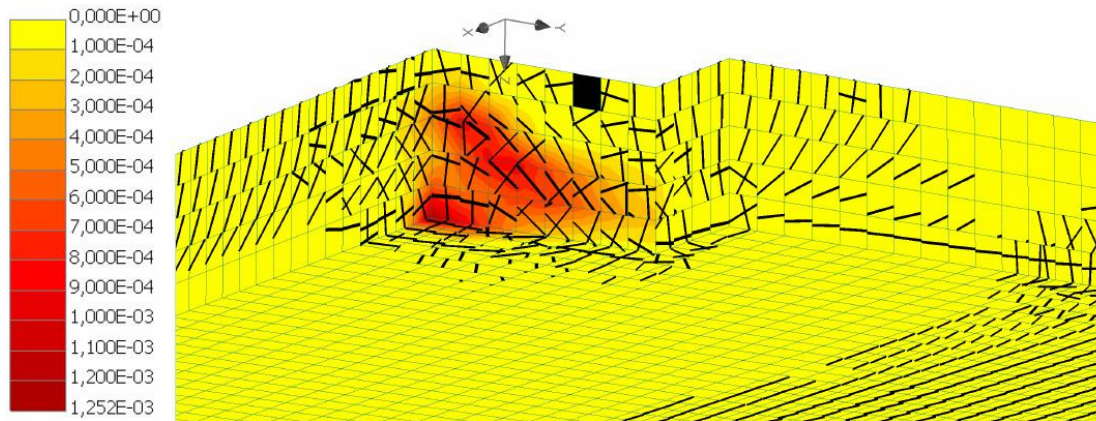


Figure 8.19 All numerically derived cracks plotted against crack widths [m] at $P=94$ kN (LS 14) corresponding to event (C).

The maximum stress in the reinforcement was reached at a column load of 96 kN. The reinforcement was close to yielding, however, it can be noted in Figure 8.20 that plastic strains were not developed. Thus yielding was not yet initiated.

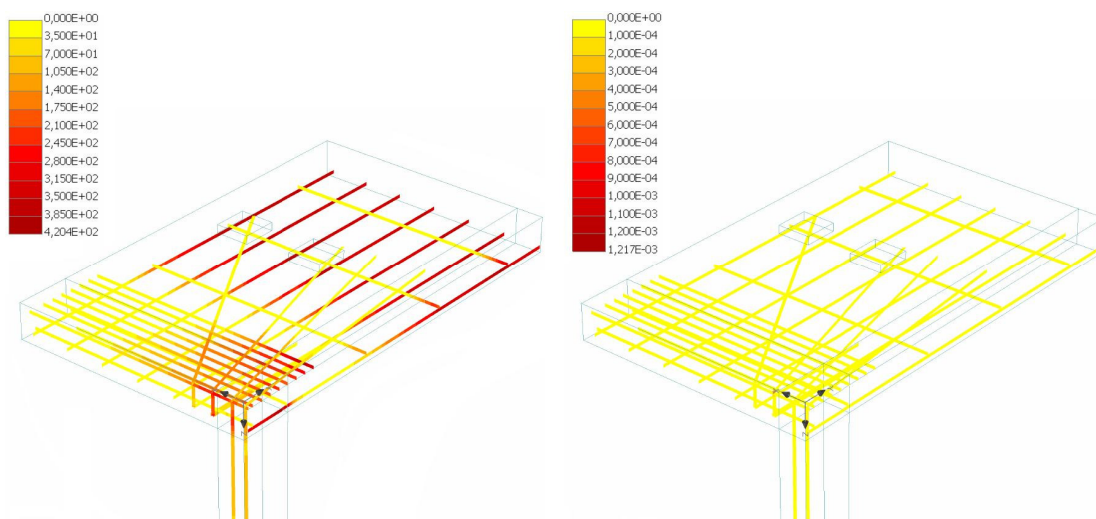


Figure 8.20 Left: principal stresses [MPa]; right: principal plastic strains [-] at $P=96$ kN (LS 16).

When the column load reached its maximum value, the previously initiated concrete crushing progressed and at event (D) the concrete in the bottom of the slab was crushed all around the column periphery (see Figure 8.21). The previously formed horizontal cracks' dilation and progressive extension is illustrated in Figure 8.22. The behaviour resulted in a loss of load-bearing capacity and structural failure.

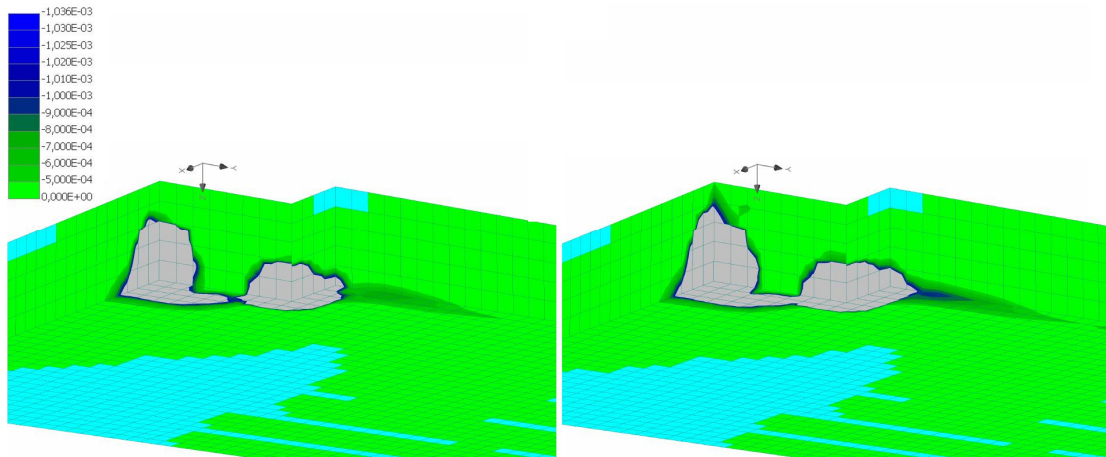


Figure 8.21 Principal plastic strains [-] indicate concrete crushing (grey regions) around the column at event (D).

(a) $P=99 \text{ kN}$ (LS 19),

(b) $P=95 \text{ kN}$ (LS 22).

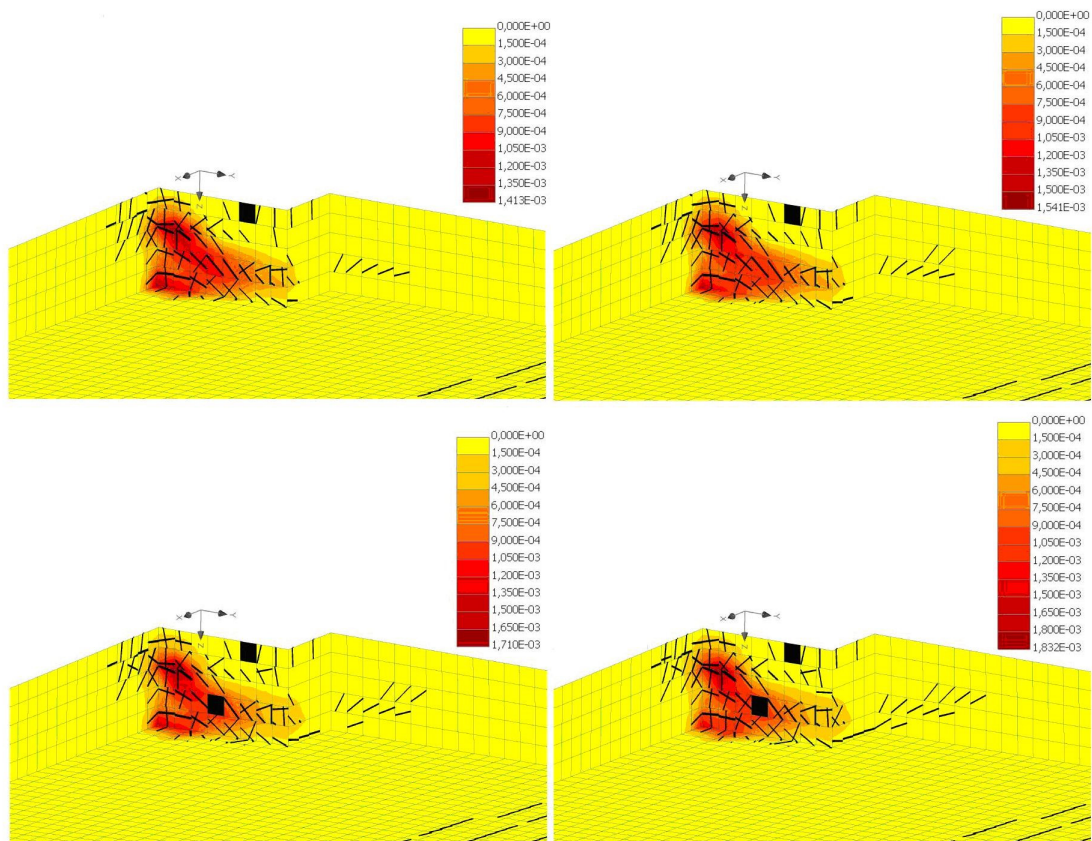


Figure 8.22 Propagation of horizontal cracks at event (D) plotted against crack widths [m].

(a) $P=99 \text{ kN}$ (LS 19),

(b) $P=99 \text{ kN}$ (LS 20),

(c) $P=96 \text{ kN}$ (LS 21),

(d) $P=95 \text{ kN}$ (LS 22).

The deformation of the structure confirms how the column punched through the slab. At failure, the elements along the failure surface became deformed. In Figure 8.23 the green and blue areas indicate upward vertical displacements.

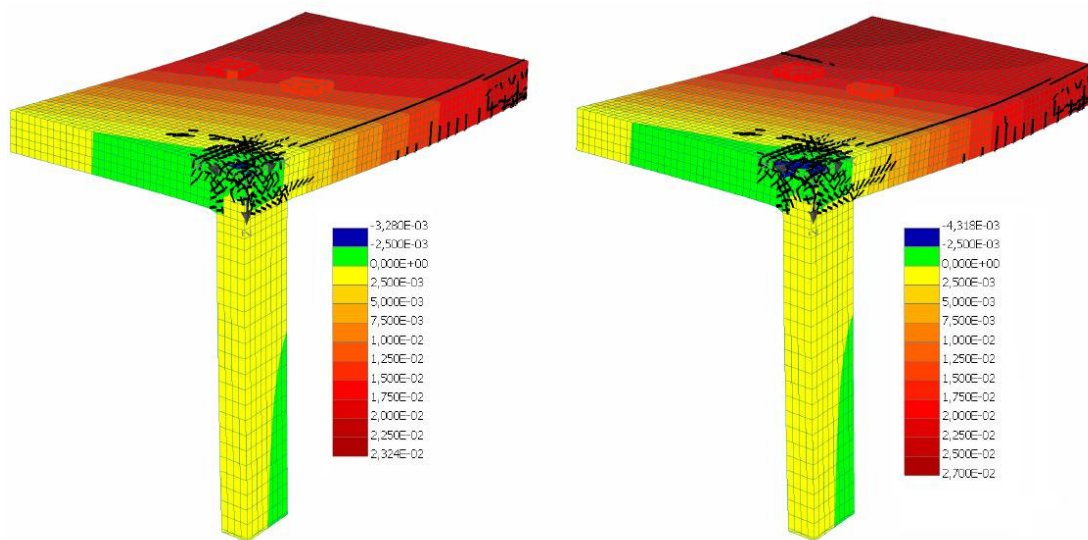


Figure 8.23 Deformed shapes (magnified by a factor 10) and cracks (>0.05 mm) at failure (event D).

(a) $P=99$ kN (LS 19), (b) $P=95$ kN (LS 25).

8.4 Comments on verification

The results from the simulation of the test specimen *RI* showed good agreement with the behaviour as described in the documentation by Ingvarsson (1977). The ultimate load was well simulated although the displacements differed somewhat. The larger deflection in the FE-analysis indicated a less stiff behaviour and a softer response compared to the experiments.

In the FE-analysis of specimen *No. 2*, the ultimate load was smaller than reported by Kinnunen (1971). The mid deflections at the maximum load were very similar for the computer simulation and what was reported from the experiment.

- Despite of the slight deviations that were encountered in the finite element analysis, it was comprehended that mean material parameters can be used to model punching failure in ATENA. Initially, the analyses showed a somewhat stiffer response than the response observed from the experiments. This is believed to be caused by the smeared crack formulation that responds, with decreased stiffness, to cracking first after the crack is fully developed within each element. In reality, cracking affects the response as cracks are initially formed.
- The FE-analyses were able to capture the structural events that were also observed during the experiments. In both the analyses of *RI* and *No. 2* the shear cracks appearing at the snap-through occurred around the same column

reaction as in the conducted experiments. In light of the FE-analysis of *RI* the ability of the reinforced concrete's capacity to resist shear despite the extensive structural damage that occurred around event (*C*) was shown. When the shear crack appeared, a new state of stress was obtained which eventually resulted in the propagation of the horizontal crack that provoked final collapse. Both the FE-analyses were able to capture the descending branch of the load-displacement curve after failure had been provoked.

- The assumption of full interaction between the reinforcement and surrounding concrete seems to have given fairly representative results. Strain hardening of the reinforcement bars had to be included for the edge column specimen *No. 2* in order to adjust for the otherwise too ductile response that was indicated by a fluctuating plateau in the load-displacement response.
- The obtained results from the validation analyses gave indications on how to model the column in the case study. Rather large in-plane displacements were observed in the deformed shape of specimen *No. 2*, which indicates difficulties with modelling the steel edge columns with spring elements.

8.4.1 Predicted punching load for specimen *No. 2*

The predicted punching load for specimen *No. 2* has been determined according to EC2 using mean values to enable comparison with the experiment and the FE-simulation (see **Appendix V**). The calculated punching resistance $V_{Rd,c}$ was only 62% and 79% of the ultimate load according to the experiment and the FE-analysis respectively.

8.4.2 Previous comparisons with ATENA

During 2006 Öman and Blomkvist investigated whether it was possible to simulate the complex behaviour of reinforced concrete flat slabs and hence conducted simulations of Broms' experiments. The stiffer response in ATENA was also observed during these investigations. Furthermore, Öman and Blomkvist conducted a parametric study in order to assess the influence of the concrete material properties. It was concluded that for models subjected to high compressive stresses parameters regarding critical displacement at compressive edge, plastic strain and plastic flow were influential. However, the tensile and compressive strengths did not influence the response markedly; neither did the model for the interface behaviour between reinforcement and surrounding concrete. The fracture energy and the coarseness of the mesh were the two parameters that highly influenced the response.

9 Numerical investigation of case study

In this project the punching phenomenon in case of edge supports on steel columns has been studied by means of FE-analyses of the corner supported element that was first introduced in Section 5.2, here illustrated in Figure 9.1. The connection detailing used in the investigations was presented in Section 2.2 and is constituted of a hollow steel section through the slab thickness.

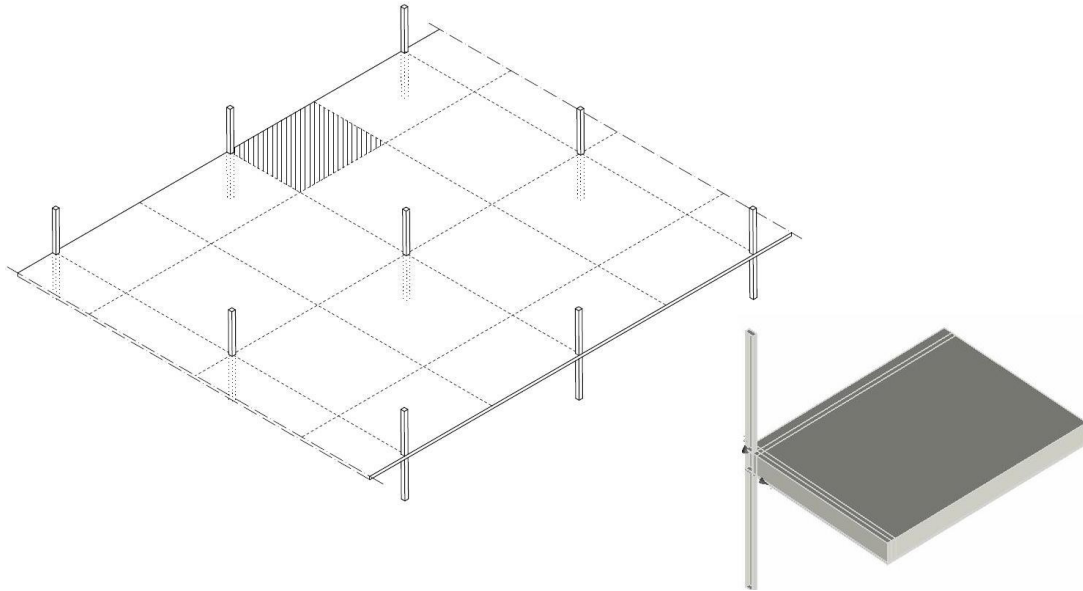


Figure 9.1 In the investigation considered corner supported element from the infinite flat slab.

9.1 General modelling considerations

Since the type of structural system modelled in this work is not within the range of available experimental data, the validation models can only give some indications on proper modelling techniques. Since the previous analysis on specimen *No. 2* indicated horizontal translation within the column-slab connection (see Figure 9.2) it is indicated that the concrete column responds to the movement of the slab in the perpendicular direction to the edge. Steel columns, being more prone to this response, are therefore not well represented by line spring elements. Hence, half the column length above and half the column length below the slab have been modelled, assuming that the cut-off sections correspond to the inflection points of the columns.

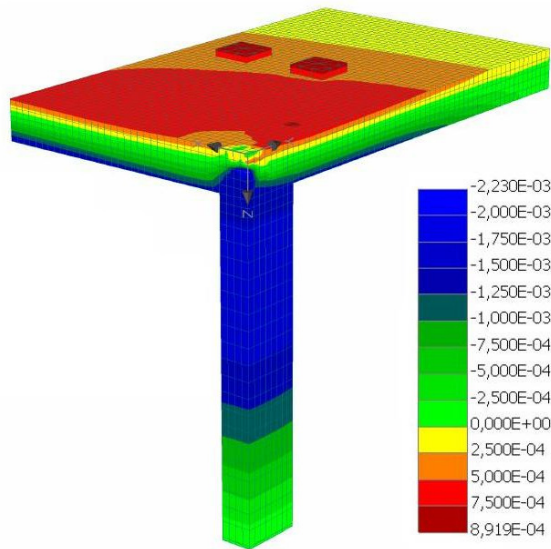


Figure 9.2 Horizontal translations in y-direction for specimen No. 2.

The effects of the lattice girders and the horizontal joint within the composite floor elements have not been taken into consideration in the modelling. Instead, the slab has been modelled as a solid homogenous concrete slab.

9.1.1 Geometrical specifications

The investigated corner supported element (illustrated in Figure 9.3) was supported on a square steel column of hollow section through a supporting steel plate projecting outside the column face. The geometrical specifications are presented in the Table 9-1. Reinforcement arrangements for the different models are presented in **Appendix IV**. The modelled element had the length a along its simply supported edge and the length b towards the interior support.

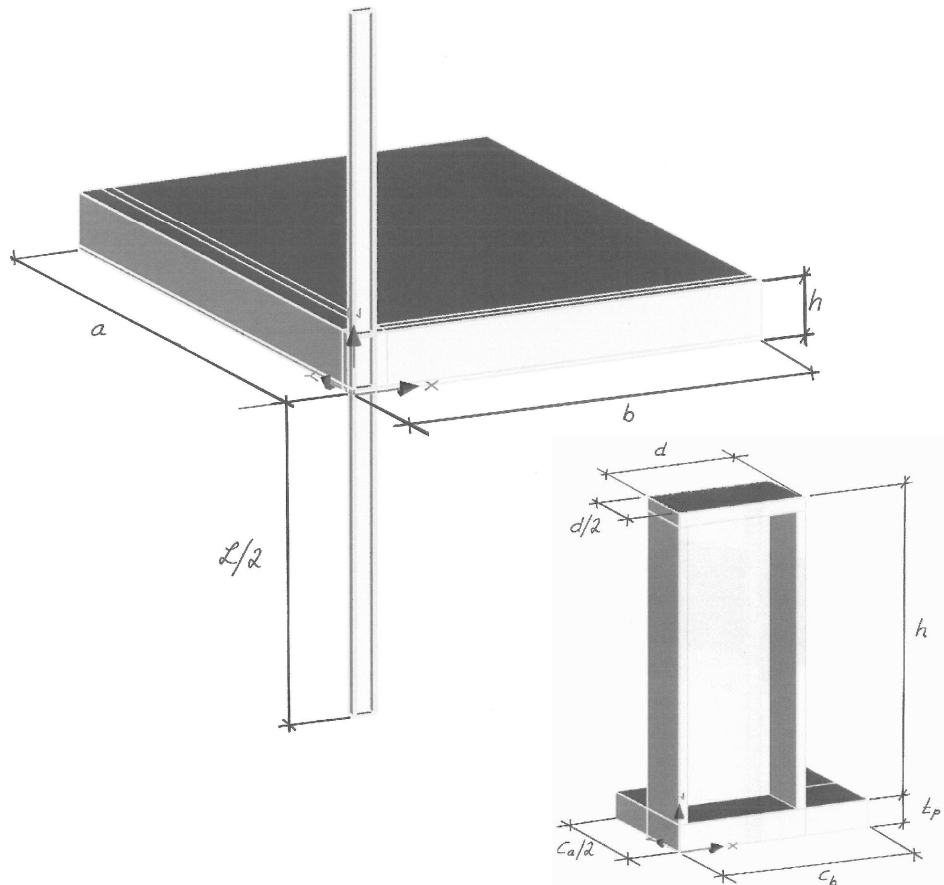


Figure 9.3 Geometry of investigated corner supported element. Note that the column and supporting steel plate are also cut at the symmetry in the x-z plane.

Table 9-1 Geometrical specifications of the investigated corner supported element.

Slab Element			Steel Column			Supporting Steel Plate		
a	b	h	d	t	L	c_a	c_b	t_p
[mm]	[mm]	[mm]	[mm]	[mm]	[mm]	[mm]	[mm]	[mm]
2500	1875	250	100	6.3	3000	200	150	20

9.1.2 Boundary conditions and loading

As the considered slab element is limited by the chosen bending moment peaks, rotations and translations have been prevented in the corresponding sections. In order to accurately place the boundary conditions at the inflection points located in the cavity of the columns, a rigid plate was added to the ends of the modelled columns. For the upper column, horizontal translation (x and y-direction) was prevented, whilst

the lower column was pinned, i.e. translations in all directions were prevented. Figure 9.4 illustrates the loading and boundary conditions that have been applied to the models.

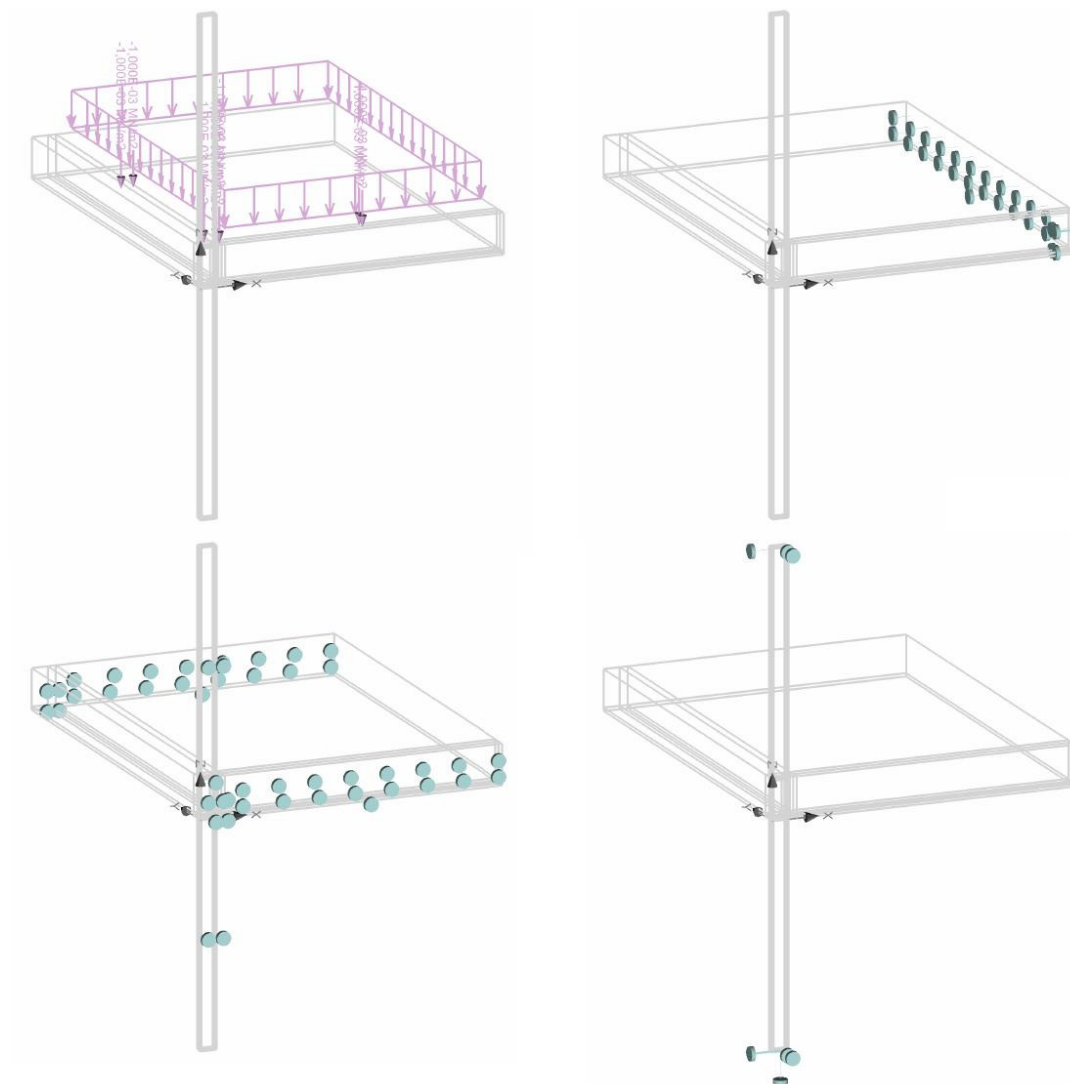


Figure 9.4 Loading and boundary conditions.

- (a) Distributed load, (b) Symmetry in x -direction,
(c) Symmetry in y -direction, (d) Column inflection points.

9.1.3 Material models

Material properties have been chosen in accordance to what has been described in Chapter 7. The basic parameters for the concrete strength class C30/37 and reinforcing steel of type B500B are presented in Table 7-1 and further specified in **Appendix II**. Unlike for specimen *No. 2*, the reinforcement model in specimen *R1* did not include strain hardening. Since the response from the simulation of specimen *R1* agreed better to the reported data than specimen *No. 2*, the reinforcement model in the investigations was chosen to bilinear without strain hardening.

Table 9-2 Basic parameters (mean values) for concrete and reinforcement.

Concrete					Reinforcement	
f_c [MPa]	f_t [MPa]	E [GPa]	G_F [N/m]	ε_{cp} [-]	f_y [MPa]	E_s [GPa]
38	2.9	32.8	96.7	$1.005 \cdot 10^{-3}$	500	210

The steel quality in the columns was assumed to have a yield strength f_y of 355 MPa and the same modulus of elasticity as for the reinforcing steel.

The contact between the concrete slab and the steel detailing of the connection was modelled with interface elements, where the transmittance of tensile stresses was prevented.

9.2 Modelling scheme

The aims of the simulations are chronologically listed below and the modelling scheme is presented in the following and describes the path along which the study elapsed.

1. Successful simulation of punching shear failure;
2. Conduct a mesh convergence study on the model that failed in punching;
3. Assess the influence of the reduced compressive strength as lateral tensile strains develop.

9.2.1 Simulation of punching shear failure

The investigation commenced with the analysis of the corner supported element, designed according to the Strip Method. The model is referred to as *A1* and the derivations for the reinforcement design are presented in **Appendix I**. During the analysis the steel columns were found to be the weakest members in the structure as buckling prior to any significant damage of the concrete slab was encountered. However, in order to attain information about the failure process in the concrete slab, the steel columns and the detailing of the connection were modelled with linear-elastic material responses excluding plastic behaviour (i.e. yielding).

The slab in model *A1* failed in bending. The investigation continued with yet another model, *A2*. In order to prevent flexural failure in the slab, model *A2* was provided with additional reinforcement bars between the previous, increasing the reinforced area in the critical section with 94%. The study of punching failure did not succeed for this model either and failure was also in this case determined to have been caused by bending. Placing additional bars was not feasible considering engineering practice. Thus for the third attempt *A3* the same reinforcement arrangement was kept as for model *A1*, although increasing all bar diameters to $\phi 16$. This measure was taken to

provoke failure of the slab in the region near the support and it corresponded to an increase of 156% for the contributing reinforcement area in the direction where bending failure had previously occurred. Figure 9.5 illustrates the alternative reinforcement arrangements in the three models A1, A2 and A3 and the corresponding amounts are presented in Table 9-3. For the three models bent bars were provided in order to ensure required anchorage for the bottom reinforcement perpendicular to the edge.

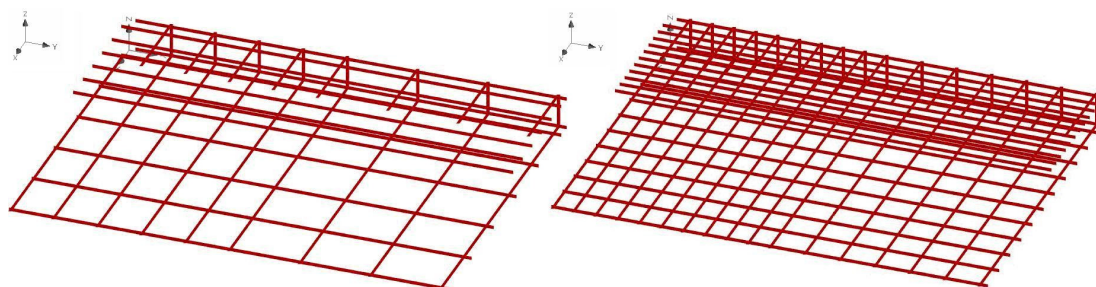


Figure 9.5 Left: Reinforcement arrangement used in models A1 and A3; Right: Reinforcement arrangement used in model A2. In all models the bar perpendicular to the simply supported edge along the symmetry in x - z plane was modelled with its half area.

Table 9-3 Reinforced section in the y - z plane for models A1, A2 and A3.

Model	Number of bars [-]	ϕ [mm]	$A_{s,x}$ [mm ²]	$A_{s,x.1}/A_{s,x.i}$
A1	9	10	668	100%
A2	17	10	1296	194%
A3	9	16	1709	256%

9.2.2 Mesh convergence study

As punching shear failure was achieved for model A3, a mesh convergence study was carried out in order to attain a proper mesh configuration with respect to punching shear. The original mesh configuration $M_{0.13}$ (which was used in models A1 and A2) was altered to a coarser ($M_{0.16}$ and $M_{0.26}$) and a finer ($M_{0.10}$) configuration. The indexes denote the assigned global mesh sizes⁵. The mesh configurations are presented in Figure 9.6 and Table 9-4.

⁵ The global mesh size [m] is the attempted size of the brick elements in a FE-mesh.



Figure 9.6 Mesh configurations for the mesh convergence study.

(a) $M_{0.10}$

(b) $M_{0.13}$

(c) $M_{0.16}$

(d) $M_{0.26}$

Table 9-4 Global element sizes and finite elements in the mesh convergence study.

Mesh configuration	$M_{0.10}$	$M_{0.13}$	$M_{0.16}$	$M_{0.26}$
Global element size [m]	0.100	0.130	0.160	0.260
Number of elements	11200	6864	4667	1631

For the mesh convergence study, the load-displacement responses have been assessed. The responses describe the column reaction versus the vertical displacement in the outermost point opposite the simply supported edge across the column for the four mesh configurations as presented in Figure 9.7. It can be seen that the finest mesh configuration $M_{0.10}$ captured many numerical deviations that were believed to not be of significant importance in the present study. By the mesh convergence study it could be concluded that the configuration $M_{0.13}$ was sufficient and fairly accurate. The response obtained from the configuration $M_{0.13}$ was smoother and representative for the structural events. Thus, in the further investigation the configuration denoted $M_{0.13}$ has been employed.

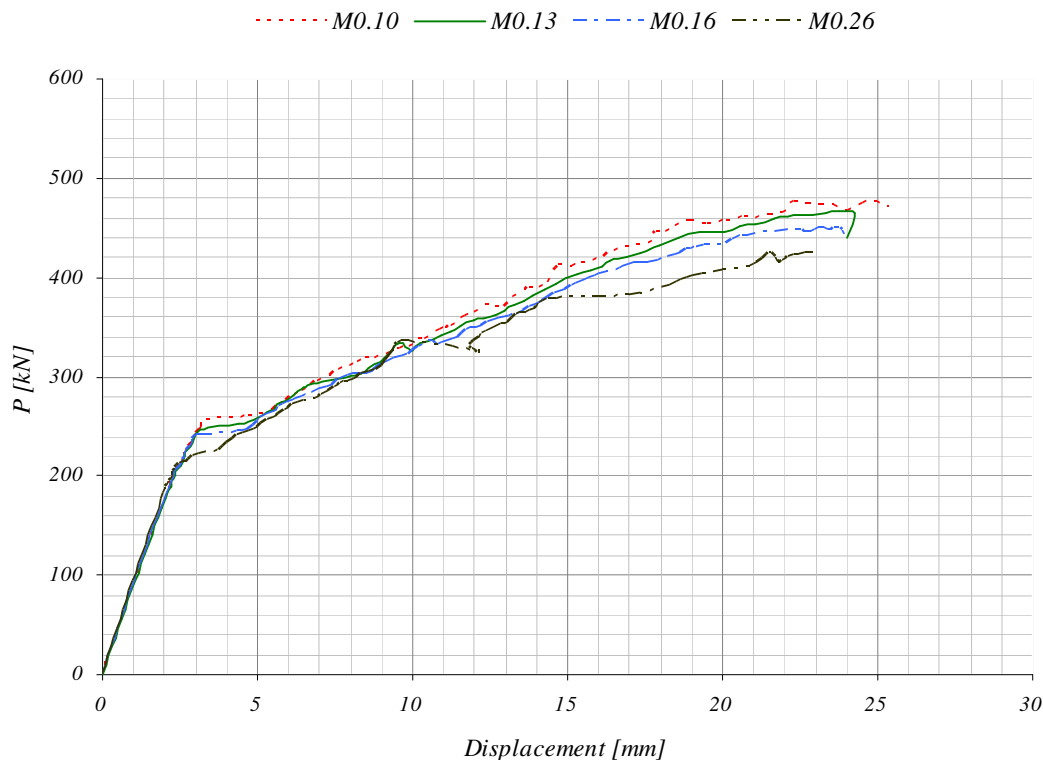


Figure 9.7 Load-displacement responses for the four mesh configurations used in the mesh convergence study.

9.2.3 Influence of the reduced compressive strength as lateral tensile strains develop

The effect of the new parameter in ATENA $r_{c,lim}$ was investigated on the model denoted A3. The effect of this parameter is of interest due to its correlation to shear cracking.

9.3 Results from FE-Analyses

Results from the investigations are presented by means of the here presented observations.

- Load-displacement responses present the vertical column reaction P in the lower column versus the vertical displacement in the outermost point opposite the simply supported edge across the column.
- In order to better correlate column reactions to load steps (LS), the loading histories are presented by plotting the column reactions at each load step.
- Residual errors for the convergence criteria are presented in **Appendix VI**.
- In order to represent the deflection of the slab, displacement curves have been plotted along the simply supported edge and also across the symmetry line in the direction perpendicular to the edge for several levels of column force P .
- The evolution of crack patterns throughout loading reflects the structural responses and indicates where the structure is strained. For the detailed assessment of failure cause, the concrete state of stresses and strains has been studied in the region close to the column. Microcracks are assumed to be smaller than 0.05 mm and are not always illustrated.
- Reinforcement stresses and strains indicate where extensive concrete damage is to be expected.

The illustrations are oriented such that they are viewed from the column support. The simply supported edge of the slab is parallel to the y -axis and the z -axis starts in level of the bottom surfaces of the slab and the supporting steel plate. In the following illustrations the edge (y -axis) is to the left and the symmetry across the support (x -axis) is to the right.

9.3.1 Analysis of *A1*

The load-displacement response of model *A1* clearly indicated bending failure of the slab in the span perpendicular to the edge as the final path of the curve constituted a plateau with increasing displacement at a constant load level. It was concluded that the reinforcement reached yielding and a mechanism was formed, slowly resulting in a loss of load-bearing capacity. As the response showed bending failure, the analysis was interrupted, although larger displacement than the one shown in Figure 9.8 could be expected. The loading history is presented in Figure 9.9.

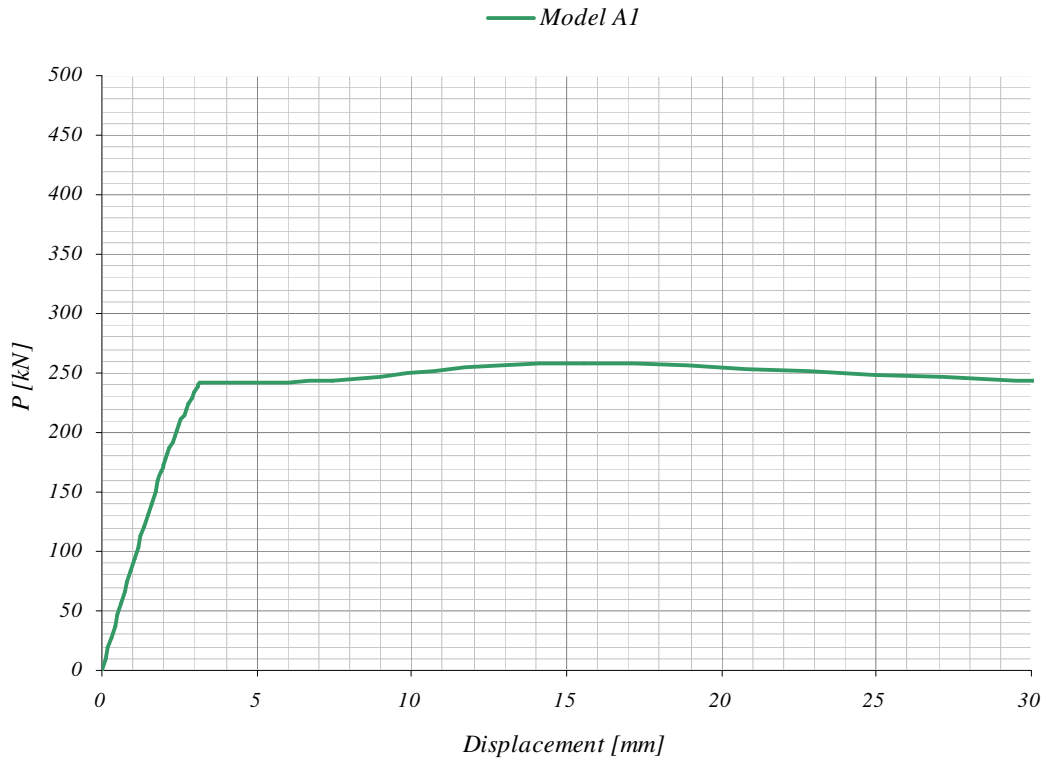


Figure 9.8 Column reaction P versus displacement for model A1.

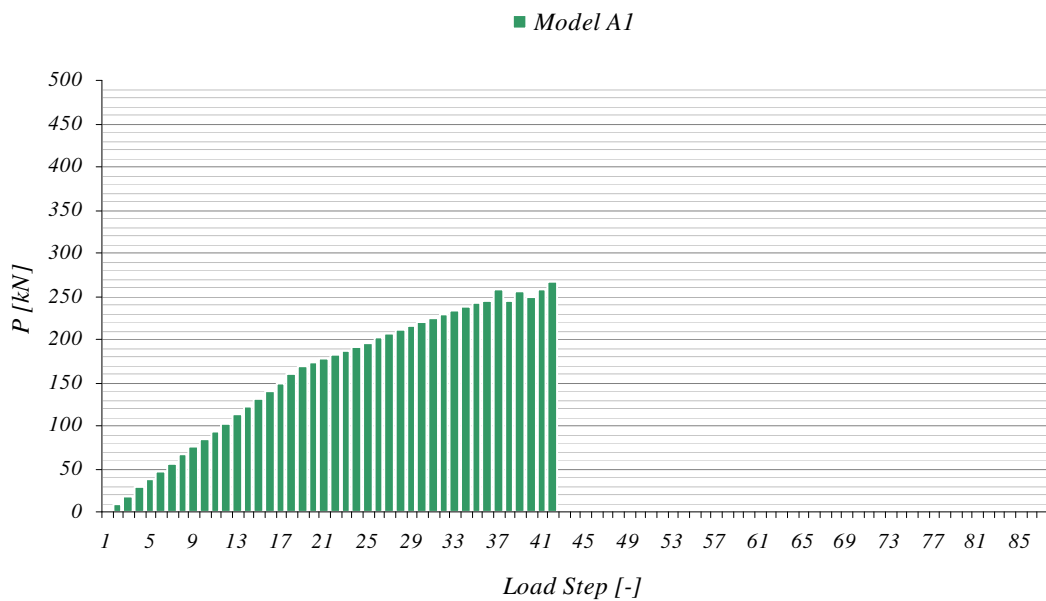


Figure 9.9 Column reaction at each load step in the analysis of model A1.

As the slab started to have a plastic response, large convergence errors were encountered. The difficulties to obtain convergence in the FE-analysis are believed to depend on the instability caused by the formation of large cracks along the yield line. The convergence errors (presented in **Appendix VI**) indicate that the errors exceeded 5% between load steps 35 and 40.

The crack propagation is presented in Figure 9.10. The first microcracks appeared above the column in the top surface of the slab at a column load of 37 kN. The direction of the microcracks showed that the cracks were the effect of hogging moment in the direction parallel to the edge. After further loading, the widths of the microcracks increased at a column load of 94 kN. Cracking propagated downwards the slab as the column reaction approached 170 kN, about the load level when the cracks first became visible. Flexural microcracks caused by sagging moment were first formed at a column load of 242 kN. The cracks were located in the middle of the span perpendicular to the edge and are indicated by the shaded areas in the figure. During further loading the largest cracks were found in proximity to the column. However, at a load of 258 kN these cracks were exceeded by the cracks in the span that extended swiftly up the thickness of the slab. When the column reaction reached 255 kN the cracks in the mid span were extended throughout the entire thickness of the slab and the first shear cracks were formed near the column in the strip perpendicular to the edge. The shear cracks started from the bottom of the column-slab intersection and had a course perpendicular to the edge. The inclinations of shear cracks were estimated to between 30° and 45°. As the slab reached failure at a load of 267 kN, several regions of the slab were extensively cracked and the largest cracks in the span perpendicular to the edge were about 10 mm. Notable were the tangential cracks at the top surface of the slab.

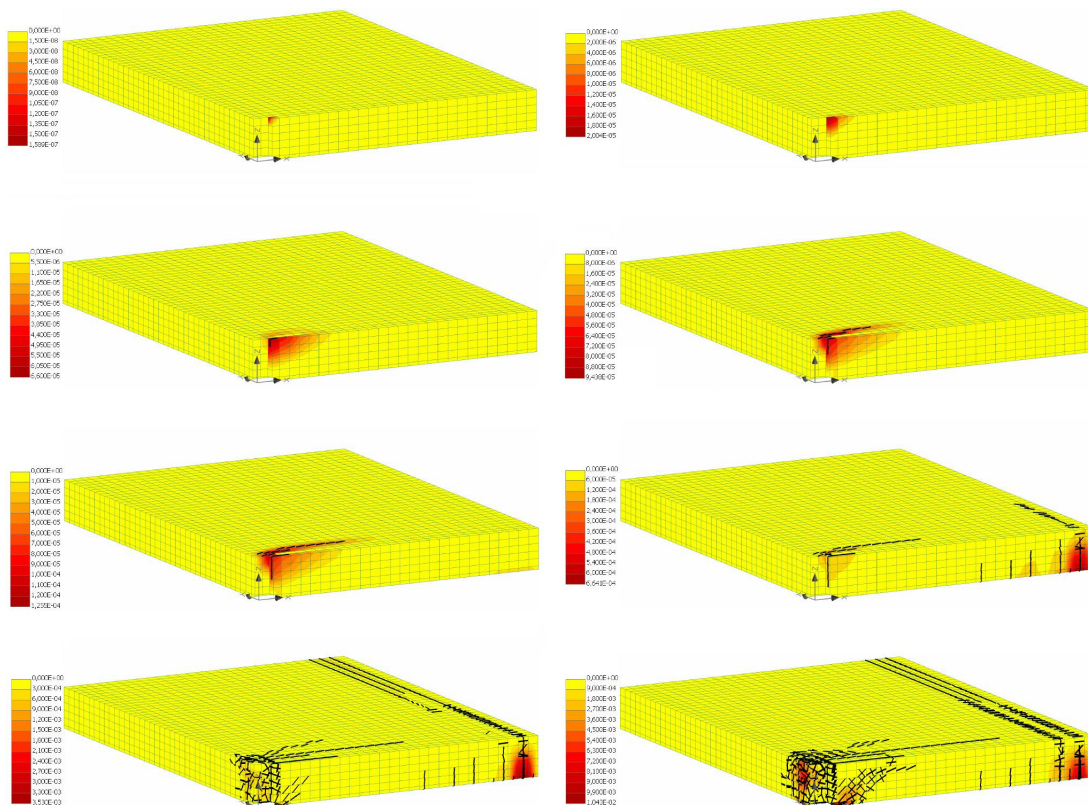


Figure 9.10 Propagation of cracks (>0.05 mm) plotted against crack widths [m].

- | | |
|-------------------------|-------------------------|
| (a) $P=37$ kN (LS 4), | (b) $P=94$ kN (LS 10), |
| (c) $P=168$ kN (LS 18), | (d) $P=215$ kN (LS 28), |
| (e) $P=242$ kN (LS 34), | (f) $P=258$ kN (LS 36), |
| (g) $P=255$ kN (LS 38), | (h) $P=267$ kN (LS 41). |

When cracking in the mid span commenced, the stresses in the reinforcement were increased markedly. An increase of stresses was also detected in the bars above the column at a column force of 255 kN. However, the presence of plastic strains indicated that a yield line was only developed in the bars in the mid span perpendicular to the edge and the flexural resistance of this section was critical for the failure of the slab. The stresses and strains in the reinforcement as the slab approached failure are illustrated in Figure 9.11.

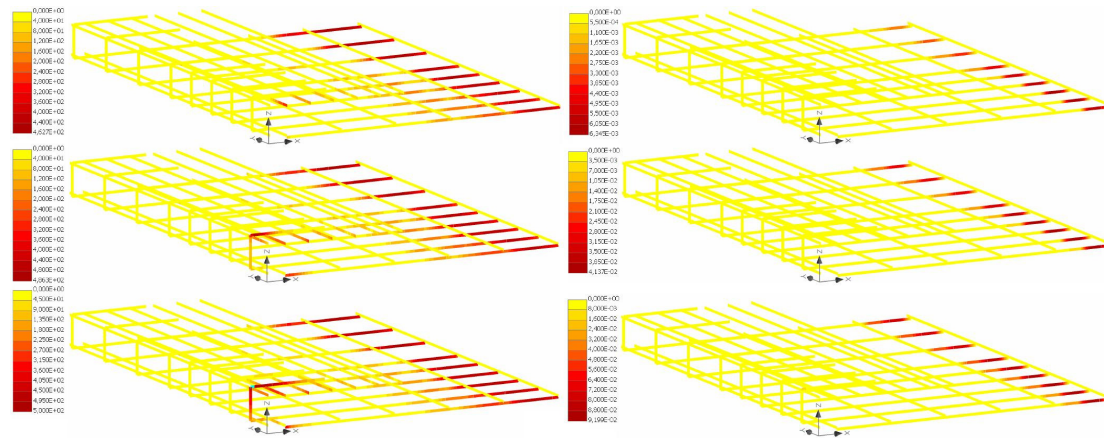


Figure 9.11 Left: principal stresses [MPa]; right: principal plastic strains [-].

(a) $P=258$ kN (LS 36),

(b) $P=255$ kN (LS 38),

(c) $P=267$ kN (LS 41).

Yielding of the reinforcement and the progressive cracking was followed by crushing of the concrete in vicinity of the column. This process is illustrated in Figure 9.12. The crushing process started at a column load of 255 kN, corresponding to the extensive crack propagation in Figure 9.10 (g). As the slab reached failure, at a column reaction between 249 kN and 267 kN, this zone with damaged concrete increased and involved both the top and bottom surface of the slab. The crushing is believed to have been caused by the yield line inducing redistribution of forces and the support region became highly strained.

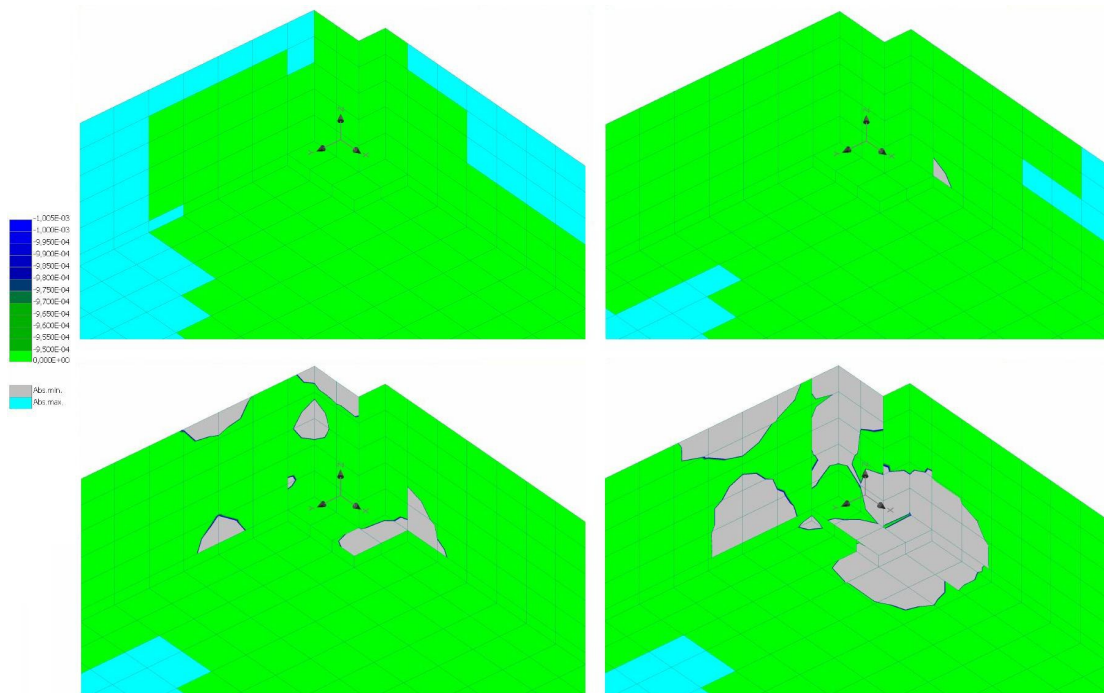


Figure 9.12 Principal plastic strains [-] indicate concrete crushing (grey regions) in the vicinity of the column.

- (a) $P=258 \text{ kN}$ (LS 36), (b) $P=255 \text{ kN}$ (LS 38),
(c) $P=249 \text{ kN}$ (LS 39). (d) $P=267 \text{ kN}$ (LS 41).

Under successive loading the slab deformed analogously in both directions. It was observed that the steel plate followed the end rotation of the slab in the direction perpendicular to the edge. The deformed shapes throughout the loading are illustrated in Figure 9.13. At a load of 258 kN when yielding in the mid span dominated the structural response, the deflection was concentrated in the strip perpendicular to the slab's edge.

The deformation of the slab followed the expected curvature until bending failure was approaching, which signifies that the boundary conditions were assumed reasonably. Furthermore, the obtained response showed that for the actual reinforcement amount and detailing the ultimate load was determined by bending failure in the span perpendicular to the edge. In order to provoke punching shear failure the reinforcement amount had to be increased.

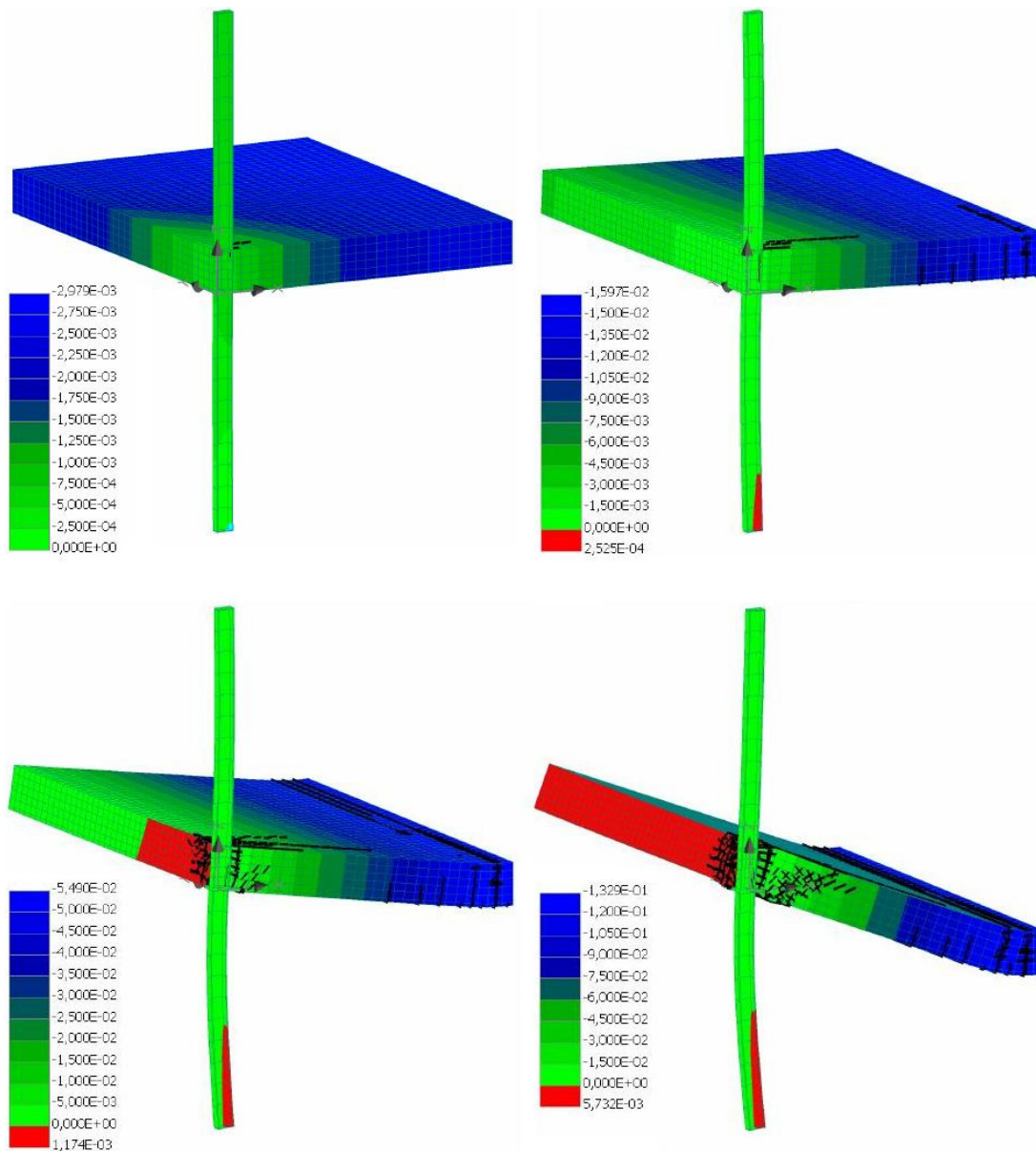


Figure 9.13 Deformed shapes (magnified by a factor 5) of the slab plotted against vertical displacement [m], cracks >0.05 mm are illustrated.

- (a) $P=201$ kN (LS 25), (b) $P=258$ kN (LS 36),
(c) $P=255$ kN (LS 38), (d) $P=267$ kN (LS 41).

9.3.2 Analysis of A2

As no punching failure occurred in model A1, the amount of reinforcement had to be increased which brought forth model A2. The same bar diameters as for model A1 were employed, although the reinforced section was increased by halving the bar spacing. The load-displacement response for model A2 (Figure 9.14) did however clearly indicate flexural failure and it was concluded that the reinforcement amount was still not enough to provoke punching failure. The model reached failure along the same critical section as for A1 but for a higher load. The loading history for model A2 is presented in Figure 9.15.

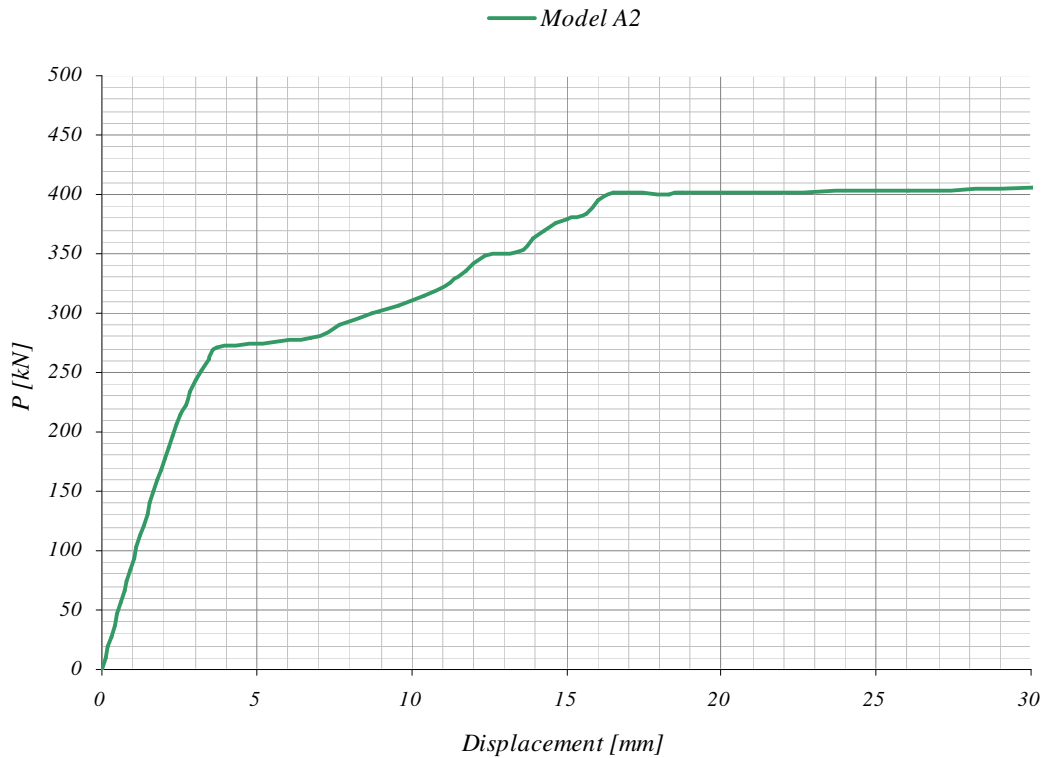


Figure 9.14 Column reaction P versus displacement for model A2.

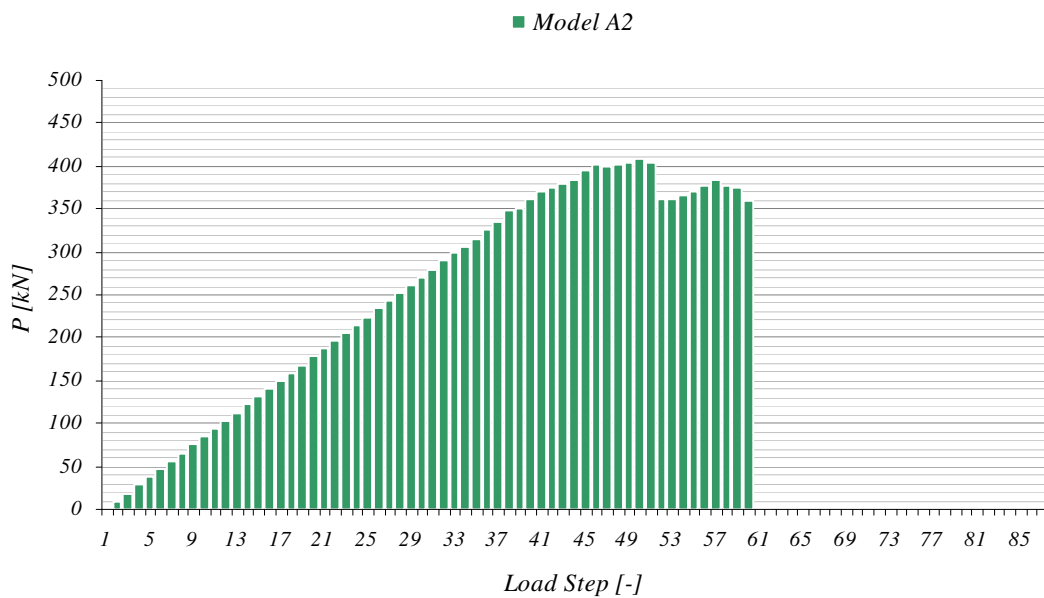


Figure 9.15 Column reaction at each load step in the analysis of model A2.

Although failing in bending as model A1 the slab's response showed a significant stiffness decrease ($P \sim 270$ kN) prior to the yielding plateau. The crack pattern (Figure 9.16) illustrates that a first plateau was initiated as flexural cracks propagated. A redistribution of forces seems to have been taken place as shear cracks were formed above the column, which limited the deformations in the span. In addition to the crack pattern showing the largest cracks along the critical section in the span perpendicular

to the edge, the reinforcement stresses and strains (illustrated in Figure 9.17) confirm that failure was caused by bending.

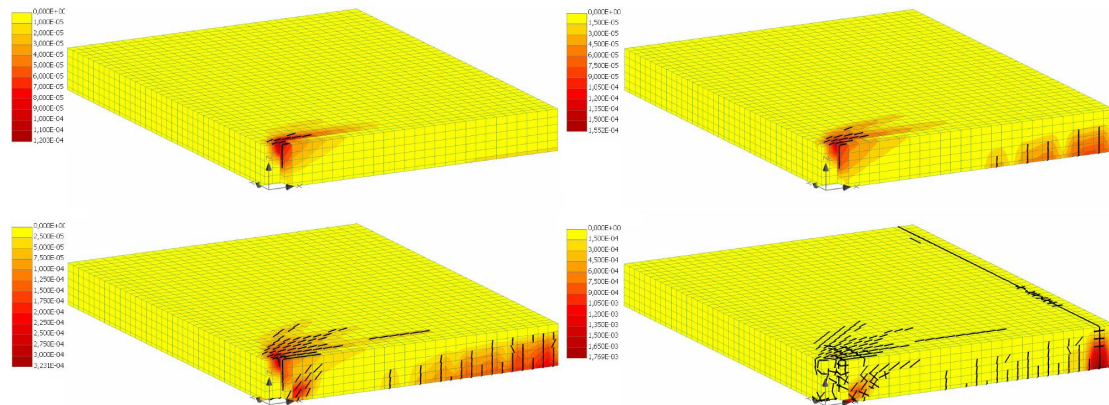


Figure 9.16 Propagation of cracks (>0.05 mm) plotted against crack widths [m].

- (a) $P=261$ kN (LS 28), (b) $P= 279$ kN (LS 30),
(c) $P=401$ kN (LS 45), (d) $P= 404$ kN (LS 50).

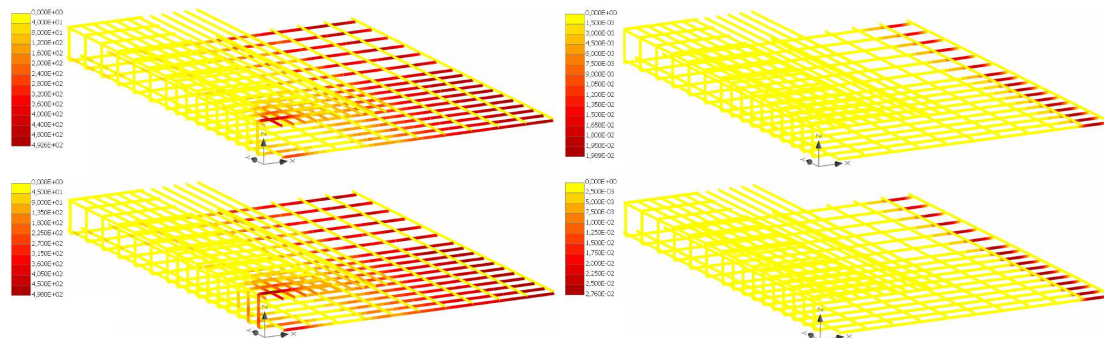


Figure 9.17 Left: principal stresses [MPa]; right: principal plastic strains [-].

- (a) $P= 404$ kN (LS 50),
(b) $P=377$ kN (LS 55).

9.3.3 Analysis of A3

The reinforcement in model A3 was arranged as for model A1, although the bottom reinforcement in the direction perpendicular to the edge consisted of $\phi 16$ bars. As the model succeeded to simulate punching failure a mesh convergence study was carried out in order to guarantee satisfying accuracies for the results as no test data were available for comparison. The load-displacement response is presented in Figure 9.18, where the sudden decrease of load-bearing capacity for a column force of 470 kN depended on a punching shear failure. Unlike for the FE-analyses of specimens R1 and No. 2 difficulties were encountered when attempting to capture the post-peak

behaviour. The main events are denoted as (A) to (D) in the graph and the column reaction at each load step can be ascertained from Figure 9.19.

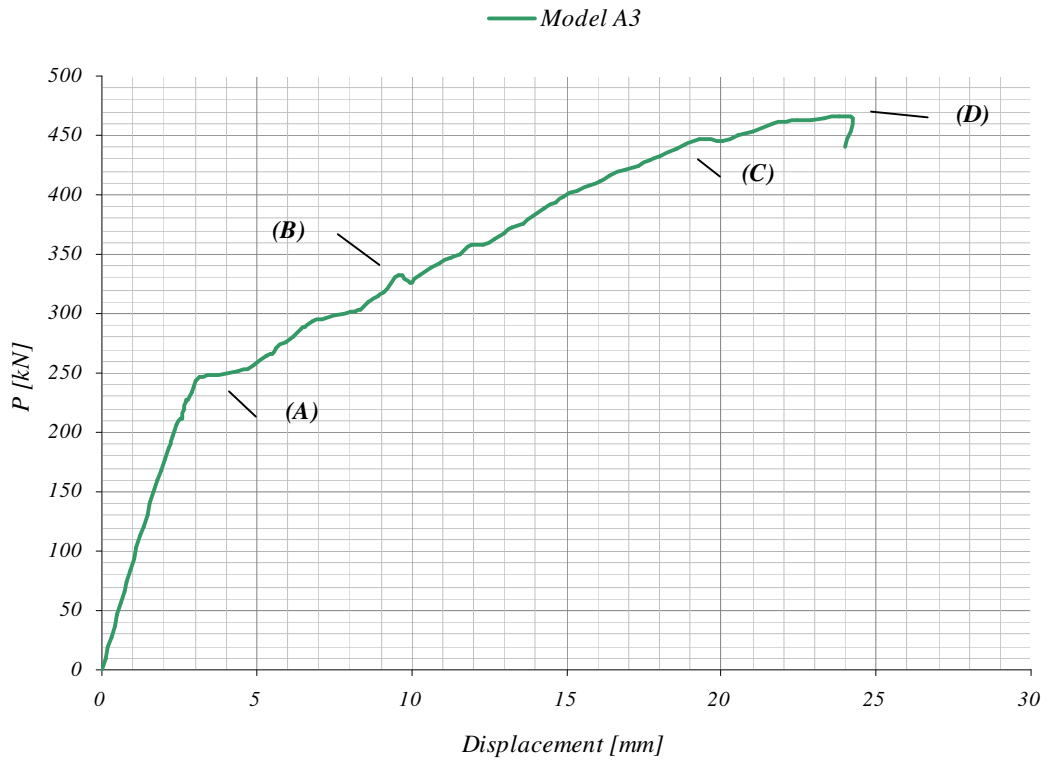


Figure 9.18 Column reaction P versus displacement for model A3.

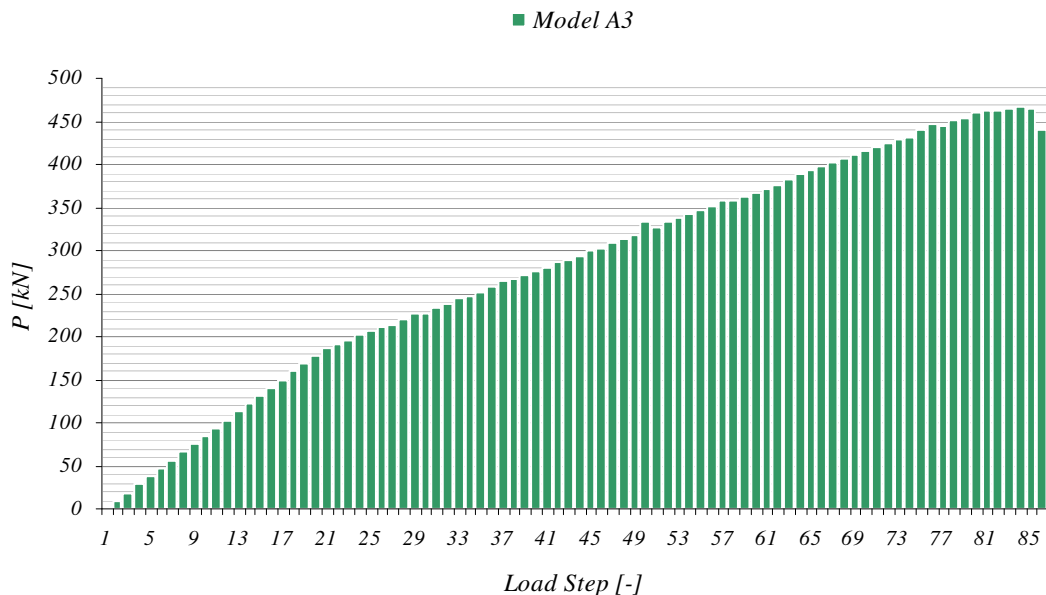


Figure 9.19 Column reaction at each load step in the analysis of model A3.

To begin with the displacements increased linearly with the applied load. The initial crack development in the concrete slab is illustrated in Figure 9.20. The first flexural cracks appeared due to hogging moment above the column in the strip along the edge.

At a column load of 37 kN they were only microcracks indicated by the shaded areas, whilst visible when the column reaction reached 178 kN. After further loading the cracks continued to increase at the top surface of the slab.

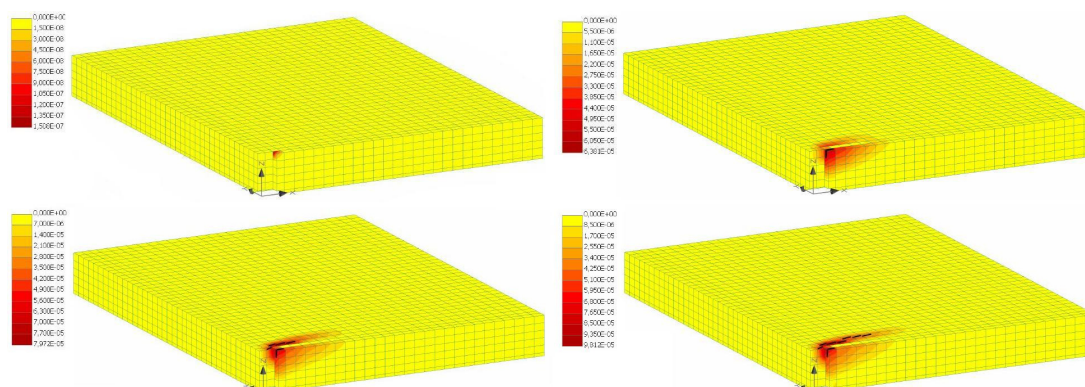


Figure 9.20 Propagation of flexural cracks (>0.05 mm) above column plotted against crack widths [m].

- (a) $P=37$ kN (LS 4), (b) $P=178$ kN (LS 19),
(c) $P=206$ kN (LS 24), (d) $P=226$ kN (LS 28).

The linear relation between load and displacement was interrupted at event (A). The stiffness of the structure decreased due to the formation of deep flexural cracks in the span perpendicular to the edge as illustrated in Figure 9.21. This occurred when the column load increased from 247 kN to 252 kN. Furthermore, the cracks above the column developed further down the column face through the thickness of the slab.

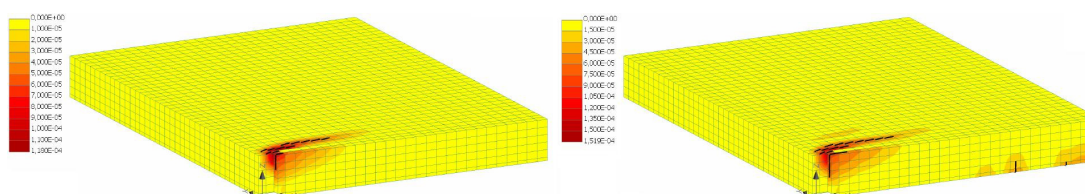


Figure 9.21 Propagation of flexural cracks (>0.05 mm) in field at event (A) plotted against crack widths [m].

- (a) $P=247$ kN (LS 33), (b) $P=252$ kN (LS 34).

The response between events (A) and (B) depends on the stiffness in the cracked state. The peak at event (B) is believed to be caused by the first significant shear crack that appeared when the column reached about 330 kN. The crack had its root at the supporting steel plate and had an inclination of about 45° . The crack patterns at event (B) are illustrated in Figure 9.22.

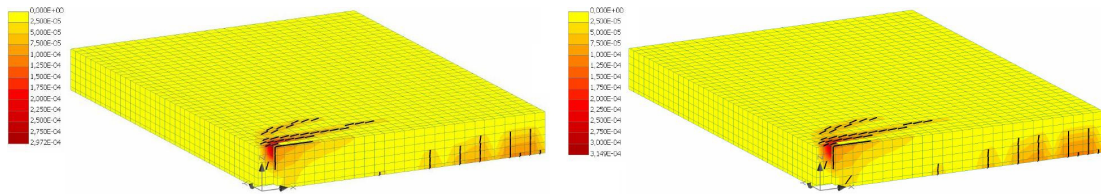


Figure 9.22 Propagation of shear cracks (>0.05 mm) adjacent to the supporting steel plate at event (B) plotted against crack widths [m].

(a) $P=318$ kN (LS 48), (b) $P=333$ kN (LS 49).

Further loading caused the initiation of failure around event (C). The concrete above the support experienced progressive crushing between events (C) and (D). The reduction of the stiffness at event (C) is believed to be caused by the crushing process and the extension of horizontal cracks at the bottom surface of the slab. Crushing of the concrete above the supporting steel plate began in the intersection between the steel plate and the column stud at a column reaction of 416 kN. The crushed area grew for a small load increase as illustrated by Figure 9.23.

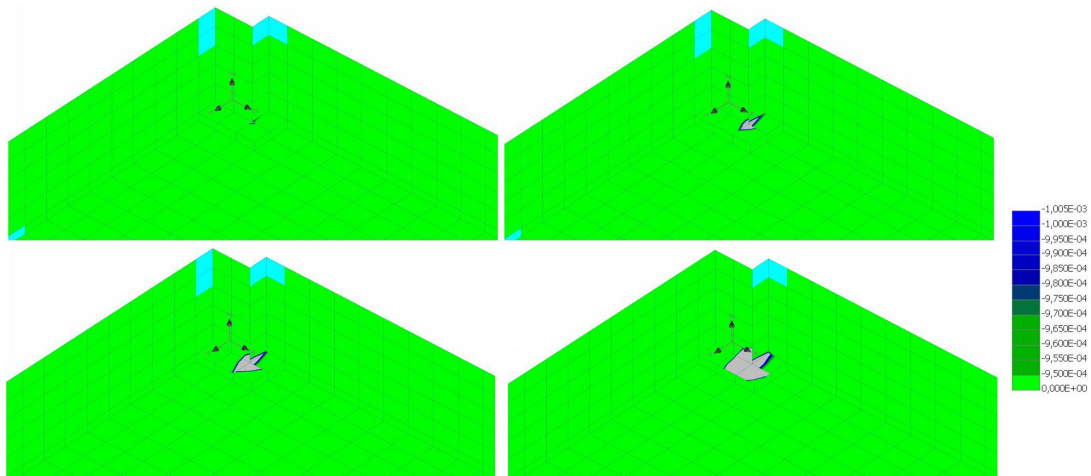


Figure 9.23 Principal plastic strains [-] indicate concrete crushing (grey regions) above the supporting steel plate at event (C).

(a) $P=416$ kN (LS 69), (b) $P=424$ kN (LS 71),
(c) $P=432$ kN (LS 73), (d) $P=451$ kN (LS 77).

The area around the column experienced a triaxial state of compression up to a column load of 451 kN. The impairment of the triaxially compressed zone is illustrated in Figure 9.24 where the visible cracks are indicated.

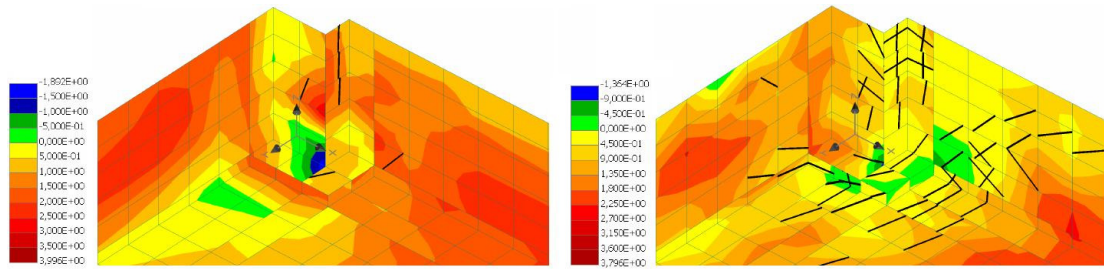


Figure 9.24 Principal tensile stresses [MPa] at event (C), negative values (blue areas) indicate triaxial compression.

(a) $P=333\text{ kN}$ (LS 49), (b) $P=451\text{ kN}$ (LS 77).

The damaged concrete region grew as crushing of the concrete outside the steel plate began at a column reaction of 451 kN, starting in a small area adjacent to the column face perpendicular to the edge. This area increased upwards and eventually towards the corner of the support plate. At the ultimate load, the crushed region had spread along the periphery of the support. The propagation of concrete damage outside the supporting steel plate is illustrated by Figure 9.25.

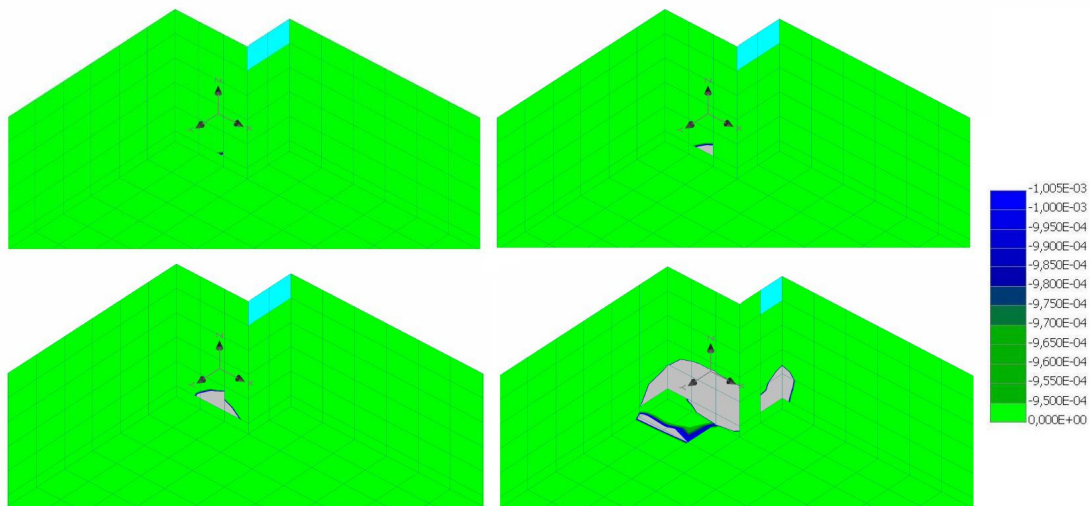


Figure 9.25 Principal plastic strains [-] indicate concrete crushing (grey regions) outside the supporting steel plate at event (D).

(a) $P=451\text{ kN}$ (LS 77), (b) $P=459\text{ kN}$ (LS 79),
(c) $P=463\text{ kN}$ (LS 81), (d) $P=440\text{ kN}$ (LS 85).

As the concrete plasticised around the column eventually causing the crushing process, the steel stresses in the reinforcement increased. The stresses and plastic strains in the reinforcement are presented in Figure 9.26. At a column load of 467 kN the reinforcement reached the yield stress in the critical section in the span perpendicular to the edge. Plastic strains were developed in some bars, although a yield line was not formed as in the previous models. Thus, bending failure could be excluded.

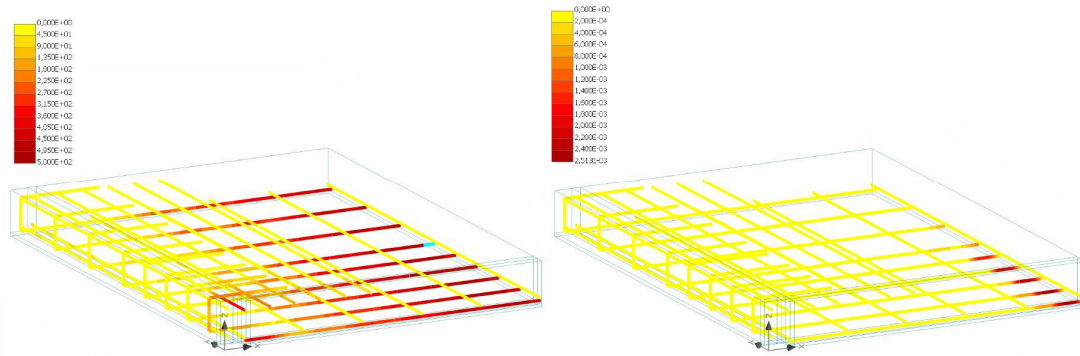


Figure 9.26 Left: principal stresses [MPa]; right: principal plastic strains [-] at $P=467$ kN (LS 83) corresponding to event (D).

Event (D) denominates the final collapse (when the column reaction reached 440 kN) that seemed to be caused by the formation of tangential cracks around the column downwards the slab section to the already damaged concrete area in the region near the column parallel to the edge. The largest cracks on the bottom surface, adjacent to the plate, approached 4 mm. The crack propagation is illustrated in Figure 9.27.

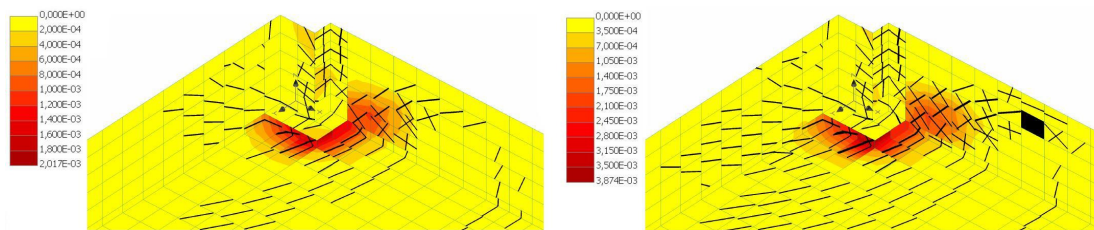


Figure 9.27 Propagation of tangential cracks at failure.

(a) $P=467$ kN (LS 83), (b) $P= 440$ kN (LS 85).

The concrete region outside the steel plate, in the direction perpendicular to the slab's edge experienced an expansion of the triaxial state of compression when the structure approached failure. This seems to have been caused when a crack reached the triaxial compressive zone in the region along the edge and impaired the capacity of the compressed zone. The region of triaxial compression grew in the other direction as the slab here compensated for the loss of capacity along the edge.

The loss of resistance in both directions resulted in structural failure. The crack pattern clearly indicated that failure was caused by punching due to the concentration of large cracks around the column. In order to establish an idea about the punching cone, the vertical strains were analysed in proximity to the column. The vertical strains along the thickness of the slab and at the bottom of the slab are shown in Figure 9.28. At the bottom of the slab the vertical strains were present outside the supporting steel plate. Notable was that, apart from the bottom surface, strains were only found in the slab strip perpendicular to the edge. The deformed shape of the slab at failure is shown in Figure 9.29.

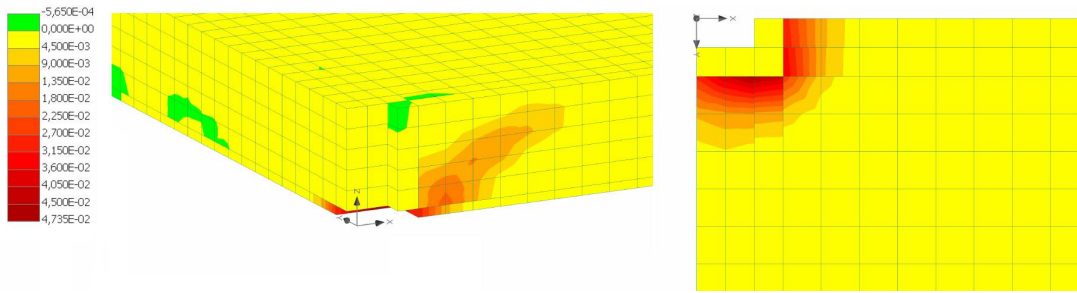


Figure 9.28 Vertical strains at failure, $P \sim 440$ kN.

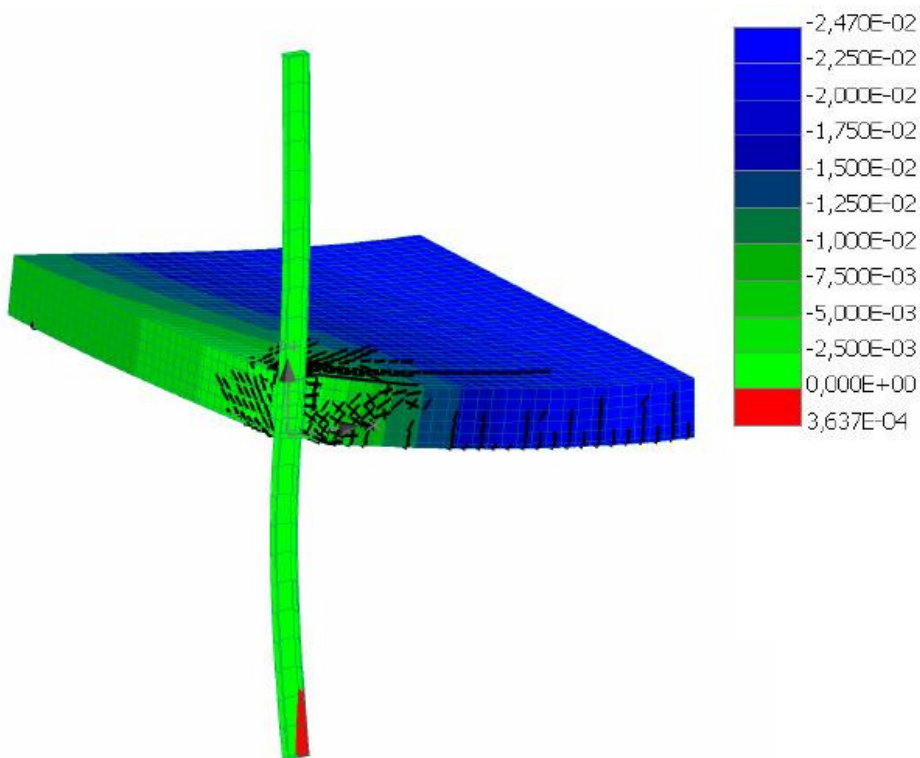


Figure 9.29 Deformed shape (magnified by a factor 10) of the slab plotted against vertical displacement [m], cracks >0.05 mm are illustrated.

9.3.4 Influence of the parameter $r_{c,lim}$ on model A3

The parameter $r_{c,lim}$ that governs the reduction of compressive strength due to the presence of lateral tensile strain was not activated for the previous models. In order to determine whether this parameter has any significant influence on the results, this feature was later activated in model A3 and compared to its previous results. As seen in Figure 9.30, the parameter $r_{c,lim}$ while cracking propagates is of little influence. However the load at which the slab suffers failure in punching is somewhat lower.

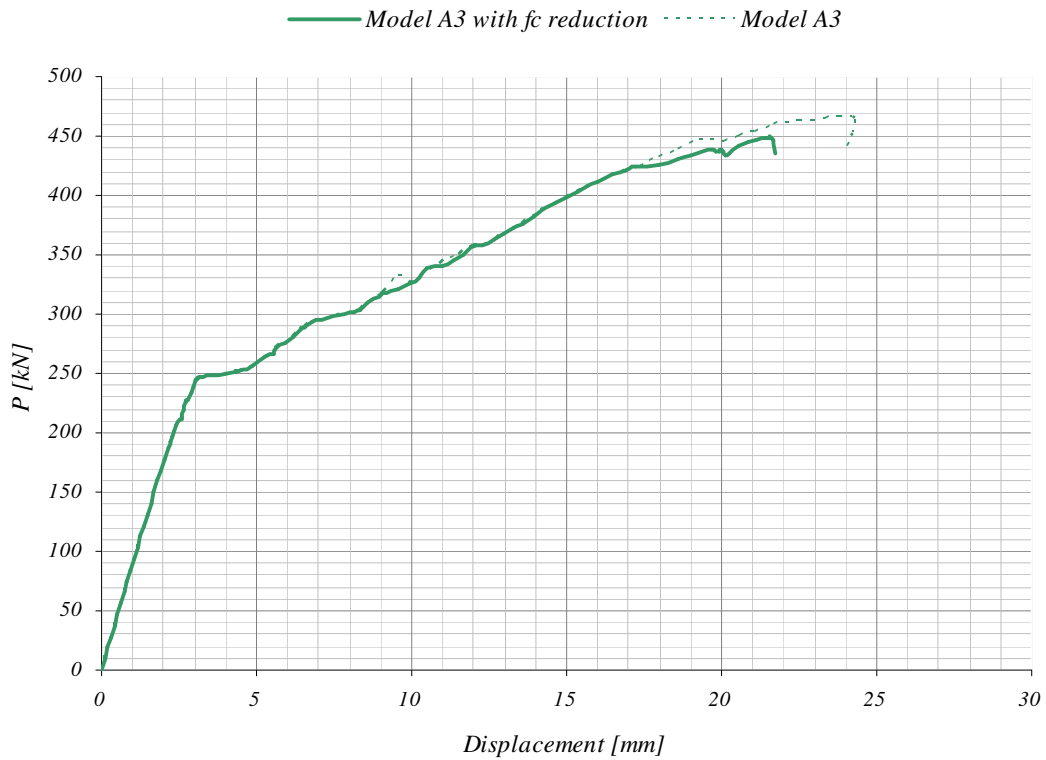


Figure 9.30 Column reaction P versus displacement for model A3 with and without the reduction of the compressive strength due to lateral tensile strain activated.

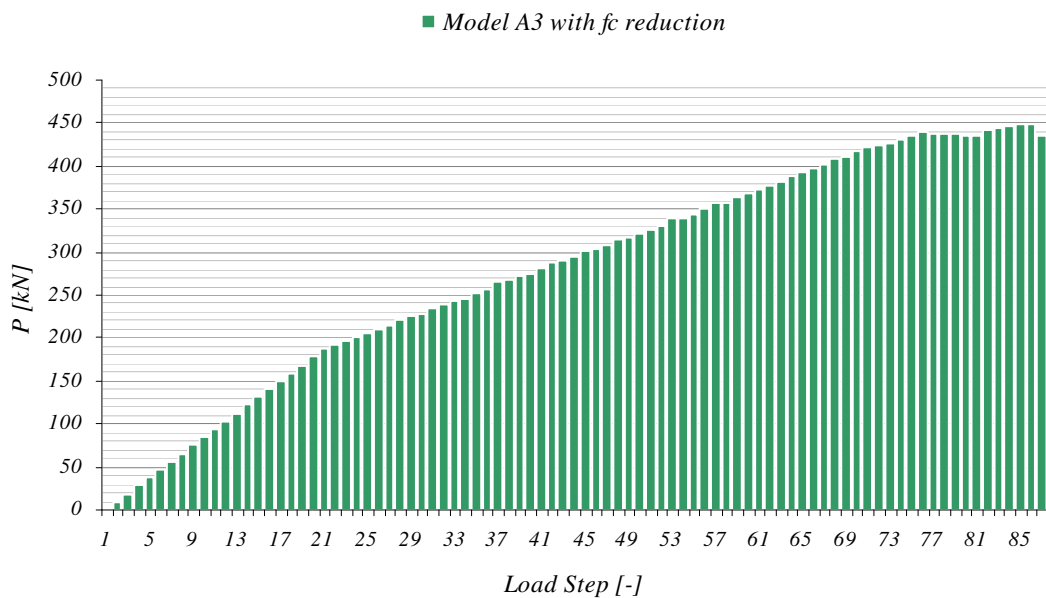


Figure 9.31 Column reaction at each load step in the analysis of model A3 with $r_{c,lim}$ activated.

After a thorough study of the crack propagation, it was noted that considering the compressive strength's dependency on lateral tensile strains had no influence on cracking. The deviation between the two load-displacement curves at a load level of

320 kN is believed to be a numerical error as the crack propagation was identical for model A3 and A3 with reduced compressive strength. However, the parameter $r_{c,lim}$ showed a big influence on the crushing progress.

The progressive crushing for model A3 was illustrated in Section 9.2.3. A similar process is shown in Figure 9.32 and Figure 9.33 for the model where $r_{c,lim}$ was activated. When comparing the two models it was discovered that crushing was initiated earlier in the model where $r_{c,lim}$ was activated and the region around the column was more severely cracked at failure.

As the crushing progress is closely correlated to the failure mode, the activation of the parameter $r_{c,lim}$ reduced the maximum load and is therefore concluded to model punching shear failure more appropriately. However, as the difference between the maximum loads is rather small (4.4%), neglecting the compressive strength's dependency on lateral tensile strains still gives a fairly representative simulation of the failure mode.

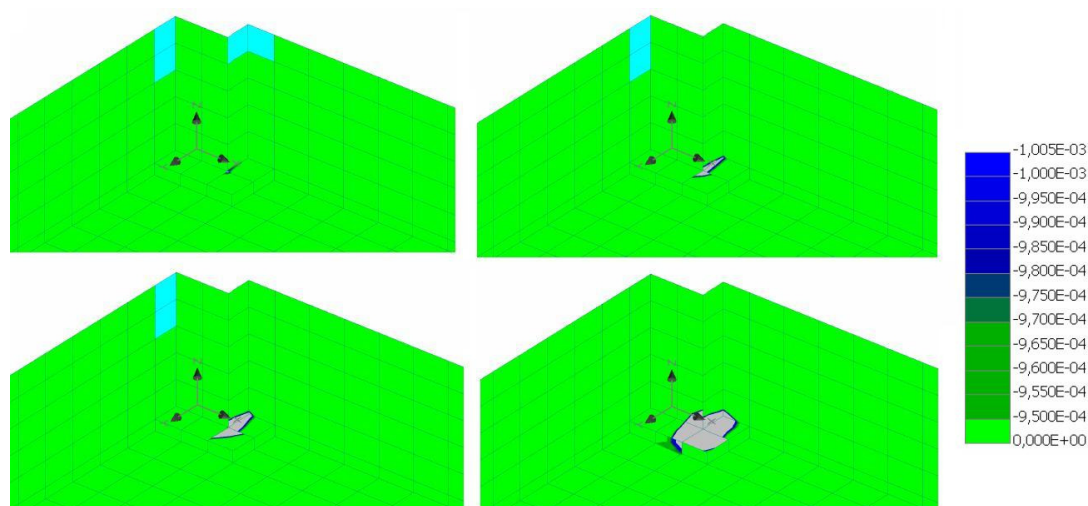


Figure 9.32 Principal plastic strains [-] indicate concrete crushing (grey regions) above the supporting steel plate.

(a) $P=411$ kN (LS 68),

(b) $P= 417$ kN (LS 69),

(c) $P= 421$ kN (LS 70),

(d) $P=431$ kN (LS 73).

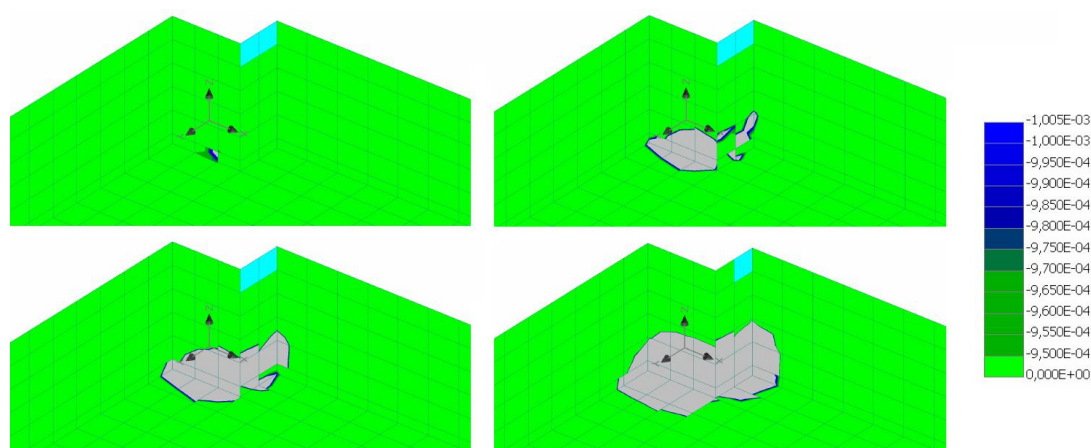


Figure 9.33 Principal plastic strains [-] indicate concrete crushing (grey regions) outside the supporting steel plate.

- (a) $P=431$ kN (LS 73), (b) $P=438$ kN (LS 77),
(c) $P=442$ kN (LS 81), (d) $P=436$ kN (LS 86).

9.4 Comments on results

In light of the previously presented results from FE-analyses the main observations from the four simulations are summarised in this section.

9.4.1 Models failed in bending, A1 and A2

The simulated loadings of model A1 and model A2 ceased by bending failure, nevertheless the crack pattern above the column support showed the influence of shear. Initially, the slab strip in the perpendicular direction to the edge behaved analogously to simply supported beams subjected to shear forces as cracks propagated from the bottom face upwards the slab with an inclination of about 45° . However, the propagation of tangential cracks from the top surface of the slab parallel to the edge depicted that the behaviour of the strip perpendicular to the simply supported edge was somewhat more complex than the assumed beam analogy. The tangential cracks might be an effect of restraint in this direction. The restraint is most likely a consequence of compatibility as a hogging moment occurred in the parallel direction. The concrete damage that was observed above the steel column in the top part of the slab might indicate that spalling occurred. As a yield line was formed in the mid span, redistribution of moment capacity caused a stress concentration above the support. Even if punching failure was not achieved, the models A1 and A2 gave valuable information regarding boundary conditions and structural response for the case study. Consequently during loading, the deformed shapes of the slab illustratively confirmed the relevance of the boundary conditions. The appointed contact elements between the concrete slab and the support plate resulted in the sought response, as the slab could separate from the supporting steel plate and the hollow steel profile under deformation.

9.4.2 Model failed in punching, A3

Compared to the required flexural reinforcement according to the Strip Method, it was found that more than twice this area was needed in order to provoke punching shear failure. The observations regarding the failure mode of model A3 that suffered punching failure are described in the following. Punching failure was identified as concrete crushing around the perimeter delimited by the supporting steel plate was observed. The crushing seemed to have been preceded by the formation of cracks with horizontal plane. The horizontal cracking is believed to correspond to the splitting of concrete that was observed by Marinković and Alendar (2008). The cracks appear to have resulted in a redistribution of stresses above the supporting steel plate. Prior to the propagation of horizontal cracks, the triaxially compressed zone was found in the region around the column closest to the edge. The state of triaxial compression was impaired as cracking approached this zone. In order to compensate for the impaired compressed conical shell the region across the edge suffered increased triaxial compression. Also the zone to which the redistribution was addressed would later experience concrete crushing, leading to final collapse of the structure as the column punched through. What is believed to be the cause of failure is summarised in Figure 9.34.

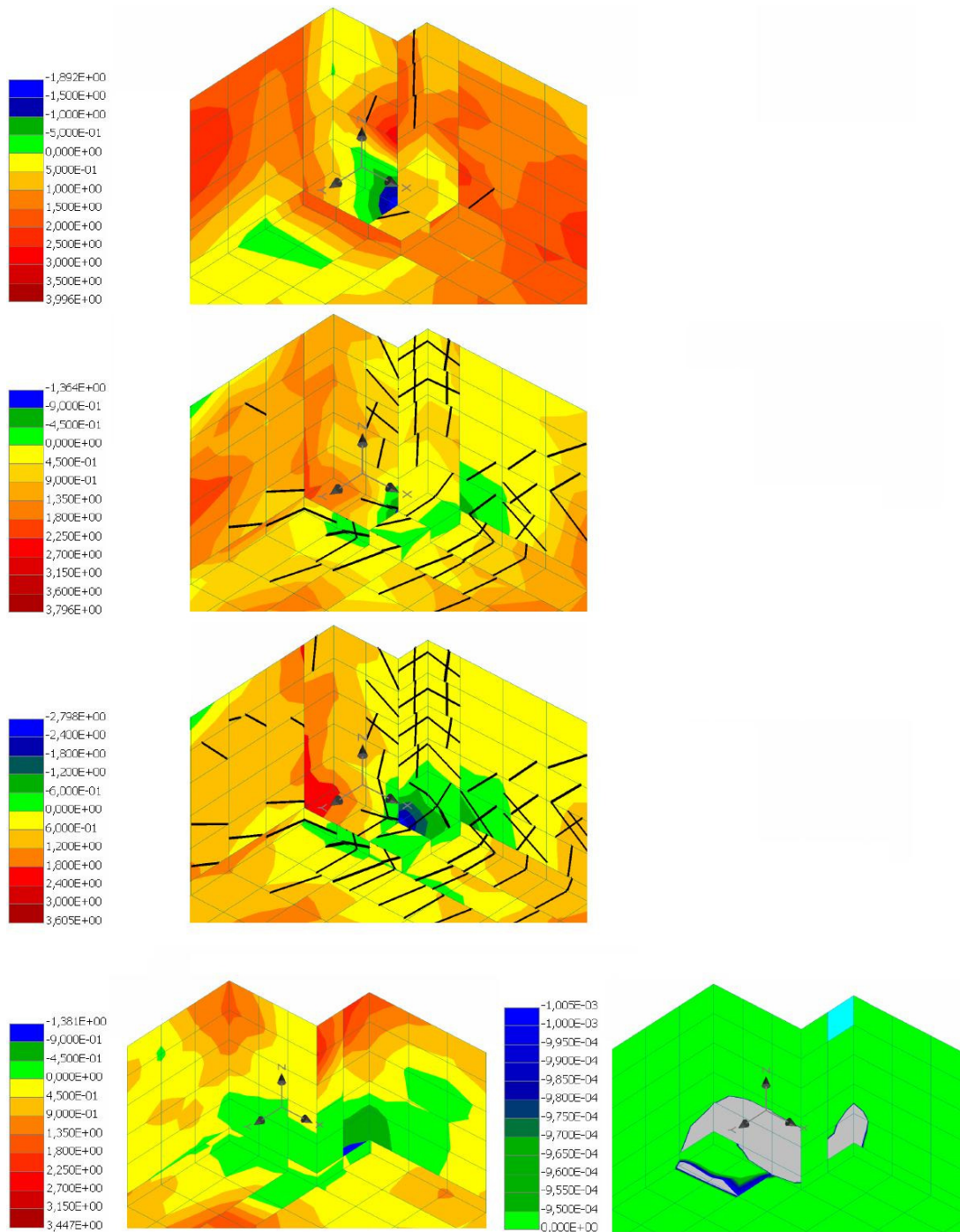


Figure 9.34 Assumed cause of punching failure for model A3.

- (a) Presence of triaxial compression in the region closest to the edge (LS 49),
- (b) Impairment of this zone as splitting occurred (LS 77),
- (c) Redistribution of compressed zone towards the simply supported strip (LS 81),
- (d) Compressed zone outside the supporting plate causing propagation of crushing (LS 85).

Similar to the state of triaxial compression that was observed in the simulated specimen *No. 2*, there was little or no triaxial compression outside the supporting plate in the region closest to the edge, which could be expected due to the slab discontinuity across simply supported edges. In the experimental investigation carried out by Marinković and Alendar (2008) the size of the supporting steel plate was discovered to be decisive for punching shear. Also in the investigation of model *A3* the failure surface coincided with the perimeter of the supporting steel plate, although crushing was initiated adjacent to the intersecting steel profile.

The largest shear cracks were situated perpendicular to the edge. As for the previous models, the initiation of the shear cracks took place at the bottom surface of the slab, adjacent to the supporting steel plate. Also along the edge shear cracks appeared at the bottom surface of the slab, however they were preceded by the formation of tangential microcracks at the top surface of the slab. In addition to the presence of tangential cracks on the top surface the triaxial state of compression in the bottom of model *A3* also indicated dissimilarity from the assumed analogy with a simply supported beam. What distinguishes punching failure from shear failure in a simply supported beam is the presence of multidirectional compression that provides an increased capacity to the region subjected to concentrated forces. Also characteristic for shear failure adjacent to the support in a beam when no shear reinforcement is provided is that shear sliding takes place in the web rather than crushing of the bottom surface. The imaginary web in model *A3* did not suffer crushing.

The predicted punching cone could be identified by means of the crack pattern of microcracks. The distance from the support to the failure surface (as seen in Figure 9.35) was determined to be about $1.6h$ and $1.9h$ in the direction parallel and perpendicular to the edge respectively. The failure surface was determined from the outermost tangential cracks that coincided with the inclined cracks towards the supporting periphery.

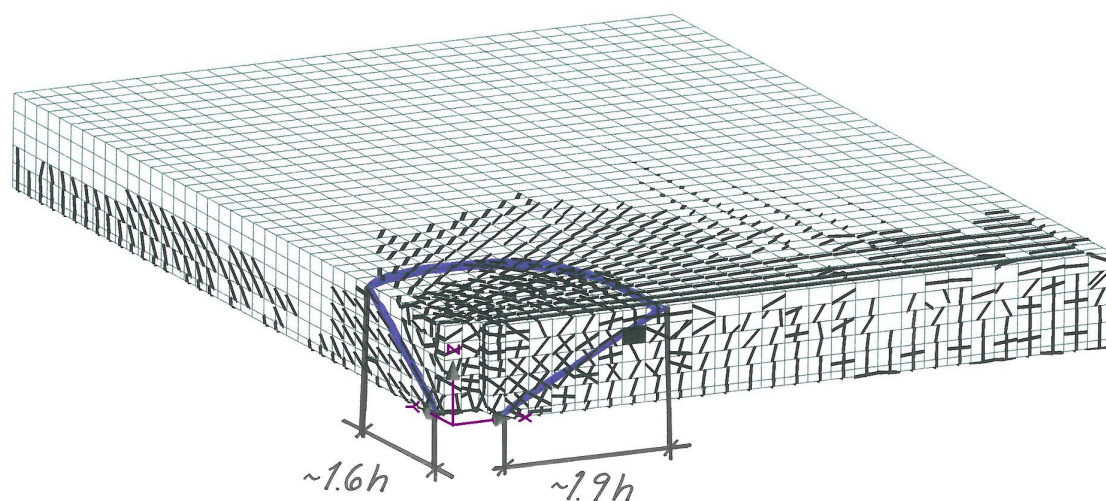


Figure 9.35 Predicted failure surface of punched cone in model *A3*.

It was also shown that the reduction of compressive strength with regard to lateral tensile strain (related to the parameter $r_{c,lim}$) had little effect on the structural response. Nevertheless, punching failure occurred at a load level 4.4% lower when this effect was considered.

Like for the edge supported specimen *No. 2*, the punching resistance has been calculated according to EC2 for the three models in this investigation. Mean values of the strength parameters have been used in order to enable comparison with the obtained results from the FE-analyses and the partial safety factor γ_c has been set to 1.0. The predicted punching loads $V_{R,c}$ (derived as seen in **Appendix V**) are presented in Table 9-5 and compared to the column reactions at bending (P_b) and punching failure (P_p) respectively.

Table 9-5 Predicted punching loads estimated using mean values and ultimate loads from analyses.

Model	$V_{R,c}$ [kN]	P_b [kN]	P_p [kN]
A1	157	250	-
A2	196	400	-
A3	200	-	467

Due to the increased amount of flexural reinforcement, punching failure could be provoked with model A3 despite the higher punching resistance that was also gained. The punching load according to the FE-analysis was much higher than the calculated capacity according to EC2.

9.4.3 Summary of investigation

- The steel columns were found to be the weakest members in the structure as buckling occurred prior to any significant damage of the reinforced concrete slab. In order to prevent failure of the columns, they were modelled as linearly elastic. The steel columns were initially considered to have the yield strength f_y of 355 MPa.
- In order to provoke punching shear failure, the critical section with regard to bending needed to be provided with over twice the required reinforcement area as assessed by means of the Strip Method.
- The behaviour of the strip perpendicular to the simply supported edge resembled the response of a simply supported beam as shear cracks propagated from the bottom surface. Nevertheless, the presence of tangential cracks on the top surface and the triaxial state of compression in the concrete near the support in the strip perpendicular to the simply supported edge depicted that some restraint could be expected.
- The effect of concrete compressive strength reduction due to lateral tensile strain is of less importance for the investigated models.

10 Conclusions

Nonlinear finite element analyses have been conducted in order to assess the structural behaviour with respect to punching shear of flat slabs supported at the edge by slender steel columns. The investigations on the case study were preceded by validation of the modelling technique. The simulation of the test specimens *R1* and *No. 2* showed good correspondence to the observations from the experiments. However, certain observations were made, namely;

- The FE-analyses showed a somewhat stiffer response than the conducted experiments. This is believed to derive from the smeared crack formulation that is used in the concrete model.
- Ability to capture snap-through responses when shear cracking took place.
- Strain hardening in order to compensate for a ductile response needed to be included for specimen *No. 2*.
- The ultimate load was for specimen *R1* very well corresponding to reality, although predicted deformations were much larger. This might be due to the inability of the FE-analysis to simulate fracture between the elements.
- For specimen *No. 2* the predicted ultimate load was 22.7% smaller than in the experiment.
- Notable in the simulation of specimen *R1* was the available residual capacity after the snap-through response, where extensive crushing took place. After the snap-through response about 1/5 of the ultimate load could be added before the slab reached its failure. As the simulation corresponded quite well to reality, it seems that corner supported slabs can hold residual capacity in spite of the critical events that occurred in this case.
- The verifications indicated in-plane translations in the connections between slab and column. It was concluded that line springs would not be able to resemble a steel column supported structure.

In light of the FE-analysis the case study indicated that the edge supported element was not as simply supported in the perpendicular direction to the edge as first assumed. From the illustrated crack patterns it could be concluded that the slab in this direction was subjected to some restraint as tangential cracks were formed opposite to the edge. The restraint is most likely due to geometrical restrictions with regard to compatibility. Furthermore, the presence of triaxial state of compression in the bottom of the assumed beam (strip perpendicular to edge) indicates the interference from the surrounding slab and hence the monodirectional beam analogy could be disclaimed.

The predicted punching loads according to EC2 were calculated for all three cases in this investigation (*A1 – A3*). For model *A3*, that suffered punching failure, the column reaction according to the FE-analysis was 130% higher than the punching load according to EC2. However, it is important to bear in mind that the method in EC2 does not result in mean capacities, even if mean material properties are inserted in the

expressions. Furthermore, it is important to emphasise the need for further assessment of safety coefficients in order to account for proper design margins when employing results from FE-analyses in structural design.

The obtained punching cone showed resemblance to the previously observed on edge and corner columns of concrete as the cone shaped perforation was more vertical at the face towards the edge than interiorly. Compared to the by Kinnunen conducted experiments on edge supported flat slabs, the shear cracks inwards the slab in model A3 were more flat, resulting in a longer distance to the critical section. In the conducted experiments on concrete column supported specimens, Kinnunen (1971) concluded that this distance was about $1.8h$, whilst in model A3 the distance appears to be about $1.9h$. Also Andersson (1966) predicted the shape of the failure surface, which indicated a larger distance to the failure surface perpendicular to the edge. The difference between the failure surfaces observed by Kinnunen and by the observations from the analysis of model A3 is illustrated by comparing Figure 9.35 to Figure 4.13, where it can be seen that the distance from the support to the failure surface is similar at the face of the edge. It seems that the shear cracks in model A3 are enabled to propagate without any significant interference of the tangential cracks since these are not deviating from the top surface of the slab as was the case for the edge supported flat slabs in Kinnunen's experiments. The differences in behaviour might be influenced by the different slab thicknesses, supporting sections and reinforcement amounts.

The parameter $r_{c,lim}$ that governs the reduction of concrete compressive strength with regard to lateral tensile strains had little influence in this investigation. Nevertheless, this consideration affected the ultimate load and the extent of concrete crushing.

Previous research (Jensen, 2009) on slabs supported on edge steel columns indicated that the strip perpendicular to the edge ought to be regarded as a pinned support. As hogging moments solely parallel to the edge were believed to develop, the strip would resemble a simply supported beam due to the believed monodirectional behaviour. Moreover, the design approach with regard to punching shear in the codes seemed to result in an increase of top reinforcement where no flexural moment was expected. However, the reinforcement to account for in the codes seems to be a question of interpretation. According to EC2 it is the tensioned reinforcement that enhances the capacity, meaning the bottom reinforcement if the edge supported strip is regarded as simply supported. Thus providing unnecessary top reinforcement is not proposed by the codes.

The connection detailing was simplified in the analyses, since the pin provided to the through-slab section, in order to prevent progressive collapse, has been excluded. The influence this pin might have on the results and whether it would increase the restraint of the slab at the support has not been investigated.

As the finite element analyses are based on an approximate method and convergence tolerances are exceeded as the models reach failure, numerical errors are to be expected. This was also the case in the present study, although the consistency of results throughout the full range of load steps indicated a reasonable response.

This study has exclusively been conducted by means of nonlinear finite element analyses. FE-analyses are convenient and economically efficient to use compared to

full scale laboratory testing that are seldom an alternative due to high costs. However, in order to verify the obtained results it is recommended to conduct a series of laboratory tests, especially since the FE-analyses have been carried out on simplified models.

If full scale laboratory testing were to be conducted on similar cases to the one investigated within this work, difficulties to obtain punching failure could be expected. Aside from increasing the flexural reinforcement, the steel columns need to be strengthened in order to eliminate other failure modes.

11 References

11.1 Literature references

- Andersson, J L., (1965): Inspänningsmoment i kantpelare vid plattor utan kantbalkar. *Nordisk Betong*, Vol. 9, No. 1, pp. 61-78
- Andersson, J L., (1966): Genomstansning av plattor understödda av pelare vid fri kant. *Nordisk Betong*, Vol. 10, No. 2, pp. 179-200
- Broo, H., Lundgren, K., Plos, M. (2008) *A guide to non-linear finite element modelling of shear and torsion in concrete bridges*. Department of Civil and Environmental Engineering, Chalmers University of Technology, Report 2008:18, Göteborg, Sweden, 2008, 27 pp.
- CEB-FIP (1993): *CEB-FIP Model Code 1990*. Bulletin d'information, 213/214, Lausanne, Switzerland, 1993 pp. 33-51
- Cervenka, V; Cervenka, J, *User's Manual for ATENA 3D*, ATENA Program Documentation, Part 2-2, Prague, 2009
- Cervenka, V, *Theory, ATENA Program Documentation, Part 1*, Prague, 2009
- Collins, M. P., Mitchell, D. (1991): *Prestressed Concrete Structures*, Prentice Hall, Englewood Cliffs, New Jersey, 1991, pp. 338-343
- European Committee for Standardization (2005): *Eurocode 2: Design of Concrete Structures – Part 1-1: General rules and rules for buildings*. Brussels, Belgium, xx pp. 94-103
- Hallgren M. (1996): *Punching Shear Capacity of Reinforced High Strength Concrete Slabs*. Ph.D. Thesis. Department of Structural Engineering, The Royal Institute of Technology, Bulletin 23, Stockholm, Sweden, 1996, 206 pp.
- Hillerborg A. (1959): *Strimlemetoden för plattor på pelare, vinkelplattor m.m.*, Sv. Byggtjänst, Stockholm, 54 pp.
- Ingvarsson, H. (1974): *Experimentellt studium av betongplattor understödda av hörnpelare* (An experimental study of concrete slabs supported on corner columns). Department of Structural Engineering, The Royal Institute of Technology, Meddelande Nr 111, Stockholm, Sweden, 1974, 25 pp.
- Ingvarsson, H. (1977): *Betongplattors hållfasthet och armeringsutformning vid hörnpelare* (Load-bearing capacity of concrete slabs and arrangement of reinforcement at corner columns). Department of Structural Engineering, The Royal Institute of Technology, Meddelande Nr 122, Stockholm, Sweden, 1977, 143 pp.

- Jensen M. (2009): *Dimensionering av betongbjälklag vid kant- och ståpelare*. B.Sc. Thesis. Department of Structural Engineering, The Royal Institute of Technology, Publication no. 279, Stockholm, Sweden, 2009, 75 pp.
- Kinnunen, S., Nylander, H. (1960): *Punching of Concrete Slabs Without Shear Reinforcement*. Transactions of The Royal Institute of Technology, No.158, Stockholm, Sweden, 1960, 112 pp.
- Kinnunen, S. (1971): *Försök med betongplattor understödda av pelare vid fri kant*. Statens institut för byggnadsforskning, Rapport R2, Stockholm, 1971, 103 pp.
- Marinković, S B., Alendar, V H. (2008): Punching failure mechanism at edge columns of post-tensioned lift slabs. *Engineering Structures*, Vol. 30, No. 10, October 2008, pp. 2752-2761
- Walraven, J C. (2002): *6.4 Punching shear. Background document for prENV 1992-1-1:2001*, Delft University of Technology, The Netherlands, 2002, pp.
- Öman, D., Blomkvist, O. (2006): *Icke-linjär 3D finit elementanalys av genomstansade armerade betongplattor*. M.Sc. Thesis. Department of Structural Engineering, The Royal Institute of Technology, Publication no. 233, Stockholm, Sweden, 2006, 119 pp.

11.2 Electronic references

- Baumann Research and Development Corporation (2004) The Vaughtborg Lift Slab System, William Vaughtborg, Inventor. *Baumann Research and Development Corporation - Product Development*. <http://www.brdcorp.com> (2010-04-28)

11.3 Complementary literature

- Broms, C. E., (1990): Punching of flat plates – a question of concrete properties in biaxial compression and size effect. *ACI Structural Journal*, Vol. 87, No. 3, May-June 1990, pp. 292-300
- Crisfield, M A. (1991): *Nonlinear Finite Element Analysis of Solids and Structures. Volume 1 - Essentials*. Publisher, City, {Nation/State}, {year}, pp. 6-13, 254-258
- Cook, R D., Malkus, D. S., Plesha, M. E., Witt, R. J. (2002): *Concepts and Applications of Finite Element Analyses*. Wiley, New York, pp. 596-602
- Engström, B. (2009) *Design and analysis of slabs and flat slabs*. Department of Civil and Environmental Engineering, Chalmers University of Technology, Göteborg, Sweden
- Fédération International du Béton (2001): *Punching of structural concrete slabs: technical report prepared by the CEB/fip Task Group Utilisation of concrete tension in design dedicated to Sven Kinnunen on the occasion of his 70th*

anniversary. Fédération internationale du béton, Lausanne, Switzerland, 2001, 307 pp.

Menétréy, P. (2002): Synthesis of punching failure in reinforced concrete. *Cement & Concrete composites*, Vol. 24, No. 6, December 2002, pp. 497-507

APPENDIX I: Design of prototype slab

Identification of main strips

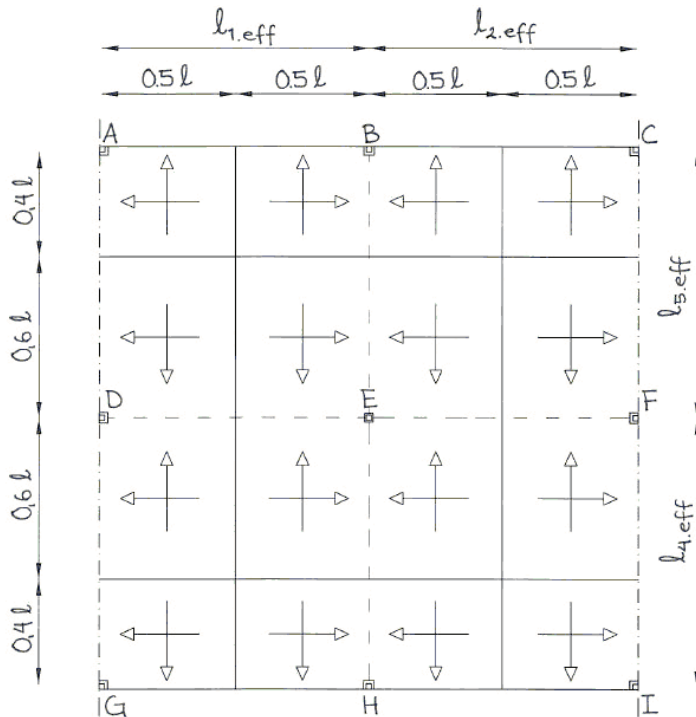
Identify main strips by sketching the load distribution roughly.

Span between fixed edge and column - subdivided about $0.5l - 0.5l$

Span between partially fixed edge and column - subdivided about $0.45l - 0.55l$ (shorter part near edge)

Span between simply supported edge and column - subdivided about $0.4l - 0.6l$ (shorter part near edge).

Span between columns - subdivided about $0.5l - 0.5l$.



Coordinate system:

x - perpendicular to slab edge

y - parallel to slab edge

z - perpendicular to slab plane

Definition of spans

Dimensions of slab and column:

Slab thickness, h : $h := 250\text{mm}$ Column width, d_c : $d_{c,x} := 100\text{mm}$

$d_{c,y} := 100\text{mm}$

Effective span width:

Effective span width, l_{eff} : $l_{\text{eff}} = l_n + a_1 + a_2$

Clear distance between faces of the support, l_n

Span 1: $l_{n,1} := 4.9\text{m}$ Span 3: $l_{n,3} := 4.9\text{m}$

Span 2: $l_{n,2} := 4.9\text{m}$ Span 4: $l_{n,4} := 4.9\text{m}$

Additional distance at each end of the span

in x-direction: $a_x := \min\left(\frac{h}{2}, \frac{d_{c,x}}{2}\right) = 0.05\text{m}$ in y-direction: $a_y := \min\left(\frac{h}{2}, \frac{d_{c,y}}{2}\right) = 0.05\text{m}$

$$\text{Span 1: } l_{1,\text{eff}} := l_{n,1} + a_x + a_x = 5 \text{ m} \quad \text{Span 3: } l_{3,\text{eff}} := l_{n,3} + a_y + a_y = 5 \text{ m}$$

$$\text{Span 2: } l_{2,\text{eff}} := l_{n,2} + a_x + a_x = 5 \text{ m} \quad \text{Span 4: } l_{4,\text{eff}} := l_{n,4} + a_y + a_y = 5 \text{ m}$$

Load

The slab is subjected to its self weight and imposed load (residential).

$$\text{Density of concrete, } \rho_{\text{concrete}} : \rho_{\text{concrete}} := 25 \frac{\text{kN}}{\text{m}^3}$$

$$\text{Self weight of the slab, } g_{\text{slab}} : g_{\text{slab}} := \rho_{\text{concrete}} \cdot h = 6.25 \cdot \frac{\text{kN}}{\text{m}^2}$$

$$\text{Variable load, } q_{\text{residential}} : q_{\text{residential}} := 2.0 \frac{\text{kN}}{\text{m}^2}$$

$$\text{Design load, } q_d : q_d := 1.35 \cdot g_{\text{slab}} + 1.5 \cdot q_{\text{residential}} = 11.438 \cdot \frac{\text{kN}}{\text{m}^2}$$

Choice of moments in statically indeterminate main strips.

In statically indeterminate strips, each unknown support moment needs to be chosen. According to the theory of plasticity any moment distribution can be chosen as long as equilibrium conditions are fulfilled in the ultimate limit state. With regard to the need for serviceability and the limited plastic rotation capacity of real structures, the chosen moment distribution should be similar to the linear elastic solution.

Hillerborg (1996) gives the following recommendations:

$$\text{Fully fixed end:} \quad m_{\text{si}} = \frac{q_d \cdot l_i^2}{12}$$

$$\text{Partially fixed end with } \zeta\% \text{ restraint:} \quad m_{\text{si}} = \zeta \cdot \frac{q_d \cdot l_i^2}{12} \quad \text{this could be applicable when the slab is connected to a supporting wall.}$$

$$\text{Support moment at interior support:} \quad m_s = \frac{m_{s,1} + m_{s,2}}{2} \quad \text{the support moment at an interior support is calculated through the average influences from two adjacent spans.}$$

$$m_{s,i} = \frac{q_d \cdot l_i^2}{12} \quad \text{when adjacent end is fully fixed.}$$

$$m_{s,i} = \frac{q_d \cdot l_i^2}{10} \quad \text{when adjacent end is partially fixed.}$$

$$m_{s,i} = \frac{q_d \cdot l_i^2}{8} \quad \text{when adjacent end is simply supported.}$$

Choice of support moments:

Support B in y-direction (interior column):

The strip is statically indeterminate, therefore the support moment must be chosen. The moment in support B is taken as the average of influences from the two adjacent spans.

$$\text{Influence from adjacent span AB: } m_{s,A,y} := \frac{q_d \cdot l_{1,\text{eff}}^2}{12} = 23.828 \cdot \frac{\text{kN}\cdot\text{m}}{\text{m}}$$

$$\text{Influence from adjacent span BC: } m_{s,C,y} := \frac{q_d \cdot l_{2,\text{eff}}^2}{12} = 23.828 \cdot \frac{\text{kN}\cdot\text{m}}{\text{m}}$$

$$\text{Support moment } m_{s,B,y}: \quad m_{s,B,y} := \frac{m_{s,A,y} + m_{s,C,y}}{2} = 23.828 \cdot \frac{\text{kN}\cdot\text{m}}{\text{m}}$$

Support B, x-direction (end support):

In the y-direction the edge is simply supported.

Degree of partial fixation in support B: $\zeta_B := 0$

$$\text{Support moment, } m_{s,B,x}: \quad m_{s,B,x} := \zeta_B \cdot \frac{q_d \cdot l_{3,\text{eff}}^2}{12} = 0 \cdot \frac{\text{kN}\cdot\text{m}}{\text{m}}$$

Support E, x-direction (interior column):

Since the strip is statically indeterminate, the support moment in E is achieved considering the average influence from the two adjacent spans.

$$\text{Influence from adjacent span - BE: } m_{s,E,x,1} := \frac{q_d \cdot l_{3,\text{eff}}^2}{8} = 35.742 \cdot \frac{\text{kN}\cdot\text{m}}{\text{m}}$$

$$\text{Influence from adjacent span - EH: } m_{s,E,x,2} := \frac{q_d \cdot l_{4,\text{eff}}^2}{8} = 35.742 \cdot \frac{\text{kN}\cdot\text{m}}{\text{m}}$$

$$\text{Support moment } m_{s,E,x}: \quad m_{s,E,x} := \frac{m_{s,E,x,1} + m_{s,E,x,2}}{2} = 35.742 \cdot \frac{\text{kN}\cdot\text{m}}{\text{m}}$$

Field moments:

Field moment between support A and B:

Due to symmetry the moment in span AB is equal to the moment in span BC. The field moments are determined by means of equilibrium conditions.

$$\text{Support reaction, } R_{B1}: \quad R_{B1} := \frac{q_d \cdot l_{1,\text{eff}}}{2} - \frac{m_{s,A,y}}{l_{1,\text{eff}}} + \frac{m_{s,B,y}}{l_{1,\text{eff}}} = 28.594 \cdot \frac{\text{kN}}{\text{m}}$$

$$\text{Section where shear force is zero, } y_{0,B1}: \quad y_{0,B1} := \frac{R_{B1}}{q_d} = 2.5 \text{ m}$$

$$\text{Field moment, } m_{f,AB}: \quad m_{f,AB} := \frac{R_{B1}^2}{2 \cdot q_d} - m_{s,B,y} = 11.914 \cdot \frac{\text{kN}\cdot\text{m}}{\text{m}}$$

Field moment between support B and E:

Support reaction, R_{B2} :
$$R_{B2} := \frac{q_d \cdot l_{3,\text{eff}}}{2} + \frac{m_{s,B,x}}{l_{3,\text{eff}}} - \frac{m_{s,E,x}}{l_{3,\text{eff}}} = 21.445 \cdot \frac{\text{kN}}{\text{m}}$$

Section where shear force is zero, $y_{0,B2}$:
$$y_{0,B2} := \frac{R_{B2}}{q_d} = 1.875 \text{ m}$$

Field moment, $m_{f,AB}$:
$$m_{f,AB} := \frac{R_{B2}^2}{2 \cdot q_d} - m_{s,B,x} = 20.105 \cdot \frac{\text{kN} \cdot \text{m}}{\text{m}}$$

Transverse moment distribution:

When the average moments across the width of the main strip have been determined, a transverse moment distribution of these moments should be carried out. The main strip is divided into a column strip and two mid strips.

Check of moment ratios:
$$\frac{m_{s,B,y}}{m_{f,AB}} = 2 \text{ OK!}$$

$$\frac{m_{s,B,x}}{m_{f,AB}} = 0 \text{ Not OK! Has to be considered in the transverse moment distribution.}$$

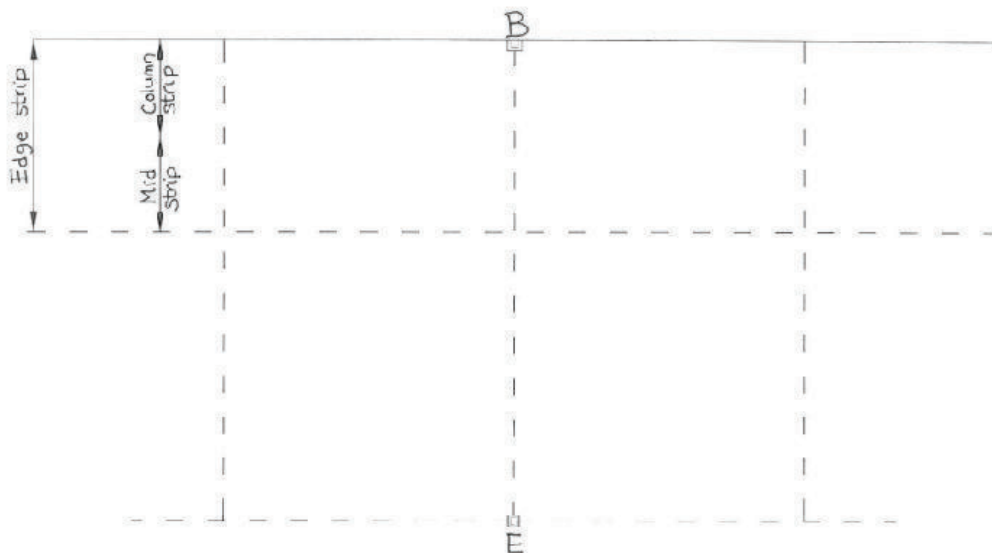
Transverse distribution of moments in y-direction:

Proportion between column and main strip, β_y :
$$\beta_y = \frac{b_{\text{column},y,B}}{b_{\text{main},y,B}}$$

$$\beta_y := 0.5$$

Width of the main strip, $b_{\text{main},y}$:

$$b_{\text{main},y} := y_{0,B2} = 1.875 \text{ m}$$



Width of column strip, $b_{column.y}$: $b_{column.y} := \beta_y \cdot b_{main.y} = 0.938 \text{ m}$

Width of mid strip, $b_{mid.y}$: $b_{mid.y} := \beta_y \cdot b_{main.y} = 0.938 \text{ m}$

Support moment, $m_{s.y}$:

No certain limitation of crack widths in the top surface is needed ; Standard solution s_f .

$m_{s.y} := 2.0 \cdot m_{s.B.y} = 47.656 \cdot \frac{\text{kN}\cdot\text{m}}{\text{m}}$ Distributed over the column strip.

Field moment, $m_{f.AB}$:

Normal solution for span moment is applied; f_f .

$m_{f.AB} := 1.0 \cdot m_{f.AB} = 11.914 \cdot \frac{\text{kN}\cdot\text{m}}{\text{m}}$ Distributed over the main strip.

Transverse distribution in x-direction:

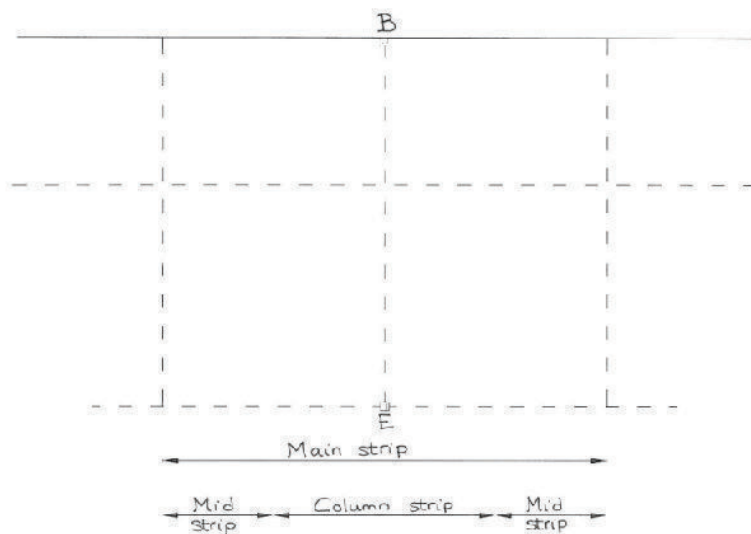
Proportion between column and mid strip, β_x : $\beta_x = \frac{b_{column.x}}{b_{main.x}}$

$$\beta_x := 0.5$$

Width of the main strip, $b_{main.x}$:

$$b_{main.x} := 2 \cdot y_{0.B1} = 5 \text{ m}$$

The main strip is divided into a column strip and a mid strip.



Width of column strip, $b_{column.x}$: $b_{column.x} := \beta_x \cdot b_{main.x} = 2.5 \text{ m}$

Total width of mid strip, $b_{mid.x.B}$: $b_{mid.x} := \beta_x \cdot b_{main.x} = 2.5 \text{ m}$

Since the criteria for moment ratio was not fulfilled, the design distribution of moment has to assure that equilibrium conditions are fulfilled. This is done making sure that the numerical sum of moments is higher in the column strip than in the mid strip.

Support moment, $m_{s,B,x}$: $m_{s,B,x} = 0$

Field moment, $m_{f,BE}$:

Assumed distribution: Column strip: $\xi_{\text{column}} := 1.3$
 Mid strip: $\xi_{\text{mid}} := 2 - \xi_{\text{column}} = 0.7$

The sum of the coefficients in the transverse distribution must be equal to 2, since the sum of the moment capacities provided must correspond to the chosen average moment.

Field moment in the column strip, $m_{f,BE,\text{column}}$: $m_{f,BE,\text{column}} := \xi_{\text{column}} \cdot m_{f,BE} = 26.136 \cdot \frac{\text{kN}\cdot\text{m}}{\text{m}}$

Field moment in the column strip, $m_{f,BE,\text{column}}$: $m_{f,BE,\text{mid}} := \xi_{\text{mid}} \cdot m_{f,BE} = 14.073 \cdot \frac{\text{kN}\cdot\text{m}}{\text{m}}$

$$\alpha := \frac{m_{s,B,x} + m_{f,BE,\text{mid}}}{m_{s,B,x} + m_{f,BE}} = 0.7$$

$$\alpha := \begin{cases} \text{"OK"} & \text{if } 0.25 \leq \alpha \leq 0.7 \\ \text{"Not OK"} & \text{otherwise} \end{cases} = \text{"OK"}$$

Reinforcement design

Required capacity: $A_s \geq \frac{m}{f_{yd} \cdot z}$

where $f_{yk} := 500\text{MPa}$ $f_{yd} := \frac{f_{yk}}{1.15} = 434.783 \cdot \text{MPa}$

Diameter of reinforcement bars: $\phi_{12} := 12\text{mm}$ $\phi_{10} := 10\text{mm}$ $\phi_8 := 8\text{mm}$

Area per reinforcement bar, A_s : $A_{s,\phi.8} := \frac{\pi \cdot \phi_8^2}{4} = 50.265 \cdot \text{mm}^2$

$$A_{s,\phi.10} := \frac{\pi \cdot \phi_{10}^2}{4} = 78.54 \cdot \text{mm}^2$$

$$A_{s,\phi.12} := \frac{\pi \cdot \phi_{12}^2}{4} = 113.097 \cdot \text{mm}^2$$

Concrete cover, EC 2, 4.4:

The nominal concrete cover, c_{nom} , consists of the minimum cover and a deviation.

Minimum concrete cover, c_{min} :

the minimum concrete cover must assure adhesion, corrosion protection for the reinforcement and fire resistance. The bigger value that fulfills the demands on adhesion and environmental effects is to be used.

Minimum demand with regard to adhesion -
at least the diameter of the reinforcement bar:

$$c_{min.b.top} := \phi_{10}$$
$$c_{min.b.bottom} := \phi_{10}$$

Minimum demand with regard to
environmental effects - exposure class XO
and structural class S4:

$$c_{min.dur} := 10\text{mm}$$
$$\Delta c_{dur.\gamma} := 0\text{mm}$$
$$\Delta c_{dur.st} := 0\text{mm}$$
$$\Delta c_{dur.add} := 0\text{mm}$$

Minimum concrete cover:

$$c_{min.top} := \max(c_{min.b.top}, c_{min.dur} + \Delta c_{dur.\gamma} - \Delta c_{dur.st} - \Delta c_{dur.add}, 10\text{mm}) = 10\text{mm}$$

$$c_{min.bottom} := \max(c_{min.b.bottom}, c_{min.dur} + \Delta c_{dur.\gamma} - \Delta c_{dur.st} - \Delta c_{dur.add}, 10\text{mm}) = 10\text{mm}$$

Allowance for variation, Δc_{dev} : $\Delta c_{dev} := 10\text{mm}$

Nominal concrete cover, c_{nom} : $c_{nom} = c_{min} + \Delta c_{dev}$

$$c_{nom.top} := c_{min.top} + \Delta c_{dev} = 20\text{mm}$$

$$c_{nom.bottom} := c_{min.bottom} + \Delta c_{dev} = 20\text{mm}$$

Approximation of internal level arms:

Effective depth, d : $d_{y.bottom} := h - c_{nom.bottom} - \phi_{10} - \frac{\phi_8}{2} = 0.216\text{ m}$

$$d_{x.bottom} := h - c_{nom.bottom} - \frac{\phi_{10}}{2} = 0.225\text{ m}$$

$$d_{y.top} := h - c_{nom.top} - \phi_{10} - \frac{\phi_{12}}{2} = 0.214\text{ m}$$

Internal level arms, z : $z_{y.bottom} := 0.9 \cdot d_{y.bottom} = 0.194\text{ m}$

$$z_{x.bottom} := 0.9 \cdot d_{x.bottom} = 0.203\text{ m}$$

$$z_{y.top} := 0.9 \cdot d_{y.bottom} = 0.194\text{ m}$$

Minimum reinforcement spacing according to EC2:

Minimum bar spacing, s_{min} : $s_{min} := \min(3 \cdot h, 400\text{mm}) = 400 \cdot \text{mm}$

At concentrated loads/ maximum moments, $s_{min.conc}$: $s_{min.conc} := \min(3 \cdot h, 250\text{mm}) = 250 \cdot \text{mm}$

Y-direction, Bottom reinforcement:

Required area, $A_{f,y}$: $A_{f,y} := \frac{m_{f.AB}}{f_{yd} \cdot z_{y.bottom}} = 140.959 \cdot \frac{\text{mm}^2}{\text{m}}$

Distribution width, $s_{f,y}$: $s_{f,y} := b_{main,y} = 1.875 \text{ m}$

Number of bars per meter, $n_{f,y}$: $n_{f,y} := \frac{A_{f,y}}{A_{s,\phi.8}} = 2.804 \frac{1}{\text{m}}$

Required bars, $n_{f,y}$: $n_{f,y} := \text{ceil}(n_{f,y} \cdot s_{f,y}) = 6$

Y-direction, Top reinforcement:

Required area, $A_{s,y}$: $A_{s,y} := \frac{m_{s.B.y}}{f_{yd} \cdot z_{y.top}} = 281.917 \cdot \frac{\text{mm}^2}{\text{m}}$

Distribution width, $s_{s,y}$: $s_{s,y} := b_{column,y} = 0.938 \text{ m}$

Number of bars per meter, $n_{s,y}$: $n_{s,y} := \frac{A_{s,y}}{A_{s,\phi.12}} = 2.493 \frac{1}{\text{m}}$

Required bars, $n_{s,y}$: $n_{s,y} := \text{ceil}(s_{s,y} \cdot n_{s,y}) = 3$

X-direction, bottom reinforcement :

Mid strip:
Required area, $A_{f,x.mid}$: $A_{f,x.mid} := \frac{m_{f.BE.mid}}{f_{yd} \cdot z_{x.bottom}} = 159.847 \cdot \frac{\text{mm}^2}{\text{m}}$

Distribution width, $s_{f,x.mid}$: $s_{f,x.mid} := b_{mid,x} = 2.5 \text{ m}$

Number of bars per meter, $n_{f,x.mid}$: $n_{f,x.mid} := \frac{A_{f,x.mid}}{A_{s,\phi.10}} = 2.035 \frac{1}{\text{m}}$

Column strip:
Required area, $A_{s,x.column}$: $A_{s,x.column} := \frac{m_{f.BE.column}}{f_{yd} \cdot z_{x.bottom}} = 296.859 \cdot \frac{\text{mm}^2}{\text{m}}$

Distribution width, $s_{s,x.column}$: $s_{s,x.column} := b_{column,x} = 2.5 \text{ m}$

Number of bars per meter, $n_{s,x.column}$: $n_{s,x.column} := \frac{A_{s,x.column}}{A_{s,\phi.10}} = 3.78 \frac{1}{\text{m}}$

Required bars:

in the mid strip, $n_{f.x.mid}$:

$$n_{f.x.mid} := \text{ceil}(s_{f.x.mid} \cdot n_{f.x.mid}) = 6$$

in the column strip $n_{s.x.column}$:

$$n_{s.x.column} := \text{ceil}(s_{s.x.column} \cdot n_{s.x.column}) = 10$$

X - direction, top reinforcement:

Required area, $A_{s.x.top}$:

$$A_{s.x.top} := 0 \cdot \frac{\text{mm}^2}{\text{m}}$$

APPENDIX II: Material properties

Specimen R1

In the following concrete properties are assessed by means of MC90 and EC2. The reported material properties are regarded as mean values.

Compressive strength according to EC2:

Mean compressive strength, f_{cm} :

For some verifications in design or for an estimate of other concrete properties it is necessary to refer to a mean value of compressive strength f_{cm} . In this case the concrete strength was estimated by means of tests on cubes.

Mean cubic strength, $f_{cm.cube}$: $f_{cm.cube} := 35\text{MPa}$

Mean cylinder strength, f_{cm} : $f_{cm} := 0.8 \cdot f_{cm.cube} = 28 \cdot \text{MPa}$

According to European standard the compressive strength f_c is based on uniaxial compression. Cylinders, with a diameter of 150 mm and height 300mm, are tested at the age of 28 days after storage in water at 20 +/- 2 °C. The test cubes in the experimental investigation conducted by Ingvarsson were measured according to a standard similar to the former Swedish standard, hence the strength is decreased by 10% to correspond to the European standard.

Mean compressive strength, f_{cm} : $f_{cm} := 0.90 \cdot f_{cm} = 25.2 \cdot \text{MPa}$

Characteristic compressive strength, f_{ck} :

f_{ck} is defined as the strength below which 5% of all possible strength measurements for the specified concrete may be expected to fail. The characteristic strength may be assessed as follows:

$$\Delta f := 8\text{MPa}$$

Characteristic cylinder strength, f_{ck} : $f_{ck} := f_{cm} - \Delta f = 17.2 \cdot \text{MPa}$

Fracture energy G_F according to MC90

The fracture energy of concrete G_F is the energy required to propagate a tensile crack of unit area. In the absence of experimental data G_F may be estimated from the following:

Base value of fracture energy, G_{F0} :

Note that in MC90 there is most likely a misprint in table 2.1.3 stating that G_{F0} is 0.058 Nmm/mm² for the third interval. The value is changed to 0.038 Nmm/mm² as it corresponds to the values of G_F given in table 2.1.4 in MC90.

Maximum aggregate size, d_{max} : $d_{max} := 20\text{mm}$

$$G_{F0} := \begin{cases} \left(0.025 \frac{\text{N}\cdot\text{mm}}{\text{mm}^2} \right) & \text{if } d_{\max} \leq 8\text{mm} \\ \left(0.030 \frac{\text{N}\cdot\text{mm}}{\text{mm}^2} \right) & \text{if } 8\text{mm} < d_{\max} \leq 16\text{mm} \\ \left(0.038 \frac{\text{N}\cdot\text{mm}}{\text{mm}^2} \right) & \text{if } 16\text{mm} < d_{\max} \leq 32\text{mm} \end{cases} = 38 \cdot \frac{\text{N}}{\text{m}}$$

$$f_{\text{cmo}} := 10\text{MPa}$$

$$\text{Fracture energy, } G_F: \quad G_F := G_{F0} \cdot \left(\frac{f_{\text{cm}}}{f_{\text{cmo}}} \right)^{0.7} = 72.571 \cdot \frac{\text{N}}{\text{m}}$$

Tensile strength f_{ct} according to EC2:

$$\text{Mean tensile strength, } f_{ctm}: \quad f_{ctm} := \begin{cases} 0.30 \cdot \left(\frac{f_{ck}}{\text{MPa}} \right)^{\left(\frac{2}{3} \right)} \text{MPa} & \text{if } f_{ck} \leq 50\text{MPa} \\ 2.12 \cdot \ln \left(1 + \frac{f_{cm}}{10\text{MPa}} \right) \text{MPa} & \text{if } f_{ck} > 50\text{MPa} \end{cases} = 1.999 \cdot \text{MPa}$$

Modulus of elasticity E_c according to EC2:

$$\text{Mean modulus of elasticity, } E_{cm}: \quad E_{cm} := 22\text{GPa} \cdot \left(\frac{f_{cm}}{10\text{MPa}} \right)^{0.3} = 29.03 \cdot \text{GPa}$$

Plastic strain ε_{cp} according to EC2:

The plastic strain is the permanent strain obtained after the maximum stress has been reached and the elastic part has been recovered.

$$\text{Strain at maximum value of stress according to EC2:} \quad \varepsilon_{c1} := \min \left[0.7 \cdot 10^{-3} \cdot \left(\frac{f_{cm}}{\text{MPa}} \right)^{0.31}, 2.8 \cdot 10^{-3} \right] = 1.903 \times 10^{-3}$$

$$\text{Plastic strain, } \varepsilon_{cp}: \quad \varepsilon_{cp} := \varepsilon_{c1} - \frac{f_{cm}}{E_{cm}} = 1.035 \times 10^{-3}$$

Specimen No. 2

In the following concrete properties are assessed by means of MC90 and EC2. The reported material properties are regarded as mean values.

Units

$$\text{pond} := \frac{196133}{20000000} \text{N}$$

$$\text{kilopond} := 1000 \cdot \text{pond}$$

Compressive strength according to EC2:

Mean compressive strength, f_{cm} :

For some verifications in design or for an estimate of other concrete properties it is necessary to refer to a mean value of compressive strength f_{cm} . In this case the concrete strength was estimated by means of tests on cubes.

$$\text{Mean cubic strength, } f_{cm.cube}: \quad f_{cm.cube} := 333 \frac{\text{kilopond}}{\text{cm}^2}$$

$$\text{Mean cylinder strength, } f_{cm}: \quad f_{cm} := 0.8 \cdot f_{cm.cube} = 26.125 \cdot \text{MPa}$$

According to European standard the compressive strength f_c is based on uniaxial compression. Cylinders, with a diameter of 150 mm and height 300mm, are tested at the age of 28 days after storage in water at 20 +/- 2 °C. The test cubes in the experimental investigation conducted by Kinnunen were measured according to a standard similar to the former Swedish standard, hence the strength is decreased by 10% to correspond to the European standard.

$$\text{Mean compressive strength, } f_{cm}: \quad f_{cm} := 0.90 \cdot f_{cm} = 23.512 \cdot \text{MPa}$$

Characteristic compressive strength, f_{ck} :

f_{ck} is defined as the strength below which 5% of all possible strength measurements for the specified concrete may be expected to fail. The characteristic strength may be assessed as follows:

$$\Delta f := 8 \text{MPa}$$

$$\text{Characteristic cylinder strength, } f_{ck}: \quad f_{ck} := f_{cm} - \Delta f = 15.512 \cdot \text{MPa}$$

Fracture energy G_F according to MC90

The fracture energy of concrete G_F is the energy required to propagate a tensile crack of unit area.

In the absence of experimental data G_F may be estimated from the following:

Base value of fracture energy, G_{F0} :

Note that in MC90, there is most likely a misprint in table 2.1.3 stating that G_{F0} is 0.058 Nmm/mm² for the third interval. The value is changed to 0.038 Nmm/mm² as it corresponds to the values of G_F given in table 2.1.4 in MC90.

$$\text{Maximum aggregate size, } d_{max}: \quad d_{max} := 20 \text{mm}$$

$$G_{F0} := \begin{cases} \left(0.025 \frac{\text{N}\cdot\text{mm}}{\text{mm}^2}\right) & \text{if } d_{\max} \leq 8\text{mm} \\ \left(0.030 \frac{\text{N}\cdot\text{mm}}{\text{mm}^2}\right) & \text{if } 8\text{mm} < d_{\max} \leq 16\text{mm} \\ \left(0.038 \frac{\text{N}\cdot\text{mm}}{\text{mm}^2}\right) & \text{if } 16\text{mm} < d_{\max} \leq 32\text{mm} \end{cases} = 38 \cdot \frac{\text{N}}{\text{m}}$$

$$f_{\text{cmo}} := 10\text{MPa}$$

$$\text{Fracture energy, } G_F: \quad G_F := G_{F0} \cdot \left(\frac{f_{\text{cm}}}{f_{\text{cmo}}}\right)^{0.7} = 69.134 \cdot \frac{\text{N}}{\text{m}}$$

Tensile strength f_{ct} according to EC2:

$$\text{Mean tensile strength, } f_{\text{ctm}}: \quad f_{\text{ctm}} := \begin{cases} 0.30 \cdot \left(\frac{f_{\text{ck}}}{\text{MPa}}\right)^{\left(\frac{2}{3}\right)} \text{ MPa} & \text{if } f_{\text{ck}} \leq 50\text{MPa} \\ 2.12 \cdot \ln\left(1 + \frac{f_{\text{cm}}}{10\text{MPa}}\right) \text{ MPa} & \text{if } f_{\text{ck}} > 50\text{MPa} \end{cases} = 1.866 \cdot \text{MPa}$$

Modulus of elasticity E_c according to EC2:

$$\text{Mean modulus of elasticity, } E_{\text{cm}}: \quad E_{\text{cm}} := 22\text{GPa} \cdot \left(\frac{f_{\text{cm}}}{10\text{MPa}}\right)^{0.3} = 28.432 \cdot \text{GPa}$$

Plastic strain ε_{cp} according to EC2:

The plastic strain is the permanent strain obtained after the maximum stress has been reached and the elastic part has been recovered.

$$\text{Strain at maximum value of stress according to EC2:} \quad \varepsilon_{c1} := \min\left[0.7 \cdot 10^{-3} \cdot \left(\frac{f_{\text{cm}}}{\text{MPa}}\right)^{0.31}, 2.8 \cdot 10^{-3}\right] = 1.863 \times 10^{-3}$$

$$\text{Plastic strain, } \varepsilon_{cp}: \quad \varepsilon_{cp} := \varepsilon_{c1} - \frac{f_{\text{cm}}}{E_{\text{cm}}} = 1.036 \times 10^{-3}$$

Prototype slabs (A1, A2 and A3)

In the following mean concrete properties are determined according to MC90 and EC2 for the considered concrete quality C30/37.

Compressive strength according to EC2:

f_{ck} is defined as that strength below which 5% of all possible strength measurements for the specified concrete may be expected to fail. MC90 and EC2 are based on the uniaxial compressive strength f_c for cylinders, 150 mm in diameter and 300 mm in height stored in water at 20 +/- 2 °C, and tested at the age of 28 days. If the characteristic strength is defined from measurements on cubic specimens, the cylindrical strength may be assessed as follows:

Characteristic cubic strength, $f_{ck.cube}$: $f_{ck.cube} := 37\text{MPa}$

Characteristic cylinder strength, f_{ck} : $f_{ck} := 30\text{MPa}$

Mean compressive strength, f_{cm} :

For some verifications in design or for an estimate of other concrete properties it is necessary to refer to a mean value of the compressive strength f_{cm} associated with a specific characteristic compressive strength f_{ck} . In this case f_{cm} may be estimated according to the following:

$$\Delta f := 8\text{MPa}$$

Mean compressive strength, f_{cm} : $f_{cm} := f_{ck} + \Delta f = 38\cdot\text{MPa}$

Fracture energy G_F according to MC90

The fracture energy of concrete G_F is the energy required to propagate a tensile crack of unit area.

In the absence of experimental data, G_F may be estimated from the following:

Base value of fracture energy, G_{F0} :

Note that in MC90, there is most likely a misprint in table 2.1.3 stating that G_{F0} is 0.058 Nmm/mm² for the third interval. The value is changed to 0.038 Nmm/mm² as it corresponds to the values of G_F given in table 2.1.4 in MC90.

Maximum aggregate size, d_{max} : $d_{max} := 20\text{mm}$

$$G_{F0} := \begin{cases} \left(0.025 \frac{\text{N}\cdot\text{mm}}{\text{mm}^2}\right) & \text{if } d_{max} \leq 8\text{mm} \\ \left(0.030 \frac{\text{N}\cdot\text{mm}}{\text{mm}^2}\right) & \text{if } 8\text{mm} < d_{max} \leq 16\text{mm} \\ \left(0.038 \frac{\text{N}\cdot\text{mm}}{\text{mm}^2}\right) & \text{if } 16\text{mm} < d_{max} \leq 32\text{mm} \end{cases} = 38 \cdot \frac{\text{N}}{\text{m}}$$

$f_{cm0} := 10\text{MPa}$

$$\text{Fracture energy, } G_F: \quad G_F := G_{F0} \cdot \left(\frac{f_{cm}}{f_{cm0}}\right)^{0.7} = 96.746 \cdot \frac{\text{N}}{\text{m}}$$

Tensile strength f_{ct} according to EC2:

$$\text{Mean tensile strength, } f_{ctm}: f_{ctm} := \begin{cases} 0.30 \cdot \left(\frac{f_{ck}}{\text{MPa}} \right)^{\left(\frac{2}{3} \right)} \text{ MPa} & \text{if } f_{ck} \leq 50 \text{ MPa} \\ 2.12 \cdot \ln \left(1 + \frac{f_{cm}}{10 \text{ MPa}} \right) \text{ MPa} & \text{if } f_{ck} > 50 \text{ MPa} \end{cases} = 2.896 \cdot \text{MPa}$$

Modulus of elasticity E_c according to EC2:

$$\text{Mean modulus of elasticity, } E_{cm}: E_{cm} := 22 \text{ GPa} \cdot \left(\frac{f_{cm}}{10 \text{ MPa}} \right)^{0.3} = 32.837 \cdot \text{GPa}$$

Plastic strain ε_{cp} according to EC2:

The plastic strain is the permanent strain obtained after the maximum stress has been reached and the elastic part has been recovered.

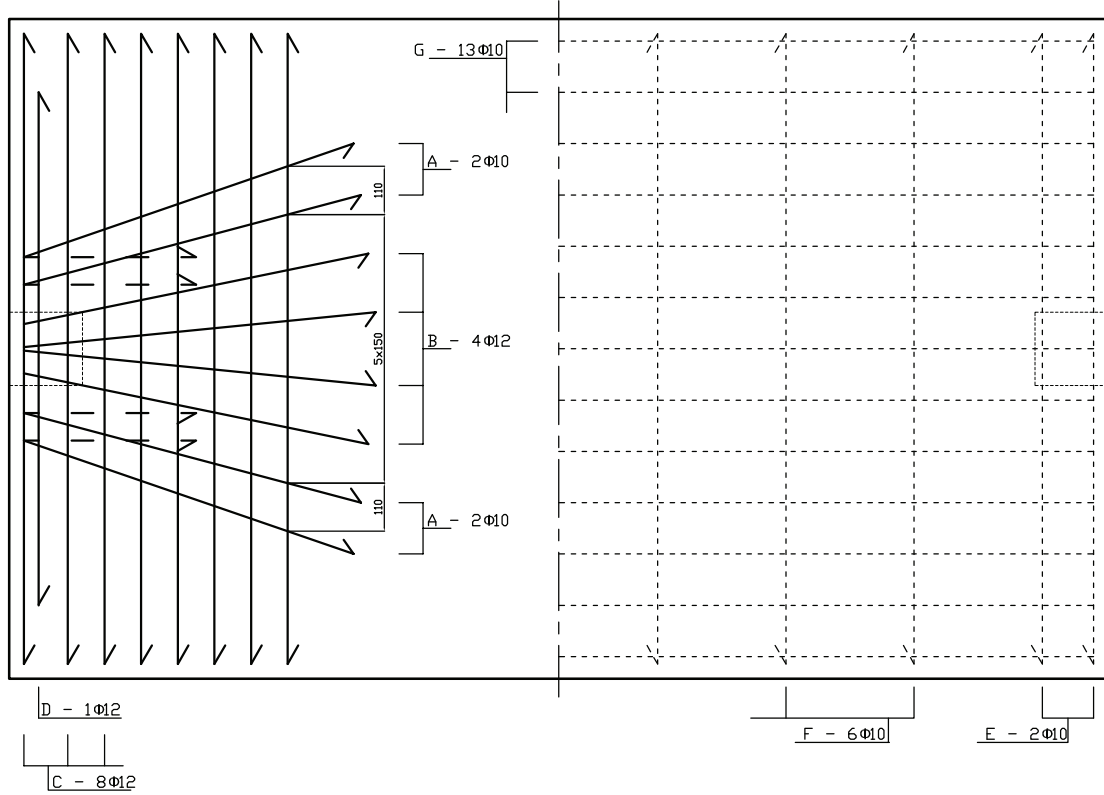
$$\text{Strain at maximum value of stress according to EC2: } \varepsilon_{c1} := \min \left[0.7 \cdot 10^{-3} \cdot \left(\frac{f_{cm}}{\text{MPa}} \right)^{0.31}, 2.8 \cdot 10^{-3} \right] = 2.162 \times 10^{-3}$$

$$\text{Plastic strain, } \varepsilon_{cp}: \varepsilon_{cp} := \varepsilon_{c1} - \frac{f_{cm}}{E_{cm}} = 1.005 \times 10^{-3}$$

Specimen No. 2

Top reinforcement

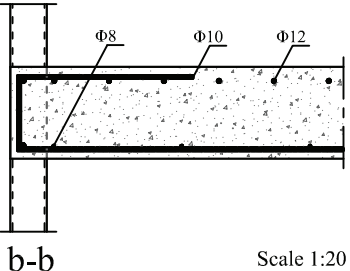
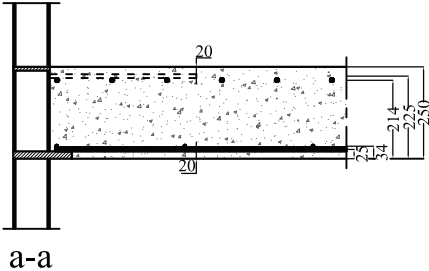
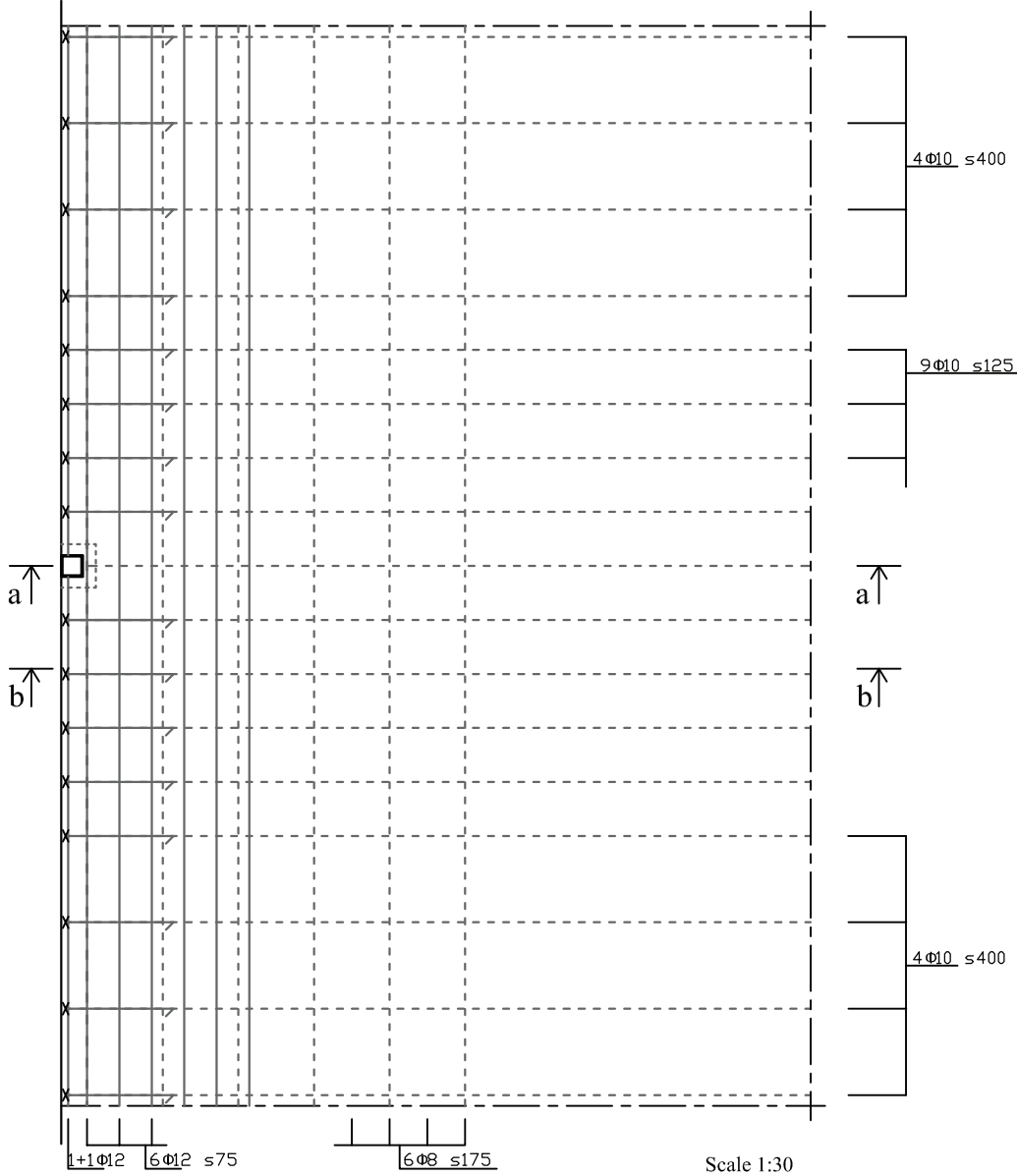
Bottom reinforcement



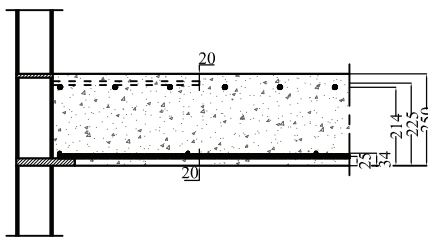
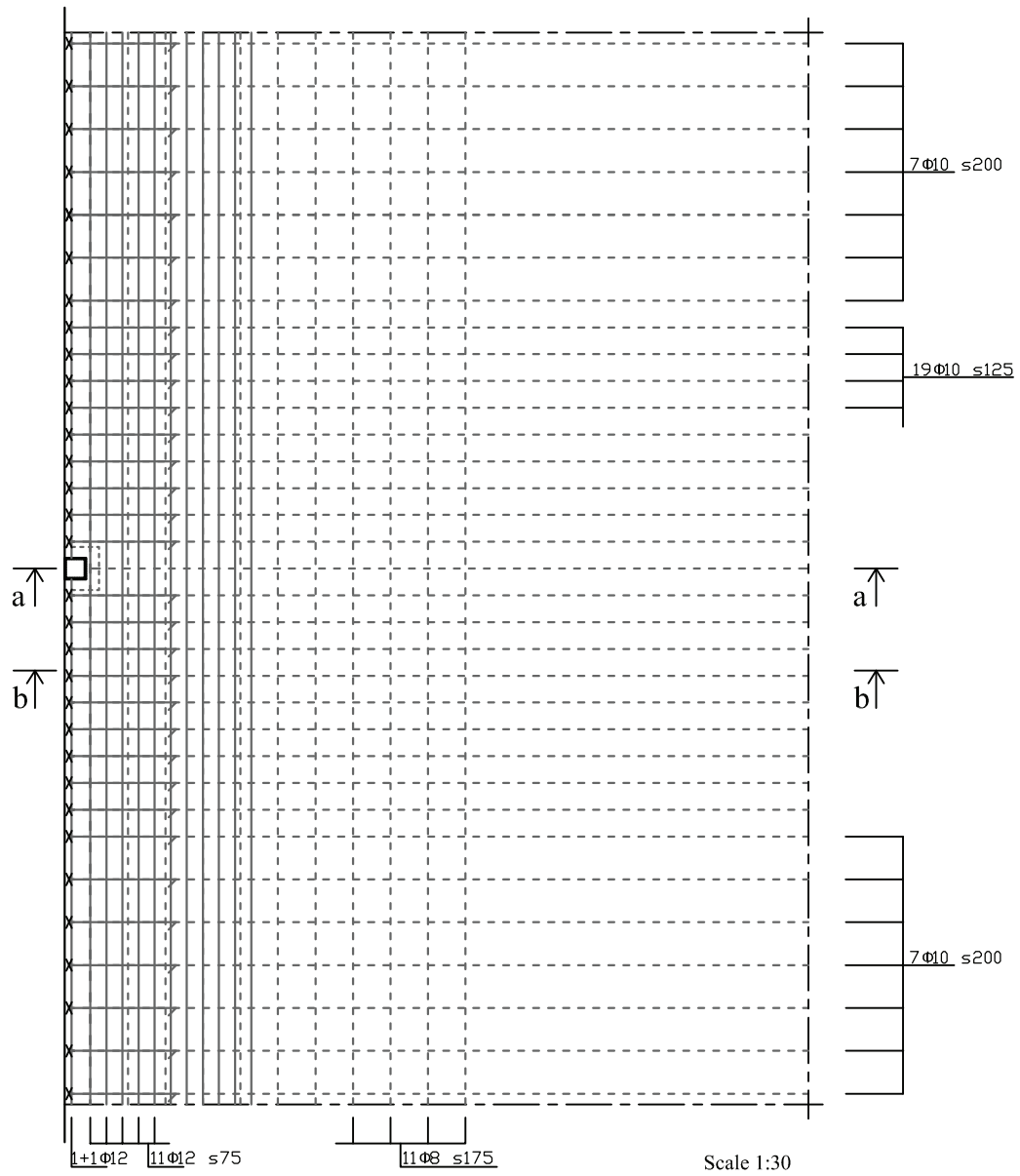
Scale 1:20

APPENDIX IV: Reinforcement arrangement in prototype models (A1, A2 and A3)

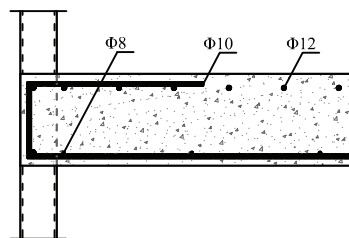
Model A1



Model A2



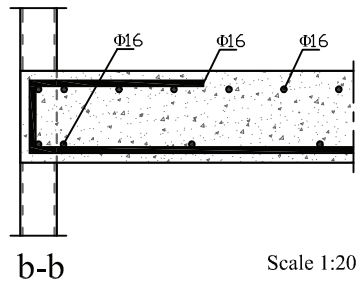
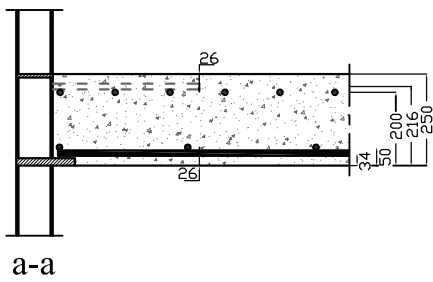
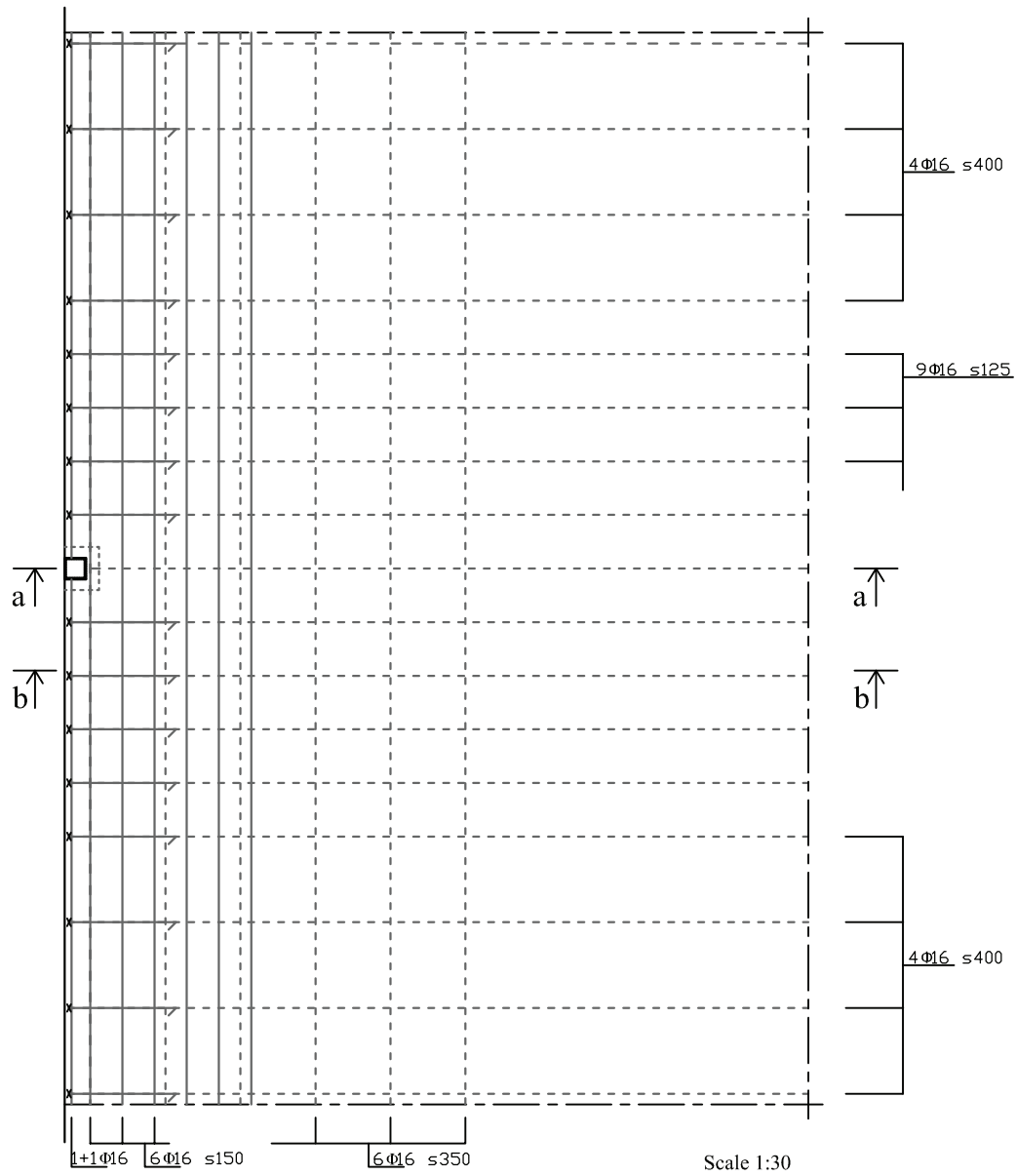
a-a



b-b

Scale 1:20

Model A3



APPENDIX V: Predicted punching load according to EC2

Specimen No. 2

Units:

$$\text{pond} := \frac{196133}{20000000} \text{N}$$

$$\text{kilopond} := 1000 \cdot \text{pond} = 9.807 \text{N}$$

$$\text{megapond} := 1000 \cdot \text{kilopond} = 9.807 \cdot \text{kN}$$

Geometry:

Coordinate system:

x - parallel to slab edge

y - perpendicular to slab edge

z - perpendicular to slab plane

Column dimensions and slab thickness:

Slab thickness, h : $h := 130 \text{mm}$

Column dimensions, d_{cx} and d_{cy} : $d_{c,x} := 200 \text{mm}$

$$d_{c,y} := 200 \text{mm}$$

Material properties:

Concrete cube strength, $f_{ck,cube}$: $f_{ck,cube} := 333 \frac{\text{kilopond}}{\text{cm}^2} = 32.656 \cdot \text{MPa}$

Concrete cylinder strength, f_{ck} : $f_{ck} := 0.8 \cdot f_{ck,cube} = 26.125 \cdot \text{MPa}$

Partial safety factor: $\gamma_{c,mean} := 1.0$

Reinforcement ratio:

$$\phi_{10} := 10 \text{mm} \quad \phi_{12} := 12 \text{mm}$$

Tensed flexural reinforcement in x-direction:

8 hairpin bars, scewed from column and out:

A-2 ϕ_{10}

B-4 ϕ_{12}

A-2 ϕ_{10}

Tensed flexural reinforcement in y-direction:

D-1 ϕ_{12}

C-8 ϕ_{12}

Effective depth, d :

The effective depth from compressed edge to tensed reinforcement.

In x-direction: $d_x := h - 25 \text{mm} = 0.105 \text{m}$

In y-direction: $d_y := h - 33 \text{mm} = 0.097 \text{m}$

Average depth: $d := \frac{(d_x + d_y)}{2} = 0.101 \text{m}$

Contributing section, A_c :

Considers bonded tensile reinforcement, within a concrete section the distance; bearing plus $3d$.

$$\text{In } x\text{-direction: } b_x := d_{c,y} + 2 \cdot 3 \cdot d = 0.806 \text{ m}$$

$$A_{c,x} := b_x \cdot h = 0.105 \text{ m}^2$$

$$\text{In } y\text{-direction: } b_y := d_{c,x} + 3 \cdot d = 0.503 \text{ m}$$

$$A_{c,y} := b_y \cdot h = 0.065 \text{ m}^2$$

Bonded tensile reinforcement within the contributing section, A_s :

$$\text{In } x\text{-direction: } A_{s,x} := 4 \cdot \frac{\pi \cdot \phi_{10}^2}{4} + 4 \cdot \frac{\pi \cdot \phi_{12}^2}{4} = 7.665 \times 10^{-4} \cdot \text{m}^2$$

$$\text{In } y\text{-direction: } A_{s,y} := 9 \cdot \frac{\pi \cdot \phi_{12}^2}{4} = 1.018 \times 10^{-3} \text{ m}^2$$

Reinforcement ratio, ρ :

$$\text{In } x\text{-direction: } \rho_x := \frac{A_{s,x}}{A_{c,x}} = 7.316 \times 10^{-3}$$

$$\text{In } y\text{-direction: } \rho_y := \frac{A_{s,y}}{A_{c,y}} = 0.016$$

Predicted punching resistance:

The ultimate punching capacity is calculated according to a simplified approach, assuming uniform shear on a reduced control perimeter.

$$\text{Control perimeter, } u: \quad u := d_{c,y} + 2 \cdot \min(1.5d, 0.5d_{c,x}) + \pi \cdot d = 0.717 \text{ m}$$

$$\text{Shear resistance per unit length, } v_{Rd,c}: \quad k := \min\left(1 + \sqrt{\frac{200 \text{ mm}}{d}}, 2.0\right) = 2$$

$$\rho_1 := \min(\sqrt{\rho_x \cdot \rho_y}, 0.02) = 0.011$$

$$v_{R,c} := \frac{0.18}{\gamma_{c,\text{mean}}} \cdot k \cdot \text{MPa} \cdot \sqrt[3]{100 \cdot \rho_1 \cdot \frac{f_{ck}}{\text{MPa}}} = 1.092 \cdot \text{MPa}$$

$$\text{Resisting punching load, } V_{Rd,c}: \quad V_{R,c} := v_{R,c} \cdot u \cdot d = 79.083 \cdot \text{kN}$$

Experimental punching resistance:

$$P_u := 13.1 \text{ megapond} = 128.467 \cdot \text{kN}$$

Model A1

Geometry:

Coordinate system:

x - perpendicular to slab edge
y - parallel to slab edge
z - perpendicular to slab plane

Dimensions of plate and slab thickness:

The supporting section of a steel column supported slab is the dimensions of the plate.

Plate dimension: $p_x := 150\text{mm}$

$p_y := 200\text{mm}$

Slab thickness: $h := 250\text{mm}$

Material properties:

Concrete mean compressive strength, f_{cm} : $f_{cm} := 38\text{MPa}$

Partial safety factor, $\gamma_{c,mean}$: $\gamma_{c,mean} := 1.0$

Reinforcement ratio:

Tensed flexural reinforcement in x-direction:

$\phi_{10} := 10\text{mm}$

$\phi_{12} := 12\text{mm}$

9 ϕ_{10} Column strip

8 ϕ_{10} Mid strip

Tensed flexural reinforcement y-direction:

6 ϕ_{12}

Effective depth:

The effective depth to from compressed edge to tensed reinforcement.

In x-direction: $d_x := 225\text{mm}$

In y-direction: $d_y := 212\text{mm}$

Average depth: $d := \frac{(d_x + d_y)}{2} = 0.219\text{m}$

Contributing section:

Considers bonded tensile reinforcement, within a concrete section the distance; bearing plus 3d.

In x-direction: $b_x := p_y + 2 \cdot 3 \cdot d = 1.511\text{m}$

$A_{c,x} := b_x \cdot h = 0.378\text{m}^2$

In y-direction: $b_y := p_x + 3 \cdot d = 0.805\text{m}$

$A_{c,y} := b_y \cdot h = 0.201\text{m}^2$

Bonded tensile reinforcement within the contributing section, A_s :

$$\text{In } x\text{-direction: } A_{s,x} := 7 \cdot \frac{\pi \cdot \phi_{10}^2}{4} = 5.498 \times 10^{-4} \cdot \text{m}^2$$

$$\text{In } y\text{-direction: } A_{s,y} := 5 \cdot \frac{\pi \cdot \phi_{12}^2}{4} = 5.655 \times 10^{-4} \cdot \text{m}^2$$

Reinforcement ratio, ρ :

$$\text{In } x\text{-direction: } \rho_x := \frac{A_{s,x}}{A_{c,x}} = 1.455 \times 10^{-3}$$

$$\text{In } y\text{-direction: } \rho_y := \frac{A_{s,y}}{A_{c,y}} = 2.808 \times 10^{-3}$$

Punching resistance:

The punching resistance of the edge column is calculated according to a simplified approach, assuming uniform shear on a reduced control perimeter.

$$\text{Reduced control perimeter, } u: \quad u := p_y + 2 \min(1.5d, 0.5p_x) + \frac{1}{2} \cdot \pi \cdot (2d) = 1.036 \text{ m}$$

$$\text{Shear resistance per unit length, } v_{Rd,c}: \quad k := \min\left(1 + \sqrt{\frac{200 \text{ mm}}{d}}, 2.0\right) = 1.957$$

$$\rho_1 := \min(\sqrt{\rho_x \cdot \rho_y}, 0.02) = 2.022 \times 10^{-3}$$

$$v_{R,c} := \frac{0.18}{\gamma_{c,\text{mean}}} \cdot k \cdot \text{MPa} \cdot \sqrt[3]{100 \cdot \rho_1 \cdot \frac{f_{cm}}{\text{MPa}}} = 0.695 \cdot \text{MPa}$$

$$\text{Resisting punching load, } V_{Rd,c}: \quad V_{R,c} := v_{R,c} \cdot u \cdot d = 157.384 \cdot \text{kN}$$

Model A2

Geometry:

Coordinate system:

x - perpendicular to slab edge
y - parallel to slab edge
z - perpendicular to slab plane

Dimensions of plate and slab thickness:

The supporting section of a steel column supported slab is the dimensions of the plate.

Plate dimension: $p_x := 150\text{mm}$

$p_y := 200\text{mm}$

Slab thickness: $h := 250\text{mm}$

Material properties:

Concrete mean compressive strength, f_{cm} : $f_{cm} := 38\text{MPa}$

Partial safety factor, $\gamma_{c,mean}$: $\gamma_{c,mean} := 1.0$

Reinforcement ratio:

Tensed flexural reinforcement in x-direction: $\phi_{10} := 10\text{mm}$ $\phi_{12} := 12\text{mm}$

19 ϕ_{10} Column strip

14 ϕ_{10} Mid strip

Tensed flexural reinforcement y-direction:

12 ϕ_{12}

Effective depth:

The effective depth to from compressed edge to tensed reinforcement.

In x-direction: $d_x := 225\text{mm}$

In y-direction: $d_y := 212\text{mm}$

Average depth: $d := \frac{(d_x + d_y)}{2} = 0.219\text{m}$

Contributing section:

Considers bonded tensile reinforcement, within a concrete section the distance; bearing plus $3d$.

In x-direction: $b_x := p_y + 2 \cdot 3 \cdot d = 1.511\text{m}$

$A_{c,x} := b_x \cdot h = 0.378\text{m}^2$

In y-direction: $b_y := p_x + 3 \cdot d = 0.805\text{m}$

$A_{c,y} := b_y \cdot h = 0.201\text{m}^2$

Bonded tensile reinforcement within the contributing section, A_s :

$$\text{In x-direction: } A_{s,x} := 12 \cdot \frac{\pi \cdot \phi_{10}^2}{4} = 942.478 \cdot \text{mm}^2$$

$$\text{In y-direction: } A_{s,y} := 11 \cdot \frac{\pi \cdot \phi_{12}^2}{4} = 1.244 \times 10^3 \cdot \text{mm}^2$$

Reinforcement ratio, ρ :

$$\text{In x-direction: } \rho_x := \frac{A_{s,x}}{A_{c,x}} = 2.495 \times 10^{-3}$$

$$\text{In y-direction: } \rho_y := \frac{A_{s,y}}{A_{c,y}} = 6.178 \times 10^{-3}$$

Punching resistance:

The punching resistance of the edge column is calculated according to a simplified approach, assuming uniform shear on a reduced control perimeter.

$$\text{Reduced control perimeter, } u: \quad u := p_y + 2 \min(1.5d, 0.5p_x) + \frac{1}{2} \cdot \pi \cdot (2d) = 1.036 \text{ m}$$

$$\text{Shear resistance per unit length, } v_{Rd,c}: \quad k := \min\left(1 + \sqrt{\frac{200 \text{ mm}}{d}}, 2.0\right) = 1.957$$

$$\rho_1 := \min(\sqrt{\rho_x \cdot \rho_y}, 0.02) = 3.926 \times 10^{-3}$$

$$v_{R,c} := \frac{0.18}{\gamma_{c,\text{mean}}} \cdot k \cdot \text{MPa} \cdot \sqrt[3]{100 \cdot \rho_1 \cdot \frac{f_{cm}}{\text{MPa}}} = 0.867 \cdot \text{MPa}$$

$$\text{Resisting punching load, } V_{Rd,c}: \quad V_{R,c} := v_{R,c} \cdot u \cdot d = 196.356 \cdot \text{kN}$$

Model A3

Geometry:

Coordinate system:

x - perpendicular to slab edge
y - parallel to slab edge
z - perpendicular to slab plane

Dimensions of plate and slab thickness:

The supporting section of a steel column supported slab is the dimensions of the plate.

Plate dimension: $p_x := 150\text{mm}$

$p_y := 200\text{mm}$

Slab thickness: $h := 250\text{mm}$

Material properties:

Concrete mean compressive strength, f_{cm} : $f_{cm} := 38\text{MPa}$

Partial safety factor, $\gamma_{c,mean}$: $\gamma_{c,mean} := 1.0$

Reinforcement ratio:

Tensed flexural reinforcement in x-direction: $\phi_{16} := 16\text{mm}$

11 ϕ_{16} Column strip

6 ϕ_{16} Mid strip

Tensed flexural reinforcement y-direction:

6 ϕ_{16}

Effective depth:

The effective depth to from compressed edge to tensed reinforcement.

In x-direction: $d_x := 216\text{mm}$

In y-direction: $d_y := 216\text{mm}$

Average depth: $d := \frac{(d_x + d_y)}{2} = 0.216\text{m}$

Contributing section:

Considers bonded tensile reinforcement, within a concrete section the distance; bearing plus $3d$.

In x-direction: $b_x := p_y + 2 \cdot 3 \cdot d = 1.496\text{m}$

$$A_{c,x} := b_x \cdot h = 0.374\text{m}^2$$

In y-direction: $b_y := p_x + 3 \cdot d = 0.798\text{m}$

$$A_{c,y} := b_y \cdot h = 0.2\text{m}^2$$

Bonded tensile reinforcement within the contributing section, A_s :

$$\text{In } x\text{-direction: } A_{s,x} := 7 \cdot \frac{\pi \cdot \phi_{16}^2}{4} = 1.407 \times 10^3 \cdot \text{mm}^2$$

$$\text{In } y\text{-direction: } A_{s,y} := 5 \cdot \frac{\pi \cdot \phi_{16}^2}{4} = 1.005 \times 10^3 \cdot \text{mm}^2$$

Reinforcement ratio, ρ :

$$\text{In } x\text{-direction: } \rho_x := \frac{A_{s,x}}{A_{c,x}} = 3.763 \times 10^{-3}$$

$$\text{In } y\text{-direction: } \rho_y := \frac{A_{s,y}}{A_{c,y}} = 5.039 \times 10^{-3}$$

Punching resistance:

The punching resistance of the edge column is calculated according to a simplified approach, assuming uniform shear on a reduced control perimeter.

$$\text{Reduced control perimeter, } u: \quad u := p_y + 2 \min(1.5d, 0.5p_x) + \frac{1}{2} \cdot \pi \cdot (2d) = 1.029 \text{ m}$$

$$\text{Shear resistance per unit length, } v_{Rd,c}: \quad k := \min\left(1 + \sqrt{\frac{200 \text{ mm}}{d}}, 2.0\right) = 1.962$$

$$\rho_1 := \min\left(\sqrt{\rho_x \cdot \rho_y}, 0.02\right) = 4.355 \times 10^{-3}$$

$$v_{R,c} := \frac{0.18}{\gamma_{c,\text{mean}}} \cdot k \cdot \text{MPa} \cdot \sqrt[3]{100 \cdot \rho_1 \cdot \frac{f_{cm}}{\text{MPa}}} = 0.9 \cdot \text{MPa}$$

$$\text{Resisting punching load, } V_{Rd,c}: \quad V_{R,c} := v_{R,c} \cdot u \cdot d = 199.971 \cdot \text{kN}$$

APPENDIX VI: Convergence criteria

